National Center for Nuclear Research

Doctoral Thesis

CFD modeling of dual fluid reactor (DFR) demonstrator

Hisham Lotfy Elgendy

A thesis submitted in fulfillment of the requirements

for the degree of Doctor of Physical Sciences

in the National Centre for Nuclear Research

Supervisor:

Prof. dr. hab. Konrad Czerski

Auxiliary supervisor:

Dr. Michal Spirzewski

Acknowledgments

I would like to express my heartfelt gratitude to the divine, who has blessed me with numerous gifts. Additionally, I am profoundly thankful to my parents, who are the cornerstone of my existence and have provided unwavering support throughout the years.

I extend my deepest appreciation to my supervisor, Prof. Konrad Czerski, for his assistance, invaluable support, effective guidance and his contribution to my academic journey.

Special thanks are due to NCBJ represented in Prof. Mariusz Dabrowski and Dr Karol Kowal and the rest of the team who have afforded me the opportunity to attain this level of knowledge.

Lastly, I wish to acknowledge the immense support from my colleagues, friends, and family, whose presence has made challenging times more manageable.

Contents

List of Figures

List of tables

List of Nomenclature

Abbreviation	Description
2D	Two Dimensional
3D	Three Dimensional
ATLAS	Advanced Thermal-Hydraulic Test Loop for Accident Simulation
BC	Boundary Condition
CFD	Computational Fluid Dynamics
DFR	Dual Fluid Reactor
DFRm	Dual Fluid Reactor (metalic fuel)
DFRs	Dual Fluid Reactor (salt fuel)
DNS	Direct Numerical Simulation
EROI	Energy Return On Investment
GenIV	Fourth Generation of nuclear reactos
GFR	Gas-Cooled Fast Reactor
GIF	Generation IV International Forum
IAEA	International Atomic Energy Agency
LES	Large Eddy Simulation
LFR	Lead-Cooled Fast Reactor
MD	Mini-Demonstrator
MSFR	Molten Salt Fast Reactor
MSR	Molten salt reactor
PPU	Pyrochemical Processing Unit

PRISM	Power Reactor Innovative Small Modular
RANS	Reynolds Averaged Navier-Stokes
RSM	Reynolds stress model
SCWR	Super Critical Water Reactor
SFR	Sodium-Cooled Fast Reactor
SGDH	Standard-Gradient Diffusion Hypothesis
SGS	Sub-Grid-Scale
SST	Shear Stress Transport Model
TRISO	Tristructural Isotropic
VHTR	Very High Temperature

Dimensionless quantities

Pr	Prandtl number
Pr_t	turbulent Prandtl number
Re	Reynolds number
Ri	Richardson number
Nu	Nusselt number
Pe	Peclet number

Greek Symbols

μ	Dynamic viscosity
μ_t	Turbulent viscosity (eddy viscosity)
v	Kinematic viscosity

ω	Specific dissipation rate
ρ	Density
τ	Shear stress
τ_w	Wall shear stress
ε	Dissipation rate
K	Thermal conduction coefiecient
m	Mass
v	Velocity
t	Time

Latin symbols

$\langle u'v' \rangle$, $\langle u'w' \rangle$, $\langle v'w' \rangle$	Turbulent shear stress components
k	Turbulence kinetic energy
T	Temperature
u, v,w	Spanwise, transverse and axial velocity components, respectively
u	Characteristic velocity
u', v, w'	Fluctuating velocity components
u_τ	Friction velocity
y	Distance from the wall
c_p	Specific heat capacity

Abstract

The Dual Fluid Reactor (DFR) is a promising Generation IV reactor concept with numerous advantages. To realize this innovative design, significant efforts are required to achieve optimal design and secure regulatory and public acceptance. While computer codes are commonly used for modeling, actual experiments hold greater credibility than simulations. Therefore, the construction of a mini demonstrator (MD) as an experimental facility targeted to the DFR research is crucial for enhancing trust in computer models dealing with low Prandtl number fluids. By comparing experimental results from the MD with modeling outcomes, validation of the model under various operational conditions provides convincing evidence for regulatory bodies and the scientific community. This validation process enables reliable modeling of the DFR across a wide range of scenarios. In this thesis a preliminary schematic of MD is proposed, and the MD core design is described together with precise dimensions and figures. The case was carefully meshed and exported to calculations based on the relative boundary layers and different scenarios.

The turbulence modeling technique employed in this study showed satisfactory agreement with DNS/LES/Experimental data which increases the confidence in capturing the correct thermal hydraulic behaviors.

Computational results revealed three primary factors influencing heat transfer and fuel velocity in the MD core, two of which are related to system geometry. The positioning of fuel pipe inlets relative to the fuel inlet direction and the placement of coolant pipes in the distribution zone, both significantly affect heat exchange, mass flow rates, and velocity uniformity in the fuel pipes. The third factor was found to be the buoyancy force affecting the direction of the fuel right after entering the MD. The counter flow configuration exhibited more uniform velocity inlets, higher heat exchange efficiency, and uniform temperature gradients compared to parallel flow. In parallel flow, swirling patterns were observed, which, although theoretically enhancing heat transfer, resulted in higher pressure, reduced mass flow rates, and increased risk of vibration-induced pipe fractures and corrosion. The choice of using 3D modelling was crucial as using 2D modelling the resulting wouldn’t be able to capture these swirling behaviors, or the observed fuel flow splitting over coolant pipes in the distribution and collection zones.

A major part of the heat transfer was found to occur in the initial contact zone between coolant and fuel in both parallel and counter flow cases. In parallel flow, the heat exchange extends over a larger region, promoting temperature uniformity in the middle core zone. In contrast, counter flow exhibits intense heat transfer in the initial contact zone, which poses safety concerns and mechanical stresses. Mass flow rates differ between parallel and counter flows, affecting heat exchange efficiency, with counter flow configurations found to be more efficient.

The observed discrepancies between parallel and counter flows provide valuable insights for DFR designers. Hot spots were observed over coolant pipes located in front of fuel inlets, which may result in corrosion and mechanical stress issues due to temperature variations. Installation of measuring instruments at specific locations is proposed to capture temperature and velocity profiles, monitor variations in temperature and heat transfer parameters, and gain a better

understanding of fuel and coolant flows within the middle core zone. Certain locations should be avoided for measurement devices, such as areas with backflows or flow separation, to ensure accurate measurements. Finally, the findings and conclusions have shown the importance of modelling the MD that alone gives a better understanding of the DFR thermal hydraulics, and together with the MD as an experimental facility for the purpose of model validation and exploring more different DFR operational scenarios during the reactor design stages.

Streszczenie

Reaktor dwufazowy (DFR) stanowi obiecującą koncepcję reaktora czwartej generacji, charakteryzującą się licznymi zaletami. Aby zrealizować ten innowacyjny projekt, wymagane są znaczne wysiłki w celu osiągnięcia optymalnego projektu oraz zapewnienia akceptacji ze strony organów regulacyjnych i społeczeństwa. Podczas gdy kody komputerowe są powszechnie używane do modelowania, faktyczne eksperymenty mają większą wiarygodność niż symulacje. Dlatego też budowa mini-demonstratora (MD) jako obiektu badawczego skierowanego na badania nad DFR jest kluczowa dla zwiększenia zaufania do modeli komputerowych zajmujących się płynami o niskiej liczbie Prandtla. Porównując wyniki eksperymentalne z MD z wynikami modelowania, walidacja modelu w różnych warunkach eksploatacyjnych dostarcza przekonujących dowodów dla organów regulacyjnych i środowiska naukowego. Ten proces walidacji umożliwia wiarygodne modelowanie DFR w szerokim zakresie scenariuszy. W niniejszej pracy doktorskiej zaproponowano wstępny schemat MD, opisano projekt rdzenia MD wraz z precyzyjnymi wymiarami i rysunkami. Przypadek został starannie podzielony na siatkę i poddany obliczeniom opartym na względnych warstwach granicznych i różnych scenariuszach. Wykorzystana w tej pracy technika modelowania turbulencji wykazała zadowalającą zgodność z danymi DNS/LES/Eksperymentalnymi, co zwiększa pewność przechwytywania właściwego zachowania termohydraulicznego.

Wyniki obliczeń wykazały trzy główne czynniki wpływające na transfer ciepła i prędkość paliwa w rdzeniu MD, z których dwa są związane z geometrią systemu. Położenie wlotów rur paliwowych w stosunku do kierunku wlotu paliwa oraz umiejscowienie rur chłodziwa w strefie dystrybucji mają istotny wpływ na wymianę ciepła, przepływ masowy i jednorodność prędkości w rurach paliwowych. Trzecim czynnikiem okazała się siła wyporu, wpływająca na kierunek przepływu paliwa tuż po jego wejściu do MD. Konfiguracja przepływu przeciwnego charakteryzuje się bardziej jednolitymi wlotami prędkości, wyższą efektywnością wymiany ciepła oraz jednorodnymi gradientami temperatury w porównaniu do przepływu równoległego. W przepływie równoległym zaobserwowano wirujące wzorce, które teoretycznie zwiększają transfer ciepła, jednak prowadzą do większego ciśnienia, zmniejszonego przepływu masowego oraz zwiększonego ryzyka uszkodzeń rur spowodowanych drganiami i korozją. Wybór modelowania 3D był kluczowy, ponieważ korzystając z modelowania 2D, nie można by uwzględnić tych wirujących zachowań ani zaobserwowanego podziału przepływu paliwa nad rurami chłodziwa w strefach dystrybucji i zbiorczych.

Stwierdzono, że znaczna część transferu ciepła występuje w strefie początkowego kontaktu między chłodziwem a paliwem zarówno w przypadku przepływu równoległego, jak i przeciwnego. W przepływie równoległym wymiana ciepła obejmuje większy obszar, co sprzyja jednorodności temperatury w strefie środkowej rdzenia. Natomiast przepływ przeciwny charakteryzuje się intensywną wymianą ciepła w strefie początkowego kontaktu, co wiąże się z obawami dotyczącymi bezpieczeństwa i naprężeniami mechanicznymi. Przepływy masowe różnią się między przepływem równoległym a przeciwnym, co wpływa na efektywność wymiany ciepła, przy czym konfiguracje przepływu przeciwnego okazały się bardziej efektywne.

Obserwowane rozbieżności między przepływem równoległym a przeciwnym dostarczają cennych wskazówek dla projektantów DFR. Zaobserwowano miejsca o podwyższonej temperaturze nad rurami chłodziwa znajdującymi się przed wlotami paliwowymi, co może prowadzić do korozji i problemów z naprężeniami mechanicznymi spowodowanymi zmiennością temperatury. Proponuje się instalację przyrządów pomiarowych w określonych miejscach w celu rejestrowania profilów temperatury i prędkości, monitorowania zmian w parametrach temperatury i wymianie ciepła oraz uzyskania lepszego zrozumienia przepływu paliwa i chłodziwa w strefie środkowej rdzenia. Należy unikać określonych miejsc do umieszczania urządzeń pomiarowych, takich jak obszary z cofaniem się przepływu lub separacją przepływu, aby zapewnić dokładne pomiary. Ostatecznie, wyniki i wnioski wykazały znaczenie modelowania MD, które samo w sobie zapewnia lepsze zrozumienie termohydrauliki DFR, oraz w połączeniu z MD jako obiektem eksperymentalnym w celu walidacji modelu i badania różnych scenariuszy eksploatacyjnych DFR podczas etapów projektowania reaktora.

1 Introduction

1.1 Motivation and Objectives

As per the International Energy Agency (IEA), approximately 770 million people across the globe currently lack access to electricity, primarily due to inadequate power generation within their countries [1]. These nations face energy deficiencies stemming from a variety of economic and political factors. In the quest to address their energy challenges, these underdeveloped countries often turn to their local energy resources, despite the potential environmental impact associated with their utilization. For instance, countries endowed with abundant coal reserves tend to heavily rely on coal as their primary energy source, while those possessing substantial underground petroleum reservoirs do the same. Not only do the undeveloped countries have the same approach, but also some underdeveloped countries are struggling with improving their carbon emissions despite running efforts towards the limitation of the carbon emissions.

Based on projections by the United States Energy Information Agency (IEA), carbon emissions are anticipated to rise steadily from the present until 2040 [1], even in light of the countries' efforts to fulfill their obligations under the Paris Climate Agreement established in 2015 [2], [3]. These findings suggest that current measures and commitments may not be sufficient to effectively curb the growth of carbon emissions within the projected timeframe, highlighting the challenges faced in achieving long-term climate goals. Despite the perceived appeal of renewable energy sources to the general public, they possess inherent limitations attributable to their reliance on natural factors beyond human control, such as the localized variability of wind and solar energies.

Regardless the occasionally ongoing debates regarding the safety and viability of nuclear power, it remains a compelling solution for addressing the current energy and environmental crisis compromise [4].

The enhanced scalability and safety features of fourth-generation reactors (GenIV) have sparked the interest of scientific researchers, driving them to dedicate efforts towards expanding our knowledge of these reactor concepts for future commercialization[5], [6]. This includes further advancements in inherent safety measures and economic feasibility to ensure widespread public and political acceptance.

Given that these reactor types are founded on novel concepts and remain in the design phase, it is imperative to address numerous safety considerations prior to licensing. This entails adopting precise and reliable modeling approaches that can effectively simulate the operation of these reactors under various operational scenarios to ensure comprehensive safety assessments[7]. However, relying solely on modeling without empirical data to validate the modeling outcomes is insufficient. Consequently, it is essential to establish experimental facilities that align with the diverse reactor types to conduct relevant experiments and enhance the accuracy of safety evaluations.

The Dual fluid reactor (DFR) is one of the novel concepts belongs to the Gen IV type of reactors[8]–[10]. The specialty of the DFR lies in its concept that is using two separated loops, one for the fuel and the other for the coolant. Both fuel and coolant are in a molten liquid state. A distinctive attribute of this technology involves the utilization of liquid fuel containing a high concentration of actinides, coupled with a coolant possessing notable thermal conductivity and heat capacity. This combination has the potential to yield higher power density, enhanced efficiency, and elevated working medium temperatures. The DFR exhibits a notable Energy Return Over Investment (EROI), indicating its high efficiency. Additionally, the DFR encompasses various advantageous characteristics, such as the ability to undergo fission reactions involving non-fertile transuranium isotopes like Pl^{240} and Am^{241}. Furthermore, the implementation of online fuel reprocessing within external distillation units offers the advantage of exceptionally high temperatures required for hydrogen production. The DFR incorporates a self-regulating reaction mechanism that operates based on temperature feedback of the reaction, thereby enhancing passive safety measures. Moreover, the DFR enables swift reduction of reactor power, with the ability to decrease from 100% to 7% within a matter of minutes. These distinctive attributes, among others, position the DFR as a reactor that surpasses the features of GenIV reactors.

Computational fluid dynamics (CFD) is essential for ensuring the safety of nuclear reactors in general and molten fuels/coolants nuclear reactors especially, this is by enabling thermal analysis, assessing accident scenarios, designing effective containment systems, evaluating material compatibility, and assessing safety system performance. It provides valuable insights into the fluid dynamics and thermal behavior of the reactor, helping engineers and researchers optimize safety measures and mitigate potential risks.

The planned experimental facility for the purpose of DFR research is the Mini Demonstrator (MD) of the DFR. The MD is the experimental facility that has the scope of this work with primary goals that include the following:

1. **Elaborating on the intricate design aspects of the mini demonstrator core:** The design of the MD core was carefully configured to closely resemble the general layout and dimensions of the DFR, specifically in terms of flow paths and pipe dimensions. This approach ensures that the modeling and future experimental results are applicable to a significant extent to the actual DFR, while minimizing the need for excessive scaling that could potentially compromise the compatibility of the results.

2. **Identifying a suitable computational fluid dynamics (CFD) methodology**: Due to the unique characteristics of the working fluid (molten metal), employing conventional modeling approaches may yield misleading outcomes. Therefore, it is crucial to select an appropriate modeling methodology that can accurately capture the distinct fluid behaviors, particularly the low Prandtl number, in the MD and in the future in DFR CFD modelling.

3. **Modelling the thermal hydraulics detailed characteristics of the MD core**: This is to model the detailed thermal hydraulics characteristics of the MD core, focusing on

capturing the specific flow and heat transfer behaviors within this particular geometry. This investigation is crucial for gaining insights, validating planned experiments, and facilitating the understanding of the possible and expected phenomenon in the DFR in various operational configurations which will be provide important information to improve the reactor during the design stages.

4. **Proposing strategically optimal positions for instrumentation in the MD core system**The conducted computational fluid dynamics (CFD) analysis provided valuable insights into the flow and heat transfer characteristics at different locations within the MD. This analysis aids in determining the optimal placement of measuring instruments within the MD core, ensuring the collection of accurate and reliable data.

This thesis comprises six chapters, each focusing on specific aspects of the research. A concise overview of the content covered in each chapter is provided below:

The first chapter serves as an introductory section to the thesis, providing a clear statement of the objectives and motivations behind the research. It also presents an overview of the current global status of nuclear energy, with a specific focus on the latest advancements in reactor technology, particularly the Generation IV (GenIV) reactors, followed by a dedicated section describing the dual fluid reactor (DFR) design concept and a brief operation description.

The second chapter highlights the crucial significance of experimental facilities in the context of reactor licensing and design. It provides an introduction to the design of the Mini Demonstrator (MD) of the Dual Fluid Reactor (DFR), including a comprehensive preliminary schematic design and a description of its components. Furthermore, the chapter presents an in-depth design description of the MD core, outlining its specific geometry and dimensions.

The third chapter provides a concise introduction to computational fluid dynamics (CFD) and its application in nuclear reactor design, addressing the associated challenges. Furthermore, it presents an overview of the turbulence modeling techniques utilized in this thesis. Additionally, the chapter discusses the specific characteristics of the fluid employed in the MD, focusing on its relevance to the research objectives.

The fourth chapter elucidates the selected turbulence modeling technique for conducting calculations. It delves into the rationale behind the choice of this technique and subsequently outlines various validation methodologies employed to assess the model's accuracy and reliability. These validation approaches are designed to provide comprehensive validation perspectives and ensure the robustness of the modeling approach.

The fifth chapter of this study presents the setup of the MD case, emphasizing the meshing process and providing an overview of the selected boundary conditions for the case calculations. Additionally, the chapter outlines the structure of the obtained results.

The subsequent section comprehensively presents and analyzes the results obtained from the parallel flow configuration, focusing on heat transfer and flow analysis. A thorough comparison is made with the corresponding boundary condition parameters of the counter flow configuration, highlighting, and discussing the main observed differences in detail.

The final section of this chapter focuses on the placement of measuring instruments, including optimal locations and areas to avoid. Various measuring instruments are introduced, accompanied by a concise description of their operational principles.

The sixth and final section in this thesis is dedicated to providing a comprehensive summary of the conclusions and findings derived from the preceding sections.

1.2 Nuclear energy status

The progression of nuclear power has a long and complex history that spans over a hundred years. It started with the basic discoveries of radioactivity and nuclear fission in the early 20th century, laying the base for approaching the power of the atom.

However, throughout the 1960s, many countries, for example France, United states of America, as well the Soviet Union, started working on their nuclear programs, constructing a significant number of reactors. The most dominant types of reactors at that time were: Pressurized Water Reactors (PWRs) and Boiling Water Reactors (BWRs).

Moreover, the 1970s and 1980s brought difficult setbacks for nuclear energy production. The Three Mile Island accident in 1979 in the United States and later the Chernobyl catastrophe in 1986 in the Soviet Union. The accidents highlighted the significance of safety and led to the establishment of stricter regulations and higher standards of safety measures. Although the accidents were a disaster in several means, they were an important lesson to the nuclear community.

Despite of the accidents, nuclear power continued to expand, adding countries like Germany, Japan, and South Korea strongly investing in nuclear energy production. However, after the Fukushima disaster in 2011 that was initiated by a massive earthquake and tsunami, triggered debates around the safety and future of nuclear energy production.

Recently, research has focused on advanced types of reactor designs, for example Generation III and Generation IV reactors, which aim to increase safety, enhance efficiency, and able to deal with other type of challenges such as waste management.

It is a fact that fossil fuels as finite energy resources tend to pose long-term sustainability challenges, either due to excess consumption that would simply lead to its end, or due to the negative environmental impact which results in the release of large amounts of greenhouse gases into the atmosphere when burned, contributing significantly to climate change and global warming. Additionally, their extraction and combustion have negative impacts on air quality, human health, and ecosystems.

For these reasons, COP 21 had a focus on the reducing the carbon emissions relying on strict requirements in the agreement signed by the participating parties of the United Nations Framework Convention on Climate Change (UNFCCC) with the objective of addressing climate change and facilitating the advancement and augmentation of endeavors and investments essential for a sustainable future characterized by reduced carbon emissions.

Despite regrettable incidents, nuclear energy remains a substantial contributor to low-carbon electricity, serving as a primary source for a considerable share of electricity generation in numerous nations, while other countries adopt a more cautious approach figure 1. Nonetheless, in the foreseeable future, nuclear power is poised to establish itself as a reliable and sustainable method of power generation, offering potential as a practical solution for addressing environmental and energy-related dilemmas.

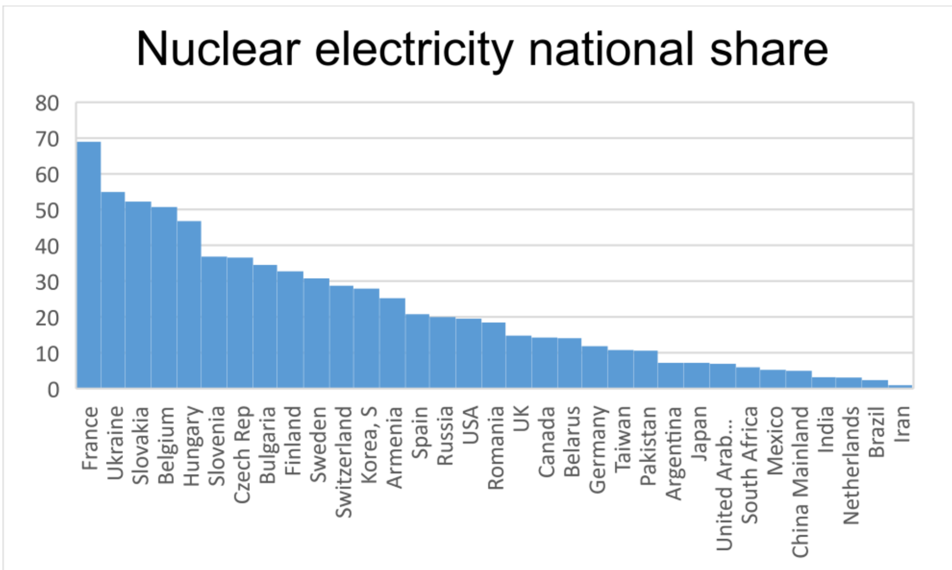

Figure 1 : Nuclear electricity national share per country
Source: IAEA Power Reactor Information System (PRIS), World Nuclear Association Reactor Database[11]

1.3 Generation IV Nuclear Reactors

Although the third generation of reactors is the most used commercially, the fourth generation of reactors is now gaining more attention from the researchers and scientists working in the field for the past three decades. Initiated by the US department of energy, in 2000 the Generation IV International Forum (GIF) was founded. Not focusing on constructing reactors, GIF targeted gathering data and researchers to add motivation to the subject and make the available data visible and accessible to interested scientists and engineers. [12]. Over the subsequent years, six novel reactor concepts were put forward, intended to serve as a technological roadmap for the future development of nuclear energy systems[13]. The Six types are: sodium-cooled fast reactor

(SFR), gas-cooled fast reactor (GFR), lead-cooled fast reactor (LFR) molten salt fast reactor (MSR). Another version of the molten salt reactor uses the thermal neutrons, in addition to two more reactors: super critical water reactor (SCWR) and (very high temperature reactor (VHTR), the last mentioned three reactors make the thermal types of the Generation IV reactor. These novel types of reactor designs are mainly targeted to fulfill multiple objectives encompassing sustainability, economic viability, safety, reliability, as well as resistance to proliferation and physical protection.[14]

In 2005 many of the original charter countries of the GIF (Argentina, Brazil, Canada, France, Japan, South Korea, South Africa, the UK and the USA. Later joined by Switzerland, China, Russia, Australia) have signed a framework agreement which formally obligates them to practically participate in the development of at least one generation VI type of reactor. Although not each country of the charters has signed the agreement, the signed parties have been continuing their research aiming to develop a better knowledge about the new generation of reactors.

Apart from GIF, other countries are pursuing their individual advanced nuclear technologies. The Russian BREST reactor is an example of a lead cooled reactor that is in focus of the country. India has a three stages program to use Thorium as a nuclear fuel. Many other projects and programs are currently running by several countries involving generation VI-related aspects like fuel recycling using different actinides for fuel assemblies.

In the SFR, as a fast reactor uses the liquid sodium as a coolant, which provides a higher working temperature possibility, unlike other types of reactors, a high pressure of the coolant here is no longer required. The working nominal temperature range is 500-550 °C. The nominal working power range is between 300 – 1500 MWth. Despite the sodium advantages as a coolant, the existence of water nearby has always been an additional safety risk and requires an extra strict safety system due to the high risk of an exothermic reaction that could occur in the planet.

The GFR is a fast and high temperature reactor cooled by gas in a closed fuel cycle. Helium and carbon dioxide are used for cooling, however, each of the coolants is more suitable for a different criticality configuration. The working temperature range is between 800-850 $^{\circ}C$. The fuel is a fractional combination of ^{235}U or ^{239}Pu. with a nominal thermal power of 2400 MWth.

LFR is also a fast reactor that operates in a temperature as high as 800 °C. in some designs, in a closed fuel cycle with a nominal power of 150 MWth that can be increased in the designs with higher temperatures. Both lead and lead-bismuth are considered as possible coolants to be used. Due to the high temperatures of operation, the LFR can be used for hydrogen production.

Both versions of the molten salt reactors (thermal MSR and fast MSFR) use liquid salt mixtures as a coolant and as a fuel. Nominal temperature range is 750 – 1000 °C. The reactor can be used as a fuel breeder and can be used as well as a UOX burner or for other types of actinides. The reactor has atmospheric operational pressure reducing which provides a lower cost by exempting the expensive pressurized systems. The Oak Ridge National Laboratory as a first introducer to this technology in the 60’s has Th-U closed fuel cycle decreasing the fuel waste and improving thermal efficiency having a nominal power of 3000 MWth.

As water is being used for cooling in the thermal SCWR, and in operational temperature as high as 375 °C up to 625 °C, the pressure must exceed 22 MPa to keep the water above its supercritical states and might go as high as 25 MPa depending on the specific design. There have been several design concepts addressing thermal power ranging from 1000 to 1700 MWe. The water exists the reactor in a high temperature and pressure. The SCWR is similar to BWR in terms of efficiency and type of cycle (direct cycle) , however, it is more similar to PWR design when it comes to fuel configuration as it uses enriched uranium oxide. Both thermal and fast designs are considered, Light or heavy water can be used for thermal design while actinides reprocessing is then suitable for the fast one. The design of this reactor is subjected to several configurations and arrangements with no full complete standard design to be used as a reference, which results in different ranges of temperature and power that can be found in literature.

Graphite serves as a moderator in the case of the thermal VHTR. Gas (helium) is used for cooling the reactor. For such a very high temperature reactor the helium outlet from the core may reach 900 - 1000 °C. A prismatic and pebble bed designs both concepts are included as possible options. The used fuel design is in the form of tristructural isotropic (TRISO) spherical particles. The spherical particle includes several tiny kernels with a diameter around 0.5 mm made of either uranium oxycarbide or uranium dioxide with a maximum enrichment of 20%. The nominated thermal power is 600 MWth, Due to the high temperature produced by the reactor, hydrogen production industry might be a good application for this type of reactor in addition to the electricity production. A summary of some mentioned features can be found in Table 1-1

Table 1-1 Fourth Generation reactors

	Neutron spectrum	Coolant	Temperature °C	Fuel	Fuel cycle	Use
GFR	fast	helium	850	U-238 +	closed, on site	electricity & hydrogen
LFR	fast	lead or Pb-Bi	480-570	U-238 +	closed, regional	electricity & hydrogen
MSFR	fast	fluoride salts	700-800	UF in salt	closed	electricity & hydrogen
MSR	thermal	fluoride salts	750-1000	U02 particles in Prism	open	hydrogen
SFR	fast	sodium	500-550	U-238 & MOX	closed	electricity
SCWR	thermal or fast	water	510-625	U02	open (thermal) closed (fast)	electricity
VHTR	thermal	helium	900-1000	UO2 prism or pebbles	open	hydrogen & electricity

In addition to the previously mentioned types of generation VI reactors, dual fluid reactor (DFR) is a novel concept that can be considered as one of these types of reactors. The DFR concept will be described in the next sections in more detail.

1.4 Dual Fluid Reactor

1.4.1 Design Concept

The Dual Fluid Reactor (DFR) represents a novel and advanced nuclear reactor concept characterized by the implementation of two distinct liquid loops dedicated to fuel and coolant.

The DFR integrates the principles of molten salt reactors and liquid-metal cooled reactors, thus, it operates in a high temperature and fast neutron spectrum, presenting a distinct approach in the field of advanced nuclear reactor design. Departing from conventional molten salt reactors, the DFR employs a separated liquid lead loop to cool the molten fuel. This innovative configuration affords notable advantages, such as enhanced power densities and superior breeding ability.

Two fluid reactor concepts have been used previously in different designs, for example the Robertson's and MacPherson's designs[15], but in these designs the molten salt is classified as fissile fuel and a fertile blanket. However, the DFR separates the two loops according to the two functions: heat removal and heat production with fuel breeding.

Consequently, the utilization of liquid fuel containing a high concentration of actinides, combined with lead coolant, demonstrates a significant advantage of the Dual Fluid Reactor (DFR) in terms of achieving higher power density compared to other reactor designs. This advantage translates into potential benefits such as reduced core dimensions, increased efficiency, and lower overall construction and operational costs, heightened operational efficiency, and reduced construction and maintenance expenses. Additionally, the DFR has a significantly high energy return on investment (EROI) compared to the classical nuclear reactors, as well as other renewable sources of energy such wind and solar energies for example [16].

Furthermore, the Pyrochemical Processing Unit (PPU) [17], [18] is an optional system that can be integrated into a nuclear facility featuring the Dual Fluid Reactor with metal fuel (DFRm). The PPU serves the purpose of continuous removal of fission products and the introduction of fresh actinides derived from spent fuel, natural or depleted uranium, or thorium into the fuel cycle. However, considering the extended operational lifespan of the DFRm reactor utilizing U-Cr fuel, the inclusion of this component is presently not under consideration.

Based on the two concepts of the reactors mentioned (molten salt and liquid metal cooled reactors) there are two designs of the DFR currently in consideration: DFRm and DFRs. DFRm utilizes a eutectic metal fuel composed of chromium or nickel in combination with uranium or thorium. Whereas DFRs employ undiluted molten salts as fuel. The DFR design facilitates a breeding fuel cycle, whereby the core can be encompassed by fertile material to enable fuel production such as the conversion of ^{238}U to ^{239}Pu and ^{232}Th to ^{233}U. The fuel supply and reprocessing can occur online in the DFR by adding a distillation unit to the cycle. This is because of the very hard neutron spectrum – fission of transuranic isotopes.

Currently, two versions of the Dual Fluid Reactor (DFR) are being developed, namely DFRs and DFRm, which combine the concepts of molten salt reactors [19] [20] [21] and liquid-metal cooled reactors [22]. The primary distinction between these models lies in the type of fuel used. In DFRs, undiluted molten salts such as UCl3, ThCl3, or PuCl3 [23]–[25] can serve as fuel. Conversely, DFRm employs a eutectic metal fuel based on chromium (or possibly nickel) with uranium (or thorium) [26], [27]. With its fast neutron spectrum and high conversion ratio, DFR facilitates a breeding fuel cycle, wherein the core can be surrounded by fertile material to enable fuel production (e.g., production of 239Pu from 238U or 233U from 232Th). DFR also offers the possibility of on-line fuel reprocessing through distillation/rectification, although this feature is not exclusive to DFRm [28]. The DFRm concept is designed for a thermal power of 250 MWth.

The aforementioned characteristics of the Dual Fluid Reactor (DFR) and its two versions highlight that the DFR not only aligns with the Generation IV of reactors but also offers additional advantages surpassing those of conventional Gen IV reactors.

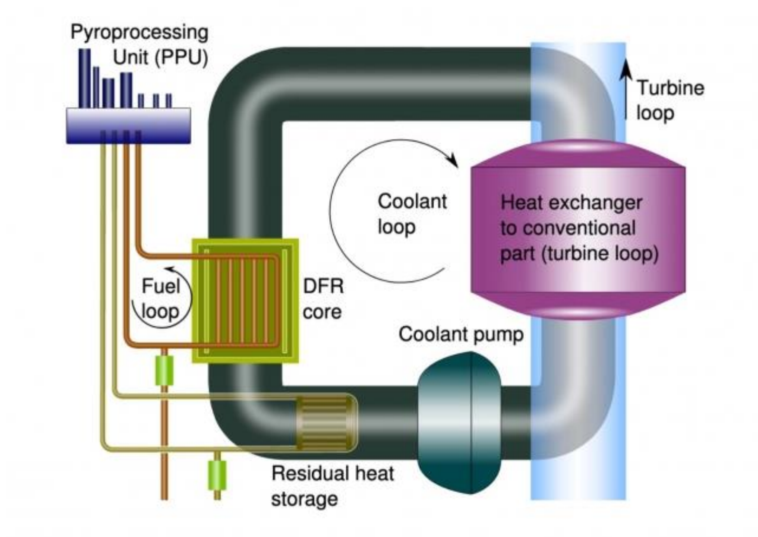

Figure 2 DFR schematic diagram

1.4.2 Operation Description

The core of the DFRm and DFRs is situated at the center of the reactor vessel and consists of numerous vertical fuel tubes where fission reactions occur. For instance, the DFRm core has around 1666 fuel tubes arranged in a hexagonal grid. These tubes connect the bottom and the top terminals of the core where the inlet and the outlet of the fuel are located, respectively. The fuel enters from the bottom going through the core where the fission reaction takes place and heat been generated. Then later exits the core from the top after an enormous amount of heat has been transferred to the coolant (liquid lead for instance). The volume of the fuel in the considered design is less than one cubic meter, which minimizes the total vessel size and compact the components and enhances safety.

The coolant (liquid lead) as well enters the core from the bottom parallelly to the fuel flow direction. The high temperature of the fuel is transferred to the coolant through the pipe wall which is made of SiC in the current design. The selection of silicon carbide (SiC) as the preferred material over other materials such as titanium carbide (TiC) and zirconium carbide (ZrC) is based on its favorable physical properties, specifically its excellent strength under high-temperature conditions. SiC exhibits desirable characteristics, it has a high thermal conductivity, low thermal expansion, and high hardness, even at such elevated operational temperatures. These features make SiC an excellent choice for applications requiring high strength materials capable of withstanding such very high thermal conditions.

In the current system, the heat absorbed by the coolant must be subsequently transferred to another medium through a distinct loop. This alternate medium is simply water, wherein water and liquid lead coexist within a heat exchanger to facilitate the necessary heat transfer for subsequent utilization. Both coolant and fuel are circulated with magnetohydrodynamic pump. Although the fuel circulation can possibly be only by natural convection, the existence of the pump is required for different operational scenarios, for example startup or shutdown where the pump will be required. Two safety plugs are to be installed at the pipes by the lowest elevation of the two loops (fuel and coolant), the plugs will be subjected to a quick melting allowing the fuel/coolant to leave the loops and evacuate the cycles in case of an unplanned extreme high temperatures occurrence cases [25], [26].

This kind of design leads to complex thermal and hydraulic phenomena that determine the safety of the reactor both in normal operation and transition scenarios. Utilizing liquid metals results in very low Prandtl numbers of the flow. Thus, they should be tested experimentally and described numerically using validated computer codes. The first step in this way would be the construction of a non-critical mini demonstrator possessing all the main features of the real reactor. The uniqueness of this design lies in the exceptionally high operating temperature and the ability to study heat transfer between two separated liquids. The design and thermal hydraulic analysis of such mini demonstrator of the DFR will be described and analyzed in detail in the next chapters.

2 Dual Fluid Reactor Mini Demonstrator (MD)

The planned experimental facility, known as the mini demonstrator, has been specifically designed to facilitate investigations into the DFR. This chapter will provide a concise discussion on the significance of employing an experimental approach in the design and licensing of a novel nuclear reactor concept. Furthermore, a detailed introduction will be presented, encompassing the MD cycle and core description, which will include the nominal dimensions and operational parameters.

2.1 Experiments Significance in Nuclear Reactor Pre-construction Stages

Like any novel reactor design, the objective is to subject the reactor to operational testing. Specifically, for fourth-generation reactors, such as the Dual Fluid Reactor which represents a relatively recent design concept, a substantial amount of research is indispensable. Although every country has its own regulations regarding reactor licensing, experiments are a common requirement in each country that adopts nuclear power generation recommended by IAEA[29]. Experiments are conducted not only for design purposes, but also as a licensing requirement in the licensing procedure. The mini demonstrator of the DFR is a planned facility to be constructed in the near future to perform several types of experiments, additionally, to be used in the licensing procedures of the DFR.

Planned experiments include -but not limited to- thermal hydraulics (heat transfer and velocity profiles) experiments, startup and shutdown procedures and methods, corrosion, MHD pump analysis, natural convection etc.)

In the next sub-sections of this chapter, the importance of experiments in designing and licensing a reactor will be briefly discussed. In a later section of this chapter, the mini demonstrator of the DFR will be described.

2.1.1 Experiments for Reactor Licensing

To be added to the theoretical evaluations, the experimental validations are a part of the licensing process of any reactor. The conducted experiments are expected to collect data, assure and evaluate the performance, safety and reliability of the reactor design and associated systems. These experiments help demonstrate compliance with regulatory standards, verify theoretical models, and ensure safe operation of the reactor under various conditions.

In the European union as an example, the experimental requirements were outlined as an obligatory requirement in the national legalization of each of the countries within the union, however, it must still have a harmonized approach towards the Euratom Treaty. Another example, the Nuclear Regulatory Commission (NRC) in the United States clearly specified in the Code of Federal Regulations (10 CFR) all the requirements of the changes to facility or procedures which may need conducting relative experiments including the nuclear-related facilities. Other countries have a similar approach whenever reactor licensing is considered.

Some examples of experiments conducted for licensing purposes include the LOFT experiment (Loss of Fluid Test) which was conducted in 1989 and intended to test the thermal hydraulics during loss of coolant LOCA in PWR. Another example is the PHEBUS FP experiment that was conducted in France by the Institut de Radioprotection et de Sûreté Nucléaire (IRSN) during the 90s in different experimental stages for the purpose of testing several severe accidents scenarios[30].

Undoubtedly, the inclusion of experiments as a mandatory requirement for licensing serves as a crucial cornerstone for ensuring the safe operation of reactors and stands as an imperative obligation for every prospective reactor seeking realization.

2.1.2 Experiments for Reactor Design

For a new reactor concept, the first design stage is the conceptual design, that's when the basic parameters and purposes are identified. In the subsequent stage known as the preliminary design stage the focus shifts towards further advancing the design and refining critical aspects such as the core configuration and the overarching system architecture. Later a detailed design stage is required to identify the specific components, structures, and systems, including control mechanisms, engineering analysis, etc. Later come the licensing and constructional stages, respectively. Experiments can be conducted at any of the mentioned stages; however, it is crucial during the preliminary and detailed design stages. The experiments assist in evaluating the behavior and performance of the main components, materials, and systems under different operating conditions. These experiments help in the selection and optimization of reactor parameters. Moreover, the execution of experiments assumes crucial significance in the validation of the models and codes utilized during the design phase, thereby augmenting the degree of confidence in the accurate representation of additional operational scenarios that may pose significant cost, time, or logistical constraints for physical experimentation.

Considering the progressive advancement of nuclear reactor technology, it is evident that a significant number of experiments have been undertaken in recent decades to address generation VI of nuclear reactors. Examples for these types of experiments are as follows: for **SFR:** PRISM (Power Reactor Innovative Small Modular) by GE Hitachi Nuclear Energy (USA), for **SCWRs:** the SCWR-500 by Rosatom (Russia). A MSFR (Molten Salt Fast Reactor) built by CNRS (France) and other international partners. Although the mentioned examples are usually critical experiments including the neutronics into the analysis, some other experiments are mainly addressing the thermal hydraulics and material testing, for example: **ACTEL** (Parallel Channel Test Loop) Experiment and **ATLAS** (Advanced Thermal-Hydraulic Test Loop for Accident Simulation) Experiment.

Regarding the DFR, the inclusion of a reactor mini demonstrator (MD) among the planned experimental facilities assumes significance. This MD facility is anticipated to offer a comprehensive scope for conducting thermal hydraulics analyses across a broad spectrum and exploring diverse operational scenarios of the reactor. Furthermore, it will play a pivotal role in validating models and facilitating the attainment of the necessary conformity with licensing procedures. The MD cycle and core will be discussed in the following sections.

There exists a significant correlation between the overall reactivity changes and localized fluctuations within the Dual Fluid Reactor (DFR) from one side and thermal hydraulic parameters from another side. One of the reasons is the thermal expansion of the utilized fluids as the DFR has a negative temperature coefficient of reactivity[31]. This neutronic-thermal hydraulic coupling plays a pivotal role in the system. The mini demonstrator (MD) offers valuable insights into the thermal expansion characteristics of liquid lead and other potential molten metals, if employed, enabling these behaviors, and observed parameters to serve as input data for coupling techniques.

2.2 The Mini Demonstrator Components and Operation

The mini demonstrator consists of multiple pipes and a vessel, arranged in a specific order to acquire a required role. The MD serves as a simplified demonstrator of the dual fluid reactor thermal hydraulics. It has been designed to investigate the flows behavior and heat removal from the fuel to the coolant regions.

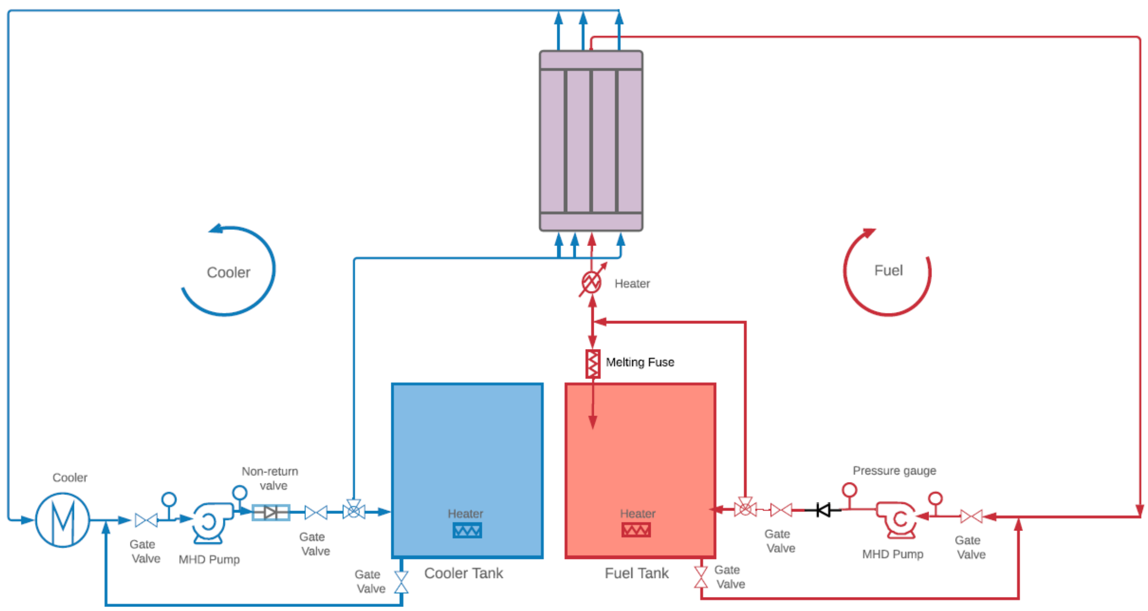

Figure 3 Mini Demonstrator Schematic diagram

The metallic version of DFR consists of two loops, namely, Uranium-Chromium eutectic loop (called fuel loop) and molten lead loop (called coolant loop). However, for a thermohydraulic testing facility, a fission reaction is not required when testing the general flow and heat transfer behaviors, and fission reaction as a source of heat, can be replaced by other means. Additionally, due to the essential strict precautions required to include U-Cr as a radioactive substance in the MD, any radioactive material has been excluded from the facility design. The MD was designed using two molten lead loops, one of them at an elevated temperature compared to the other. In this thesis, within the context of the MD discussions, the molten lead in the higher temperature will be often referred to as “fuel” while the molten lead with the lower temperature will be referred to as “coolant”.

For this type of facility, several systems need to be carefully installed, this includes cooling system (oil/water/air), control system, also proper temperature insulation, etc. However, such full details of the cycles will come in the details design stage which is beyond the work presented in the thesis in hand. As for the preliminary cycle components, it includes two tanks, one for fuel and the other for coolant. Three main heaters, one is installed in the fuel tank and the second in the coolant tank, the third heater is dedicated to the fuel entering the core. Two magnetohydrodynamic pumps, each of them is dedicated to the molten lead in each loop. A heat exchanger (cooler) is attached to the coolant side for reducing its the temperature. Several arrangements of valves were introduced to the design for the purpose of disassembling and control. Two melting plugs are located by the lowest elevation of each loop. Measuring devices like thermocouples, pressure gauges, flow meters, ultrasonic velocity profile measuring devices, etc.

The MD startup is initiated by heating the full body of the facility to temperature above the melting point of the lead (327 °C) to avoid lead solidification at any location in the loops. In the current design the two pumps then start pumping the molten lead into the already heated pipes. However, a different design for the fuel loop may consider using a pressurized inner gas (for example helium) to force the fuel into the pipes. Using the valves control, the coolant will then be directed to the core entrance after from the bottom side and exiting from the upper one. Similarly, the fuel will go through the same except that it must pass by its dedicated heater right before entering the core to add a reasonable temperature to the lead so that a noticeable heat transfer between the two loops in the core can be observed. The core description will be shown in the next section. Once both the coolant and the fuel exist the core, the coolant enters the cooling heat exchanger to lose back the heat gained in the core, and continue the cycle once more, while the fuel is directed to the core, once more through the dedicated heater. In the case of shutting down the facility, the molten lead is allowed to be collected again in the storage tanks via gravitational force and valves control.

2.3 Mini Demonstrator Core Description

The core of the mini demonstrator (MD) is constructed in the form of a cylindrical vessel, featuring three distinct zones: the distribution zone, the middle core zone, and the collection zone, arranged in a bottom-to-top order. In terms of fuel circulation, there are two inlets located at the bottom of the core, entering from the lateral side, with a flow direction perpendicular to the longitudinal axis of the MD. The fuel exits from the corresponding terminal in the opposite direction of the inlet. As for the coolant, it enters vertically in parallel with the longitudinal axis of the MD and exits from the top in the same direction Figure 4.

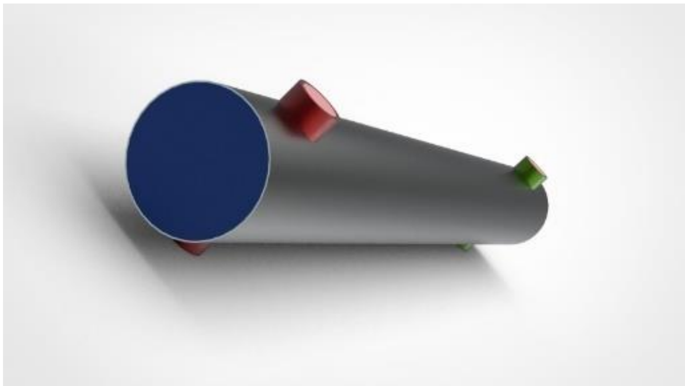

Figure 4 The mini demonstrator core vessel

The MD core vessel accommodates 12 coolant pipes in the distribution zone, the same number of coolant pipes in the collection zone, and 7 fuel pipes in the middle core. Two inlets and two exits for fuel, a single inlet and single exit for coolant. Figure 5 Figure 6. As the collection and distribution zones are identical geometrically, the zoomed in figures might show only the collection zone in the below figures unless else is mentioned in the legend.

Figure 5 Fuel and coolant domains without vessel casing (brown is fuel, blue is coolant)

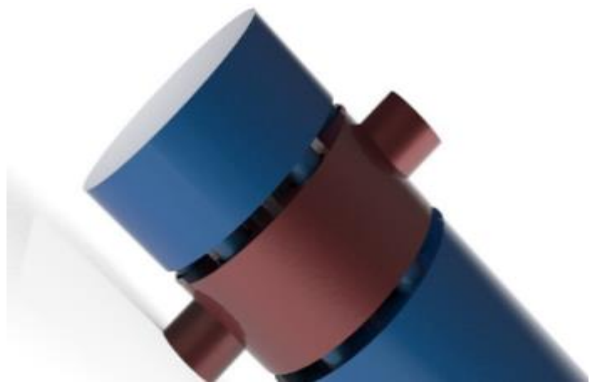

Figure 6 Collection zone showing fuel two exits, coolant single exit, and coolant pipes.

In Figure 7 and Figure 8, only the blue coolant is shown without the fuel or casing. The coolant flow enters from the bottom of the MD to be distributed in 12 pipes with two different diameters. The coolant is then discharged into the middle core zone to surround the fuel pipes. The coolant exits the middle core zone to identical 12 pipes to those by the inlet and then exists the MD core from the top.

Figure 7 Full coolant domain

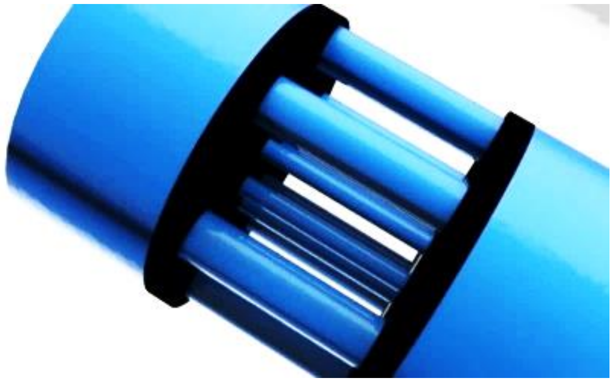

Figure 8 Coolant domain in the collection zone

The fuel domain enters as well from the bottom of the MD through two inlets opposite to each other as shown in Figure 9 and Figure 10. In the distribution zone (at the bottom) the fuel surrounds the coolant pipes (coolant pipes shown in Figure 8) before it exits to the fuel pipes along the whole core length.

Figure 9 Full fuel domain

Figure 10 Fuel domain in the collection

To show the details inside the distribution and collection zones, both fuel and coolant domains are quarterly sliced and shown in Figure 11 and Figure 12, The fuel in the reddish color enters to the distribution zone to surround the coolant pipes as described earlier. A similar arrangement is as well in the collection zone.

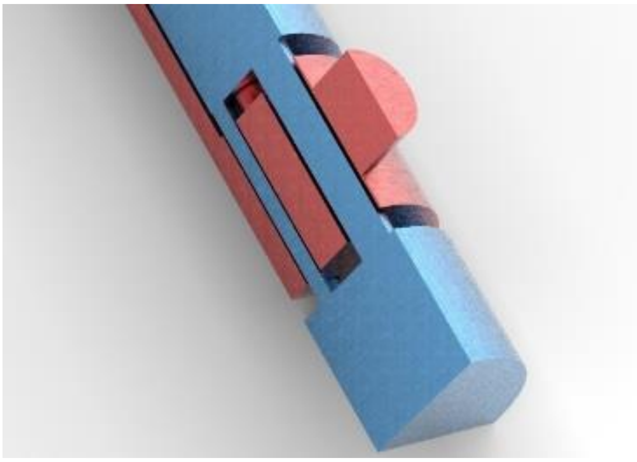

Figure 11 Distribution zone (quarterly sliced), blue color represents the coolant, red represents the fuel.

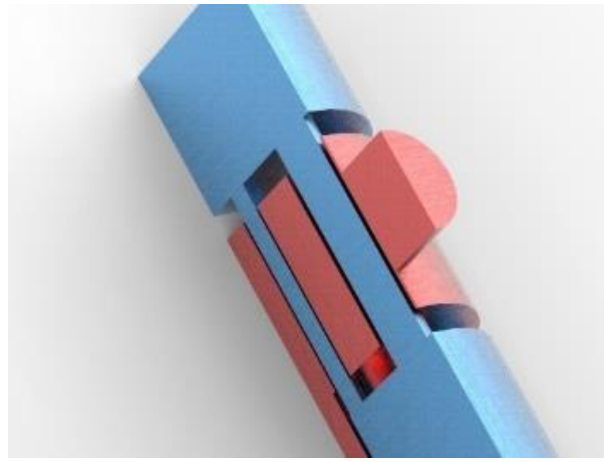

Figure 12 Collection zone (quarterly sliced), blue color represents the coolant, red represents the fuel.

The dimensions of the fuel pipes were taken from the DFR fuel pipes dimensions to have a close heat transfer behavior. Other dimensions were decided accordingly to match the general arrangement and the required facility size. Table 2.

Table 2 Dimensions of the DFR mini demonstrator core

Parameter	Values
Outer Diameter of MD (mm)	133
Inner Diameter of MD (mm)	130
Length of the MD in axial direction (mm)	880
Distribution zone height (mm)	70
Collection zone height (mm)	70
Number of fuel pipes	7
Number of large-diameter coolant pipe	6
Number of small-diameter coolant pipe	6
Fuel pin pitch (mm)	28
Outer/inner diameters of fuel pipes (mm)	23/19
Outer/inner diameters of large-diameter coolant pipes (mm)	23/19
Outer/inner diameter of small-diameter coolant pipes (mm)	10/8

In this chapter, the significance of the DFR mini demonstrator as an experimental facility was elucidated, considering its licensing, and designing implications for the DFR as an innovative reactor concept. Furthermore, the technical preliminary schematic of the loops and cycle, along with their constituent elements, as well as the core dimensions and particulars, were presented. The subsequent chapter will introduce the importance of computational fluid dynamics analysis for similar facilities and provide an overview of the fundamentals of turbulence modeling.

3 Computational Fluid Dynamics and Turbulence Modelling

This chapter provides a concise overview of computational fluid dynamics (CFD) in the context of this thesis, including the methodologies and models employed. The relevance of CFD modeling in nuclear reactor design will be emphasized, followed by an elucidation of direct numerical simulations and large eddy simulations. Furthermore, the Navier-Stokes equations and the utilized RANS models (K- ω and K- ω SST) will be introduced, accompanied by an explanation of their mathematical foundations. Lastly, the criteria for modeling low Prandtl number fluids will be discussed.

3.1 Brief Introduction to Computational fluid dynamics (CFD)

Computational Fluid Dynamics (CFD) is a computational tool widely used in engineering and scientific research to study fluid flow and related phenomena. It provides a numerical approach for solving the governing equations of fluid motion and allows for the simulation and analysis of complex flow behavior in various applications.

CFD has proven to be invaluable in investigating fluid dynamics in a wide range of fields, including aerospace, automotive, energy, environmental and nuclear engineering. It offers the ability to analyze fluid behavior, such as velocity, pressure, temperature, and turbulence, with high accuracy and efficiency. By using computational algorithms and numerical methods, CFD enables researchers to gain insights into the intricate details of fluid flow that are often difficult or impossible to obtain through experimental means alone.

One of the key advantages of CFD is its ability to simulate and visualize flow phenomena in a virtual environment, providing a cost-effective and time-saving alternative to physical experiments. It allows engineers and scientists to evaluate the performance of existing designs, optimize new designs, and explore different scenarios without the need for extensive prototyping or costly testing procedures.

In CFD simulations, the governing equations of fluid motion, known as the Navier-Stokes equations, are solved numerically. These equations describe the conservation of mass, momentum, and energy in the fluid domain. Direct numerical simulation (DNS) provides a detailed and comprehensive representation of fluid flow by directly solving the governing equations. To account for turbulent flow, various turbulence models, such as Reynolds-averaged Navier-Stokes (RANS) models or large eddy simulation (LES) models, can be employed to capture the effects of turbulence on the flow behavior.

CFD simulations involve the discretization of the fluid domain into a computational grid or mesh, where the governing equations are solved at discrete points. This numerical approach allows for the computation of flow variables at different locations and times, enabling the visualization and analysis of flow patterns, forces, and heat transfer characteristics.

In this thesis, CFD will be utilized as a tool to investigate and analyze fluid flow phenomena in the context of the DFR mini demonstrator. By employing appropriate numerical methods and models, the behavior of fluids within the MD will be explored, contributing to a deeper understanding and potential improvements in DFR design.

3.2 CFD Modelling for Nuclear Reactors Design

The design and operation of nuclear reactors necessitate a deep understanding of fluid dynamics, heat transfer, and related phenomena to ensure optimal performance, safety, and efficiency. CFD has emerged as an indispensable tool in the field of nuclear reactor design, enabling engineers and scientists to simulate and analyze the complex behavior of coolant fluids within the reactor system. This section highlights the importance of CFD in nuclear reactor design by elucidating its role in addressing critical design challenges, optimizing reactor performance, and ensuring the safe operation of nuclear power planets.

3.2.1 Realizing fluid Dynamics Phenomena

CFD plays a pivotal role in predicting and analyzing the behavior of coolant and fuel fluids within nuclear reactors. Through the utilization of advanced numerical algorithms and discretization techniques, CFD models accurately solve the governing equations of fluid flow and heat transfer, enabling detailed predictions of flow patterns, pressure distributions, temperature profiles, and turbulence characteristics. Considering molten fuel reactor designs, the fuel has as well been analyzed using CFD methods for the same mentioned reasons. This capability empowers engineers to gain insights into complex fluid dynamics phenomena, such as flow separation, recirculation zones, and fluid mixing, crucial for optimizing reactor design and performance.

3.2.2 Evaluation and Optimization

CFD provides a powerful means of evaluating and optimizing the performance of reactor components. By simulating fluid flow and heat transfer within fuel assemblies, coolant channels, heat exchangers, and other critical components, engineers can assess the impact of design modifications on reactor efficiency, core cooling, and safety margins. CFD simulations facilitate the exploration of various design alternatives, operating conditions, and parameter optimizations, enabling informed decisions to be made without the need for costly and time-consuming physical prototypes.

3.2.3 CFD Models Validation

The validation of CFD simulations against the future experimental data and analytical solutions are crucial to establish confidence in the accuracy and reliability of the models. Through rigorous benchmarking exercises, CFD predictions can be compared against well-documented experimental results, ensuring that the models effectively capture the physical phenomena within the reactor system. This validation process enhances the credibility of CFD simulations and provides assurance that they are robust tools for predicting fluid behavior and guiding reactor design decisions.

3.2.4 Addressing Thermal-Hydraulic Challenges

Thermal-hydraulic issues, such as anisotropic coolant distribution, vibrations caused by the flow, and localized temperature variations, can significantly impact the safety and performance of nuclear reactors. CFD simulations provide to engineers and scientists with trustworthy methods to identify and mitigate such challenges through offering insights into flow characteristics, pressure losses, and heat transfer distributions. By optimizing coolant flow patterns and component designs, CFD contributes to the prevention of flow instabilities, hotspots, and potential equipment failures, ensuring safe and efficient reactor operation.

CFD is a crucial tool used to understand and analyze the flow as well as validating the used models which allows the use of such models to explore better designs of the reactor and to test the flow behavior in different conditions. Some of these conditions could be fatal or destructive if intentionally created experimentally, especially in the case of nuclear reactors. The following sections in this chapter will provide basic theoretical background of CFD and turbulence models that have been employed in this thesis.

3.3 Turbulence and Modelling

Several definitions for turbulence had occurred during the last century, one of the first definitions was in 1937 by von Karman:

“Turbulence is an irregular motion which in general makes its appearance in fluids, gaseous or liquid, when they flow past solid surfaces or even when neighboring streams of the same fluid flow past or over one another”

Although Turbulence is difficult to define, there are some main features that can usually lead to its understanding namely, Chaoticity, Irregularity, Rotationality, Diffusivity, Continuity and Dissipation.

The chaoticity and the change of the flow patterns in turbulent flows appears stochastic, however, the turbulent flow is still a deterministic solution of the Navier-Stokes equations, devoid of any inherent stochastic terms.

The irregularity of the turbulence comes from the complicated nonlinear interactions among the multitude of vortices and eddies overrunning a wide range of different scales within the flow field. Due to the complexity of the turbulence, statistical treatments are approached rather than deterministic treatments.

Rotationality occurs in turbulence due to the presence of vortices and swirling motions within the flow, which result from the complex interactions between velocity gradients, pressure fluctuations, and the formation of turbulent eddies in three-dimensional manner.

The diffusivity of turbulence is mainly coming from the turbulent mixing caused by the random motion of fluid molecules. This mixing results from the interactions between various scales of turbulent vortices, which lead to the spreading of momentum, heat, and other scalar quantities within the flow. The diffusivity of turbulence enhances energy and mass transfer which is crucial in many engineering and physical processes.

The continuity of turbulence is due to the uninterrupted motion, as the irregular behavior continues within the whole flow field without any boundaries or discontinuities.

Dissipation is an important characteristic of turbulence since it represents the transformation of the kinetic energy in the flow field into thermal energy using viscous impacts. In the case of turbulence, the energy is converted from larger scales to smaller ones, leading to a cascade of energy from larger to smaller ending by the dissipation scale sizes.

3.3.1 Navier Stocks Equations

In 1822, Claude-Louis Navier formulated the first set of partial differential equations that had been expanded 20 years later by Sir George Gabriel Stokes. The equations were derived from the conservation principles of mass, momentum, and energy. While there are two commonly used versions of the equations for incompressible and compressible flow, this thesis will include solely the incompressible flow formulation, as the compressible flow aspect cases are beyond the scope of this study.

The equations as defined by the two scientists are as following:

Firstly the continuity equation; since the equation is set for incompressible fluids, a constant density is then assumed, and the continuity equation takes the form as below for one dimension steady-state condition:

$$\frac{\partial u_i}{\partial x_i} = 0 \tag{3.3.1}$$

Secondly the momentum equation: the equation provides insights into the behavior of fluid flows by relating the changes in velocity to the various forces affecting the fluid and for one dimensional incompressible fluid case it can be written as below:

$$\frac{\partial u_i}{\partial t} + u_j \frac{\partial u_i}{\partial x_j} = -\frac{1}{\rho}\frac{\partial p}{\partial x_i} + \nu \frac{\partial^2 u_i}{\partial x_j^2} \qquad 3.3.2$$

Thirdly the energy equation: it relates the changes in energy to the flow properties and energy transfers within the fluid, and it takes the below form:

$$\frac{\partial T}{\partial t} + u_j \frac{\partial T}{\partial x_j} = \frac{\nu}{\mathrm{Pr}}\frac{\partial^2 T}{\partial x_j^2} \qquad 3.3.3$$

Pr is Prandtl number (see 3.3.13)

3.3.2 Direct Numerical simulation DNS

The main difference between Direct Numerical Simulation (DNS) simulation and other used techniques is obviously readable in the name. Simulation in DNS is by definition the replicating of the exact behavior of the turbulence phenomena. While modelling is presenting an approximation of the actual turbulence behavior.

DNS is a computational method used for simulating fluid flow at high resolutions using Navier Stokes equations without any turbulence modeling. It is a technique that has been developed and utilized by various researchers in the field of CFD.

DNS is a result of advancements in computer hardware and numerical algorithms, which have enabled researchers to solve the governing equations of fluid flow (Navier-Stokes equations) at a very fine scale, capturing the smallest turbulent structures. The development and application of DNS can be attributed to numerous scientists and engineers who have contributed to the field of computational fluid dynamics over the years.

The concept of DNS can be traced back to the early work of researchers like Lewis Fry Richardson and Robert Richtmyer, who made significant contributions to numerical methods for solving fluid flow equations. However, the development and widespread use of DNS as a specific technique for simulating turbulence can be credited to a collective effort by researchers from various institutions and organizations around the world.

As DNS has evolved and been refined over time, numerous researchers, and research groups, including those from academic institutions, national laboratories, and industry, have made significant contributions to its development. They have improved the numerical algorithms, developed efficient parallel computing strategies, and applied DNS to a wide range of turbulent flows.

However, DNS has some limitations due to its high computational cost. The direct resolution of all scales of motion requires fine grids and small time-steps, which can be computationally demanding, especially for high Reynolds number flows. As a result, DNS is typically restricted to academic research and simulations of relatively simple geometries and flow configurations.

Some DNS results have been included and implied in this thesis for the reason of model validation, which will be discussed in the next chapter.

3.3.3 Large Eddy Simulation LES

As the biggest limitation of the DNS simulating method is the high computational cost which usually requires a long time to obtain the required results, Large Eddy Simulation (LES) modeling method is following the same approach except for the smaller energy scale.

The flow field is here divided into resolved and modeled scales. The large scales of motion, which contain the dominant energy-containing eddies, are resolved explicitly using a grid with sufficient resolution. On the other hand, the smaller scales, which are responsible for energy dissipation, are not resolved explicitly due to their high computational cost. Instead, they are modeled using sub-grid-scale (SGS) models.

The resolved scales in LES capture the large-scale flow structures and turbulent motions, providing detailed information about their evolution and interaction. The smaller, unresolved scales are modeled based on turbulence models or closure schemes that account for their effects on the larger scales. The SGS models in LES aim to capture the energy transfer from the resolved scales to the unresolved scales, and accurately represent the turbulent mixing and dissipation.

LES is particularly suited for flows where large-scale coherent structures play a significant role, such as in turbulent boundary layers and shear flows. Compared to DNS, LES provides good results accuracy and with relatively affordable computational cost. However, LES is still computationally demanding and requires careful grid resolution and selection of appropriate turbulence models to achieve accurate results.

Some specified LES results have been used in this thesis for validation reasons in addition to the DNS data.

3.3.4 RANS models

By separating the mean flow from turbulent fluctuations, RANS (Reynolds averaged Navier-Stokes) modelling methods were obtained. Since the flow variables are divided into two categories, mean and fluctuating, the time averaged Navier-Stokes equations together with some other models are resolved to provide information about the mean flow parameters.

The fluctuations are modelled using several possible models that have been invented by scientists in the past years. Examples of these types of models are K-ε model[32], K- ω model[33], K- ω SST model and Reynolds stress model (RSM). These models are able to provide the closures as well as some other quantities related to turbulence which cannot be directly solved using the time-averaged equations.

Not resolving the full turbulences scales makes the RANS as a modelling method much less expensive (computationally) than both DNS and LES, which allow a handy and quick modelling method available for scientists and especially for engineers in industrial applications where time is an important aspect to consider, while only a reasonable accuracy is sufficient.

However, the limitations of RANS models are coming from the fact they are built on assumptions and closures. The choice of the turbulence model is heavily affecting the accuracy of the modelling results and decides whether the model can be used for good accuracy, can be used with low accuracy or even not valid entirely. This is because some RANS models might struggle capturing turbulence features in complicated flow parameters and geometry.

In the next sub-sections one of the RANS models that has been used in the thesis will be discussed briefly.

3.3.4.1 K- ω SST model

The k-omega Shear Stress Transport (SST) model, introduced by Menter [34], integrates the favorable aspects of two eddy-viscosity turbulence models, namely the k-epsilon and k-omega models. The model begins with the transformation of the standard k-epsilon model into the k-omega formulation through the $\epsilon = \beta^{*} k\omega$. This transformation introduces an additional cross-diffusion term in the omega equation. A similar cross-diffusion term is also present in the latest version of the k-epsilon model [33].The equations of the Shear Stress Transport model are derived by interpolating the transport equations of the original k-epsilon model [35] with the transport equations of the transformed standard k-omega model [36], utilizing:

$$\phi = F_1\phi_1 + (1 - F_1)\phi_2 \qquad 3.3.4$$

The subscripts 1 and 2 in Φ represent the terms corresponding to the original and transformed k-epsilon models, respectively. The function F1 is designed to have a value of unity near the wall and zero away from the wall. Consequently, the original formulation of the k-epsilon model remains effective in the near-wall region, while the transformed standard k-epsilon model is influential in the freestream region.

The transport equations for the turbulent kinetic energy k and the specific dissipation rate ω of the k- ω SST model [37] are:

$$\frac{D(\rho k)}{Dt} = P_k - \beta^* \rho k \omega + \frac{\partial}{\partial x_j}\left[(\mu + \widetilde{\sigma_k} \mu_t)\frac{\partial k}{\partial x_j}\right] \qquad 3.3.5$$

$$\frac{D(\rho \omega)}{Dt} = \frac{\tilde{\alpha}}{\nu_t} P_k - \tilde{\beta} \rho \omega^2 + \frac{\partial}{\partial x_j}\left[(\mu + \widetilde{\sigma_\omega} \mu_t)\frac{\partial \omega}{\partial x_j}\right] + 2(1 - F_1)\sigma_{\omega 2}\frac{\rho}{\omega}\frac{\partial k}{\partial x_j}\frac{\partial \omega}{\partial x_j} \qquad 3.3.6$$

The term of production is

$$P_k = \mu_t \hat{S}^2 \qquad 3.3.7$$

The dynamic turbulent viscosity is defined by

$$\mu_t = \frac{\rho a_1 k}{max(a_1 \omega, \hat{S} F_2)} \qquad 3.3.8$$

where $a1$ is the model constant in equation 3.3.8 contains the stress limiter, similar to the stress limiter of the $k - \omega$ model[38]. $F1$ and $F2$ functions are construed as

$$F_1 = \tanh\left(\arg_1^4\right) \text{ where} \qquad 3.3.9$$

$$\arg_1 = min\left[max\left(\frac{\sqrt{k}}{\beta^* \omega y}, \frac{500\mu}{\rho y^2 \omega}\right), \frac{4\rho\sigma_{\omega 2} k}{CD_{SST} y^2}\right]$$

$$CD_{SST} = max\left(\frac{2\rho\sigma_{\omega 2}}{\omega}\frac{\partial k}{\partial x_j}\frac{\partial \omega}{\partial x_j}, 1.0e^{-10}\right) \text{ and} \qquad 3.3.10$$

$$F_2 = \tanh\left(\arg_2^2\right) \text{ where } \arg_2 = max\left(2\frac{\sqrt{k}}{\beta^* \omega y}, \frac{500\mu}{\rho y^2 \omega}\right) \qquad 3.3.11$$

The boundary conditions for turbulent kinetic energy and specific dissipation rate at the walls are prescribed in accordance with [39] ,as follows:

$$k_{\text{wall}} = 0, \omega_{\text{wall}} = 10 \frac{6\nu}{\beta_1 (\Delta y)^2} \tag{3.3.12}$$

The distance between the nearest cell center to the wall and the wall itself is denoted by Δy. Table 3 provides a summary of the closure coefficients for the k-omega Shear Stress Transport (SST) model [39].

Table 3: Closure coefficients for K-omega SST model

a_1	α_1	α_2	β_1	β_2	β^*	σ_{k1}	σ_{k2}	$\sigma_{\omega 1}$	$\sigma_{\omega 2}$
0.31	0.556	0.44	0.075	0.083	0.09	0.85	1	0.5	0.856

3.3.5 Low Prandtl Flow modelling

Prandtl number is a dimensionless number defined as the ratio between the kinematic viscosity (v) and the thermal diffusivity (α) of a fluid. It was named after the physicist "Ludwig Prandtl" in the early 20th century.

$$\mathrm{Pr} = \frac{\nu}{\alpha} = \frac{\text{momentum diffusivity}}{\text{thermal diffusivity}} = \frac{\mu/\rho}{k/(c_p \rho)} = \frac{c_p \mu}{k} \tag{3.3.13}$$

Where C_p is the heat capacity, μ is the fluid viscosity, and k is the thermal conductivity.

Excluding DNS and LES methods, when modelling fluids with Prandtl number that is more than unity (Pr >1) RANS models show very reasonable accuracy in capturing the correct behavior and features of the turbulent flow if the correct model has been chosen to best match the studied case. However, when Pr number is much lower than unity, then in this case the model accuracy can be easily affected, and accuracy deviations are then observed. By definition, this type of fluid (low Pr fluids) has a higher thermal diffusivity compared to their momentum diffusivity, which results in a larger thermal boundary layer than that for the momentum Figure 13. Pr number for molten metals can be as low as 0.01 or even less in some cases. Several efforts have been elaborated in the recent past to approach better accuracy using Reynolds analogy models as a common base for further improvements.

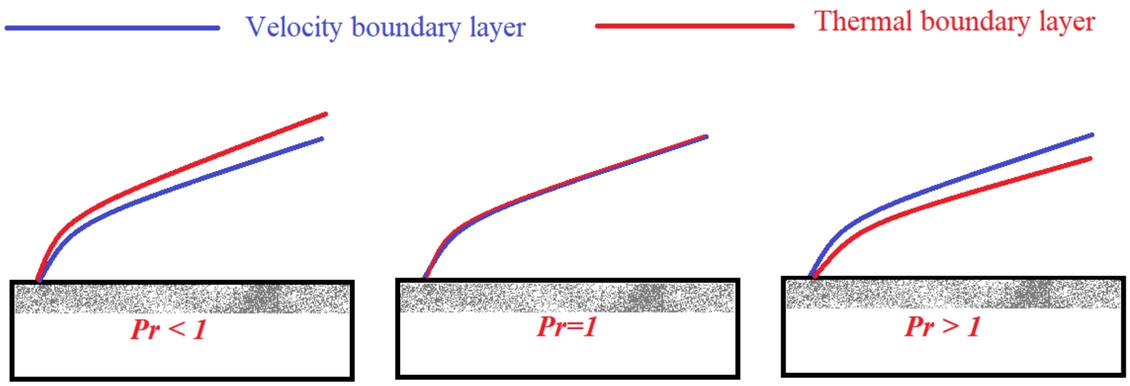

Figure 13: Velocity and thermal boundary layers in different Pr number ranges

Although modelling turbulence is well known as a challenge, modelling low Pr fluids is even a more difficult challenge due to the lack of such especially tailored models for this type of fluids specifically. The interest in the low Pr flows was gradually increasing in the past decades due to the future perspective of nuclear reactor concepts known as Generation VI reactors (Section 1.1). A comprehensive review effort about low Pr turbulent modelling challenge has been discussed in several literatures[40].

In the 1970s and earlier, a significant amount of experimental data was collected to study heat transfer in low Prandtl number fluids, particularly in molten metal systems[41]. These experiments focused on specific geometries, such as rod bundles, and resulted in the development of correlations to estimate heat transfer characteristics [42]. With the current achieved improvements in the numerical methods as well as the computational technologies, the numerical simulations are now essentially considered and should be accurate to rely on when trying to validate any modelling approach in relation to the low Pr number fluids issue.

When modelling a molten metal, from a CFD perspective it is important to increase confidence in the currently well-known models by comparing these data to the experimental ones or other numerical accurate data sets like DNS or LES.

Another approach is to come up with a new model that captures the turbulence features with reasonable accuracy. Some recent work was found to be a combination of the two approaches. Based on introducing an additional transport equation to a Re analogy model, returning a new model that is more accurate than simply using a RANS model. Despite the complications of such an approach, it fits more to the natural and mixed convection flow regimes.

Within this thesis, all examined scenarios, both globally across all cases and locally within each individual case, exhibited a distinct forced convection behavior. The corresponding Richardson number for these flows was found to be on the order of magnitude close to zero (Ri = 10^{-6} – $10^{-9)}$, indicating the dominant influence of externally imposed forces and negligible impact of buoyancy forces. Hence, the modelling in this work is based on Reynolds analogy model (K- ω

SST model) but with a variable turbulent Prandtl number taken from the corresponding correlations. The validation of this model in the next chapter will be based on the experimental data in addition to the DNS and LES data sets.

4 Model Validation

4.1 RANS Model and Turbulent Prandtl Number

In the context of this research, the Standard-Gradient Diffusion Hypothesis (SGDH) model has been utilized. However, the constant turbulent Prandtl number (Pr_t) employed in the model, which typically falls below 1, has been modified based on variations in the turbulent Peclet number Pe_t.

$$Pe_t = \frac{v_t}{v} Pr \qquad \text{(Turbulent Peclet number)} \quad 4.1.1$$

$$Pr_t = \frac{v_t}{\alpha_t} \qquad \text{(Turbulent Prandtl number)} \quad 4.1.2$$

Where v is molecular kinematic viscosity, v_t is the turbulent kinematic viscosity and α_t is turbulent heat diffusivity.

The value of Pr_t is significantly affected by the molecular Prandtl number, particularly in the case of fluids characterized by extremely low Prandtl numbers, such as liquid metals. Furthermore, the distance from the wall also plays a role in determining the turbulent Prandtl number, leading to an increase in Pr_t near the wall. This heightened Pr_t near the wall assumes particular significance for fluids with high Prandtl numbers due to the presence of an extremely thin thermal boundary layer.

Generally, the relation between the Pr_t and Pr is observed as below:

$$Pr_t \leqslant 1 \qquad \text{for} \quad Pr \geqslant 1 \text{ (gases and liquids)}$$

$$Pr_t \gg 1 \qquad \text{for} \quad Pr \ll 1 \text{ (liquid metals).}$$

Several numerical simulations of turbulent heat transfer in liquid metals have been conducted. A remarkable work was that made by Kawamura et al. and Abe et al., which showed interesting outcomes for different Reynolds numbers and low Prandtl numbers (Re_τ as high as 1020 and Pr_t as low as 0.025). Other studies used a different code (spectral codes) to conduct a DNS simulation for several different Re_τ with a Pr=0.01. an overview for some of these studies were gathered by Grotzbach [40]. The noticeable outcome of all those studies was that the classical Reynolds analogy is no longer holding true when it comes to low Pr number conditions. That is because these models have the turbulent Prandtl number and the near-wall function both based on the similarity between the temperature field and the velocity field, which doesn't apply in the case of the low Prandtl fluids.

The effective turbulent heat diffusivity is the main essential parameter to determine in RANS modelling if used for low Pr fluids. In RANS models, when modelling heat transfer (the energy equation activated), the available eddy viscosity values from the turbulence model allows the use of Pr_t.

Despite the low Pr fluids, the usual approach is to use Pr_t less than -but close to- unity (typical value = 0.85). However, in the case of the low Pr fluids, results obtained using DNS simulations have clearly shown that for this type of fluid condition the Pr_t is more than unity.

As the turbulent Prandtl number Pr_t is strongly dependent on the molecular Prandtl number Pr and the distance from the wall, efforts have been made to predict the dependability parameters and establish a model or a correlation that can fit in the low Prandtl number flow issue. These efforts were based on conducting experiments and analyzing the experimental data obtained [43]–[45]. One of the most remarkable correlations is the correlation made by Kays[46]

Kays proposed the below empirical correlation that allows to achieve a variable Pr_t depending on the Pe_t variation.

$$Pr_t = 0.85 + \frac{0.7}{Pe_t} \qquad 4.1.3$$

Figure 14 below illustrates the above correlation made by Kays.

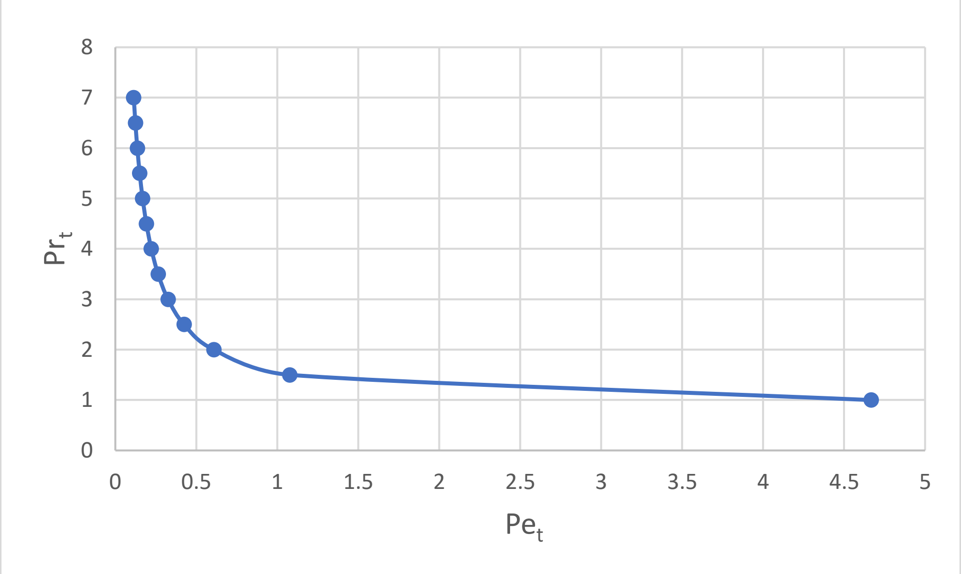

Figure 14: Variation of turbulent Prandtl number Pr_t with Peclet number Pe_t in Kays correlation

Weigand B [47] has extended Kays correlation adding the effect of Reynolds number into the correlation to provide the local and global flow parameters:

$$\frac{1}{Pr_t} = \frac{1}{2Pr_{t\infty}} + CPe_t \frac{1}{\sqrt{Pr_{t\infty}}} - (CPe_t)^2 \left[1 - \exp\left(-\frac{1}{CPe_t\sqrt{Pr_{t\infty}}}\right)\right] \qquad 4.1.4$$

Where C = 0.3, while $\mathrm{Pr}_{t\infty}$ is calculated using the following equation:

$$Pr_{t\infty} = 0.85 + \frac{100}{\mathrm{Pr}\ Re^{0.888}} \qquad 4.1.5$$

M. Duponcheel et al. [48] compared both Weigand and Kays correlations and obtained that Weigand correlation showed a better result for Pr_t with respect to the near-wall profile than Kays correlation in the high Re_τ (Re_τ =2000 and Pr = 0.01). Nevertheless, the good results of Weigand correlation near-wall accuracy have been lowered because the correlation did not follow the LES Pr_t values very close to the wall where the sharp peak occurs. Additionally, Weigand correlation showed over estimation to the values of Pr_t in the channel where the parameters of the bulk flow are different.

The significance of the correlations is relatively low in the viscous-sublayer where turbulent viscosity approaches zero (see equation (Turbulent Prandtl number) 4.1.2). This is because in this region, heat transfer is primarily influenced by molecular effects rather than turbulence.

However, the same study found that the best results was that obtained from Kays correlation giving the best Pr_t values specially for $y^+ \gtrsim 100$ in the bulk of the flow. Due to the simplicity of this correlation, as well as the accuracy, it has been chosen for calculations. In this work, the modelling will be based on the Standard Gradient Diffusion hypothesis (SGDH) and the value of Pr_t will be calculated using Kays correlation.

To be able to use the Kays correlation in the modelling in this thesis, the reliability of the model had to be tested and validated to increase the confidence in the model. The following section will show the validation strategies and the validation results.

4.2 Validation strategy

Validation is an important process used to assess the accuracy and reliability of CFD modelling by comparing the results obtained by the used models against experimental or analytical data. Another possible method of validation is instead of using experimental data, one can use a more accurate model results - usually computationally expensive - for example LES, or a numerical simulation method like DNS. The primary goal of validation is to increase confidence in the numerical models and computational techniques employed in CFD simulations.

In this work, the validation was established on three pillars based on the chosen data and experiments. The combination of these three pillars instills trust and confidence in the chosen model for the calculations. The first pillar is validating the model resulted dimensionless velocities against DNS data. The second pillar is the validation of the model resulted dimensionless temperature against LES data, and finally the third pillar is validation of temperature field against the experimental data. The next subsections will be dedicated to explaining in more detail the validation results based on the three pillars mentioned.

The flow solution in the first two pillars (DNS/LES) is obtained using SST k-omega model, as for the standard Prandtl number case (Pr=1) and a constant turbulent Prandtl number $\mathrm{Pr_t}$=0.85. However, when the heat transfer modelling is to be tested, the correlation by Kays is used for modelling providing a variable turbulent Prandtl number. In case of the flow field calculations, there is no effect of $\mathrm{Pr_t}$ number and the SST k-omega model was simply used.

4.3 Validation against DNS data

In this section and the subsequent one, the validation process is conducted using a physical case involving a fully developed turbulent channel flow. The flow under investigation has a low Prandtl number (Pr=0.025) and passes through a heated wall where an average constant heat flux is applied.

Numerically, for these two sections, the problem is addressed by simulating a time-evolving flow between two plates using periodic boundary conditions in the streamwise (x) and spanwise (z) directions until reaching a statistical equilibrium.

Frictional Reynolds number is characterized using the frictional velocity $\bar{u}_\tau$ as below:

$$Re_\tau = \frac{\bar{u}_\tau \delta}{v} \qquad 4.3.1$$

Where δ is half of the channel height, v is the kinematic viscosity, τ_w is the wall shear stress, ρ is the density and the frictional velocity is given by:

$$\bar{u}_\tau^2 = \bar{\tau}_w / \rho \qquad 4.3.2$$

The DNS and LES data were taken from literature [48] and figures have been replotted adding K- ω SST model results, and Standard-Gradient Diffusion Hypothesis (SGDH) using Kays correlation.

The first validation is of the flow field, and it is against the DNS data. The K- ω SST model was used in this case. To ensure a consistent comparison, the flow velocity has been adjusted to align with the frictional Reynolds number Re_τ and Reynolds number Re with specific values of $Re_\tau = 2000$, Re=85,000. This alignment is generally crucial for achieving a reliable correspondence between the employed model in the test case, the validation DNS/LES reference cases, and the mini demonstrator case.

The comparison plot in Figure 15 is between u^+ and y^+. From the results it can be concluded that the results of the K- ω SST model are in a fairly good agreement with the DNS data. As mentioned previously, the agreement between the used model and the DNS data was expected, as the main discrepancies are expected to be within the thermal boundary layer, but not the velocity boundary layer.

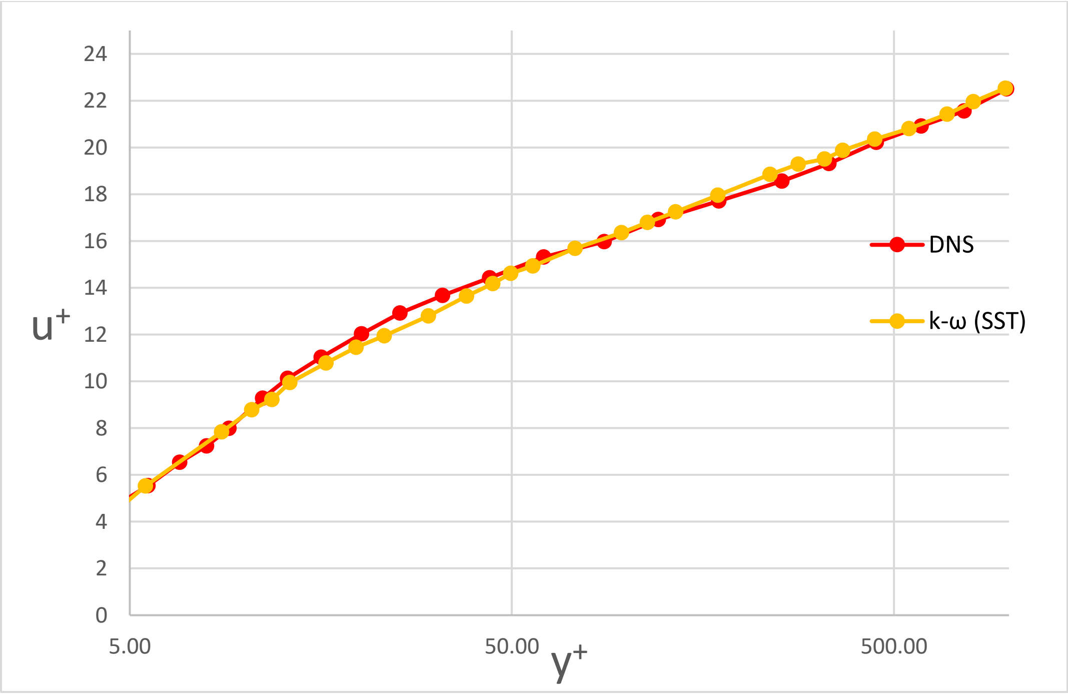

Figure 15 velocity profile: DNS, Kay and K- ω SST

4.4 Validation against LES data

In light of the unavailability of DNS (Direct Numerical Simulation) data capturing the turbulent Prandtl number within the range of the given frictional Reynolds number Re_τ and Prandtl number (Pr), LES (Large Eddy Simulation) data was employed instead. The LES data utilized in this study was obtained from the same literature source [48], where it was derived from various simulations conducted in previous research and documented in the literature.

The number of grid points for the LES is thus $\mathrm{N_x} \times \mathrm{N_y} \times \mathrm{N_z} = 384 \times 256 \times 384$ and the stretching factor is γ = 2.4, corresponding to a resolution $\Delta x^+ = 32.7, \Delta z^+ = 16.4$, $\Delta y^+_{min} = 1.25$ and $\Delta y^+_{max} = 38.22$. This resolution is typical of high-quality wall-resolved LES.

Knowing that $\bar{T}_w$ is the mean wall temperature and $\bar{T}$ is the local mean temperature, the mean temperature is then defined as:

$$\bar{\theta}^+ = \frac{\bar{\theta}}{\bar{T}_\tau} = \frac{\bar{T}_w - \bar{T}}{\bar{T}_\tau} \qquad 4.4.1$$

Where the mean frictional temperature is defined as:

$$\bar{T}_\tau = \frac{\bar{q}_w}{\rho c \bar{u}_\tau} \qquad 4.4.2$$

$\bar{q}_w$ is the average heat flux, ρ is density, C is specific heat and $\bar{u}_\tau$ is the frictional velocity.

The turbulent Prandtl number is conventionally set to 0.85 when utilizing the K-ϖ SST model. However -as mentioned earlier- in this validation pillar where the heat transfer is to be tested, the Kays correlation was employed to achieve the intended variation of the turbulent Pr number.

In Figure 16 presented below, it can be observed that there exists a satisfactory agreement between the temperature profile acquired from Large Eddy Simulation (LES) and the profile obtained using the Standard-Gradient Diffusion Hypothesis (SGDH) model with Kays correlation. However, a significant discrepancy is apparent when comparing the results of the k-omega SST model with LES, particularly as the Y+ values increase. This discrepancy arises due to the low Prandtl number (Pr=0.025) associated with this particular case. This result underscores the suitability of employing the SGDH model with Kays correlation for turbulent Prandtl number calculations in the context of the MD case wherever the heat transfer is considered. The chosen model aligns well with the conditions of the LES validation case, as evidenced by the close correspondence between the frictional Reynolds number and the laminar Prandtl number.

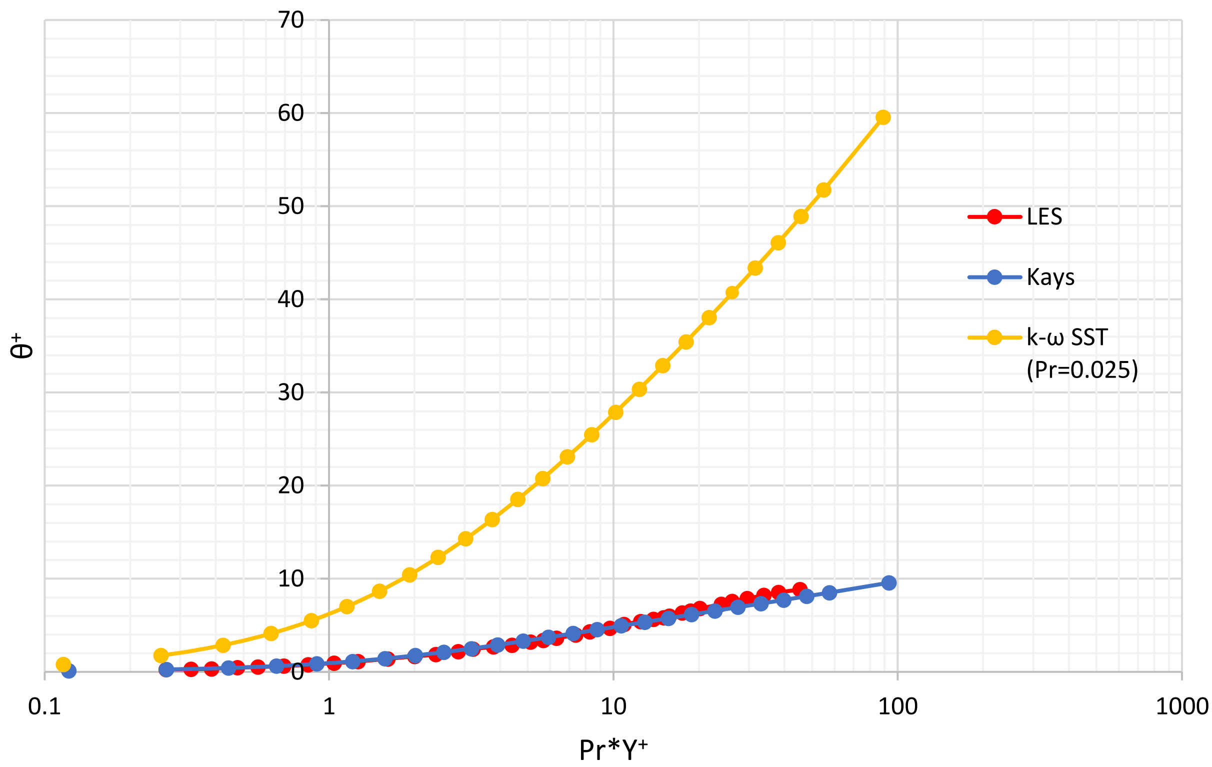

Figure 16: Temperature profiles in LES (Pr=0.025, $Re_{\tau} = 2000$), Kays (Pr=0.025) and K- ϖ SST (Pr=0.025)

4.5 Validation against experimental data

One of few facilities in the world used to test liquid lead systems to observe the behavior of the flow in various operational conditions is the TALL-3D facility in the Royal Institute of Technology, Stockholm, Sweden. An experiment has been performed in the facility that can be used here for the purpose of validation. The facility has two loops with a heat exchanger between them. Liquid lead–bismuth eutectic (LBE) was used as a coolant to the primary loop while the secondary loop has glycerol oil coolant. (More description can be found in [49])

The Loop has a testing section which consists of a pipe with a heater in the center along the whole testing section of 150 cm total length. The heater itself has a heating section only in 87 cm of its length located after a 60 cm length used for flow development, heater is then followed by 3 cm section as for the device constructional reasons.

The thermocouples used for measuring the temperatures are in four different levels, each level has four thermocouples positioned horizontally. The dimensions (in mm) of the horizontal locations of the thermocouples are shown in Figure 17

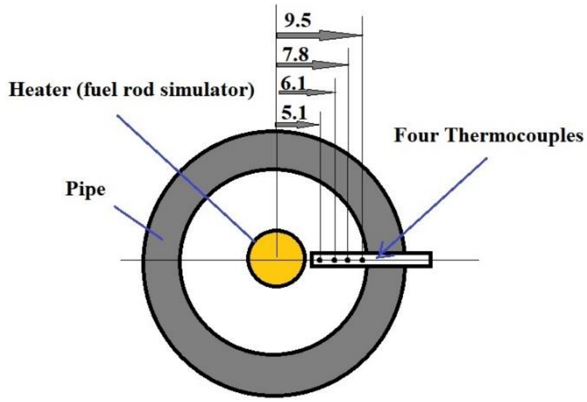

Figure 17: Radial distribution of thermocouples
in TALL testing section

The steady state experiment was set based on the nominal power of the heater, which is 21kW as a constant value, while different inlet velocities were tested (0.65, 0.93, 1.36, 1.57 and 2 m/s) and temperatures increase have been measured and presented in the article results.[49]

For the purpose of modelling, the same dimensions of the experiment have been used to establish the model geometry and the mesh using Ansys Design modeler, and Ansys meshing respectively. The minimum and maximum velocity cases (0.65 and 2 m/s) corresponding to 19,000 and 61,000 Reynolds number respectively, have been selected for testing and Ansys fluent has been used to model the two cases.

Similarly, to the previous validation cases, the K- ω SST model with the standard Pr=1 is used while the other tested case is the same model but using Kays correlation for variable turbulent Prandtl number.

The temperatures from the model calculation results were extracted using the same technique of the experiment. The average temperature of the four points equivalent to the four thermocouples in the experimental facility in each of the four levels have been recorded and compared to those found experimentally.

The differences between the models' predictions and the experiment findings (error) are shown in percentage in Figure 18 and Figure 19.

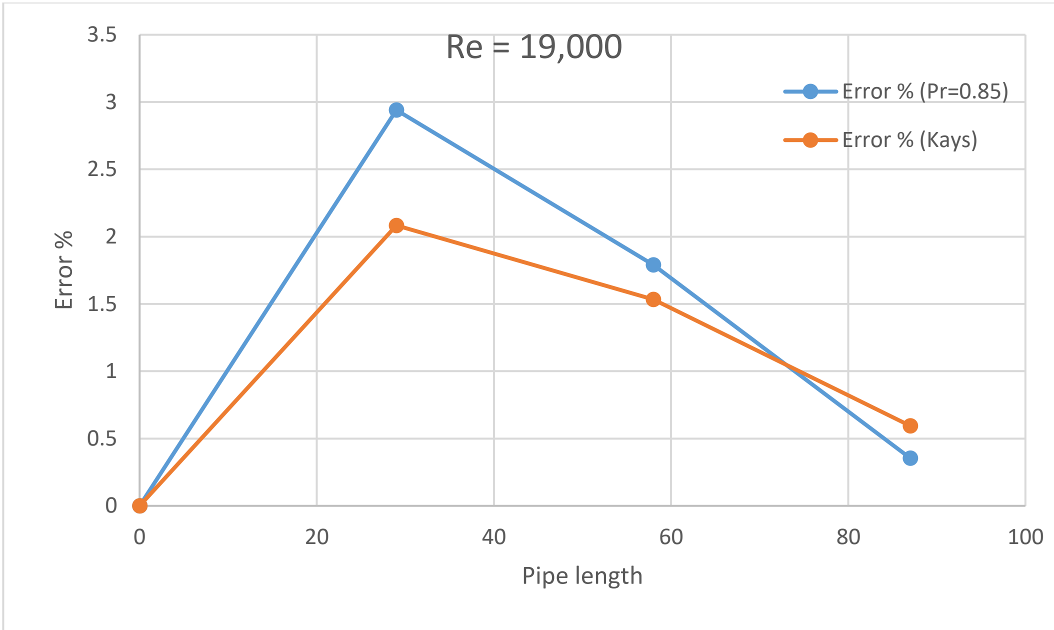

Figure 18: Error percentage in case of Pr_t calculated by Kays and constant Pr_t=0.85 compared to experiment with Re=19000.

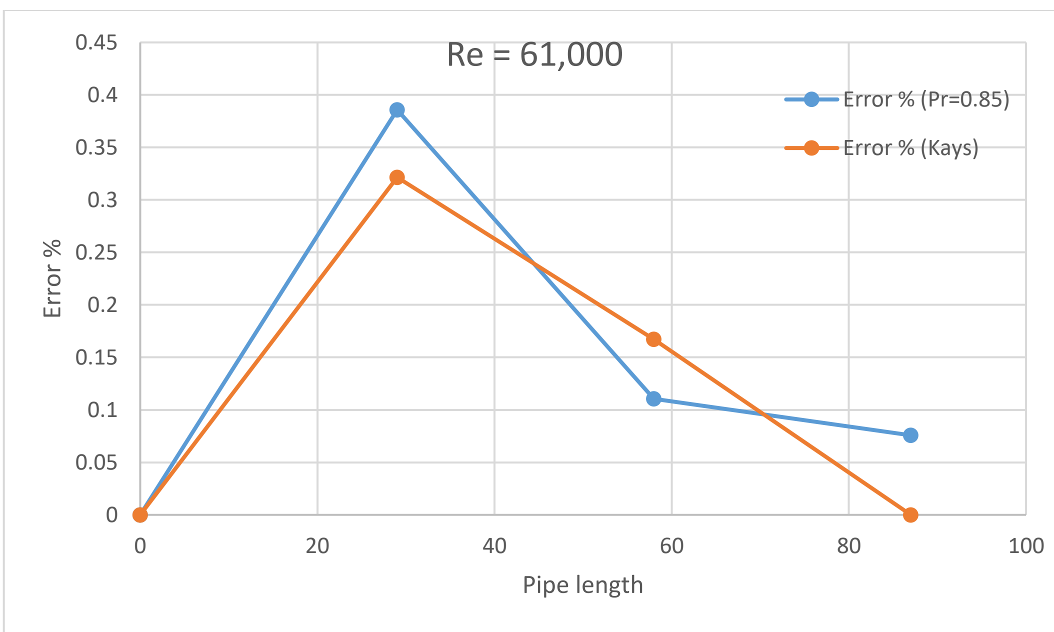

Figure 19: Error percentage in case of Pr_t calculated by Kays and constant Pr_t=0.85 compared to experiment with Re=61000.

Although the two models showed a very low error level, the Kays correlation gives a better result in the two velocity cases except for one point where it showed a slightly lower accuracy. The results obtained seem to be very good with a very low error percentage, however, this might be due to the simplicity of the flow conditions and using an average Re number.

The results of the three validation pillars all indicate that using the SGDH model together with the Kays correlation gives the best results. That was clearly visible when the thermal field was tested, as well as the experimental data were compared.

Although the results presented in this subsection (validation against experimental data) using K-ω SST model or even the Kays correlation, may give a different accuracy level if applied to a different flow conditions. However, the MD core has comparable conditions and dimensionless numbers. Hence, the shown validation approaches together are able to add a trustful amount of confidence that is enough to rely on the results obtained from using the same model in a different case that have similar dimensionless numbers and close parameters.

5 Modelling, Results and Discussions

5.1 Case set up.

This thesis focuses solely on modeling the MD core, while the investigation of the remaining loops outside of the core falls beyond the scope of this study.

In order to capture the minute flow phenomena with high fidelity, it is necessary to employ a considerably refined mesh resolution. Nonetheless, the computational expenses and practical challenges associated with such a high-resolution mesh are substantial. To address this concern, a quarter-slice approach has been adopted for the investigation of the MD core, wherein one quarter is studied while applying symmetric boundary conditions in both the X and Y directions. This approach effectively reduces the computational burden and overall computation time to a quarter of the original size, while retaining the requisite level of resolution.

As previously stated, the MD core has been partitioned into three distinct zones for individual analysis. These zones are as follows:

1. The distribution zone: This zone serves as the entry point for coolant into the MD. The coolant flows into the coolant pipes and subsequently discharges into the middle core zone. (In parallel flow case, the coolant and the fuel enter within the distribution zone).
2. Middle core zone: Positioned in the center of the MD core, this zone encapsulates the interaction between the fuel flowing through the pipes and the surrounding coolant.
3. The collection zone: Similar to the distribution zone, this zone represents the exit point for coolant from the MD core, following a comparable arrangement to that of the distribution zone (in counter flow case the fuel enters from this zone).

Note: In the nomenclature adopted for the zones in this study is based on the coolant flow condition (distribution/collection) rather than the fuel flow condition. This nomenclature choice is made specifically to prevent any potential confusion when discussing the counter flow case.

Figure 20 illustrates the zones and elements of the MD.

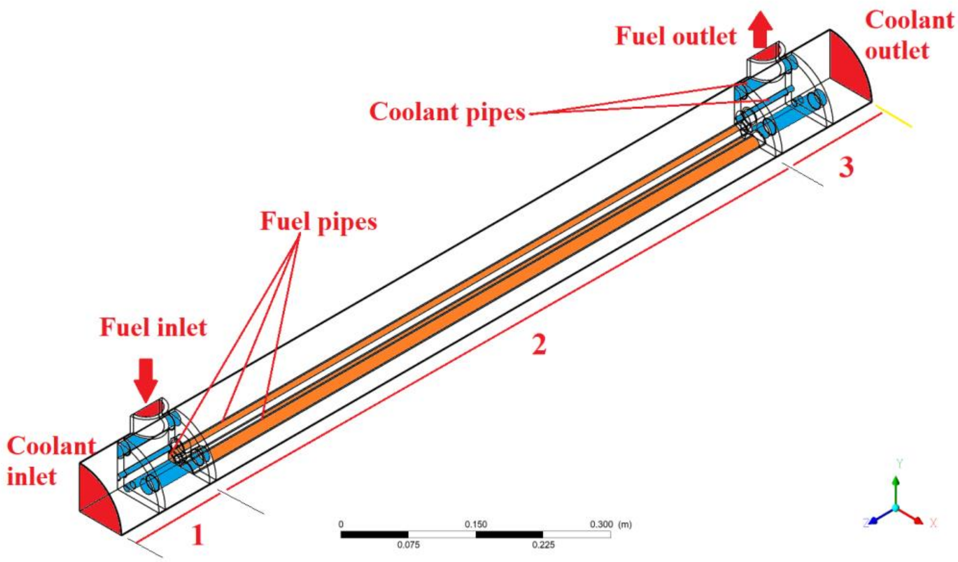

Figure 20: MD core zones and elements, 1 is Distribution zone, 2 is middle core zone and 3 is the collection zone.

5.1.1 Meshing design

In order to accommodate the geometric complexity, the mesh construction was conducted in a series of stages, with each stage dedicated to a specific element or domain. The configuration of each stage was meticulously devised to prioritize the resolution and quality of mesh elements, incorporating inflation layers whenever deemed necessary. The selection of element sizes, inflation layer placements, and meshing methods was carefully guided by the significance of each meshed region. Taking into consideration the Y^+ values to ensure that the first cell centroid is located within the viscous sublayer, capturing the important flow features near the wall. Notably, inflation layers were applied to all surfaces where significant heat transfer was anticipated.

While the overall mesh construction followed a high-resolution approach, the most refined mesh resolution was implemented in areas associated with pipe inlets and exits. This deliberate focus aimed to accurately capture the flow behavior during sudden variations in the cross-sectional area and flow velocity.

The sweep method was employed to generate meshes for all sweepable bodies within the model's components. The mesh construction process was conducted with meticulous care, particularly focusing on the boundary layers adjacent to the walls of utmost significance for the investigation. This involved incorporating appropriate inflation layers, extending up to 10 layers with a growth rate of 1.2, within the fuel and coolant domains on the inner and outer sides of both fuel and coolant pipes.

A total of 24,897,191 elements were generated to encompass the model's quarter, with the potential to reach over 99 million elements for the entire model if fully established. Figure 21 shows the mesh resolution in the collection and distribution zones (identical) as well as a part of the coolant domain in the middle core zone and fuel in the fuel pipes.

Conducting a sensitivity analysis on the mesh resolution is challenging due to the intricate geometry and the varying mesh sizes employed for areas with significant contributions to heat transfer or fluid flow. Despite efforts to obtain optimal results, the complex nature of the geometry hindered the ability to accurately capture the desired effect of grid dependency. For this reason, accountability on the Y^+ values that were kept below 10 in the majority of the areas of significance were relied on.

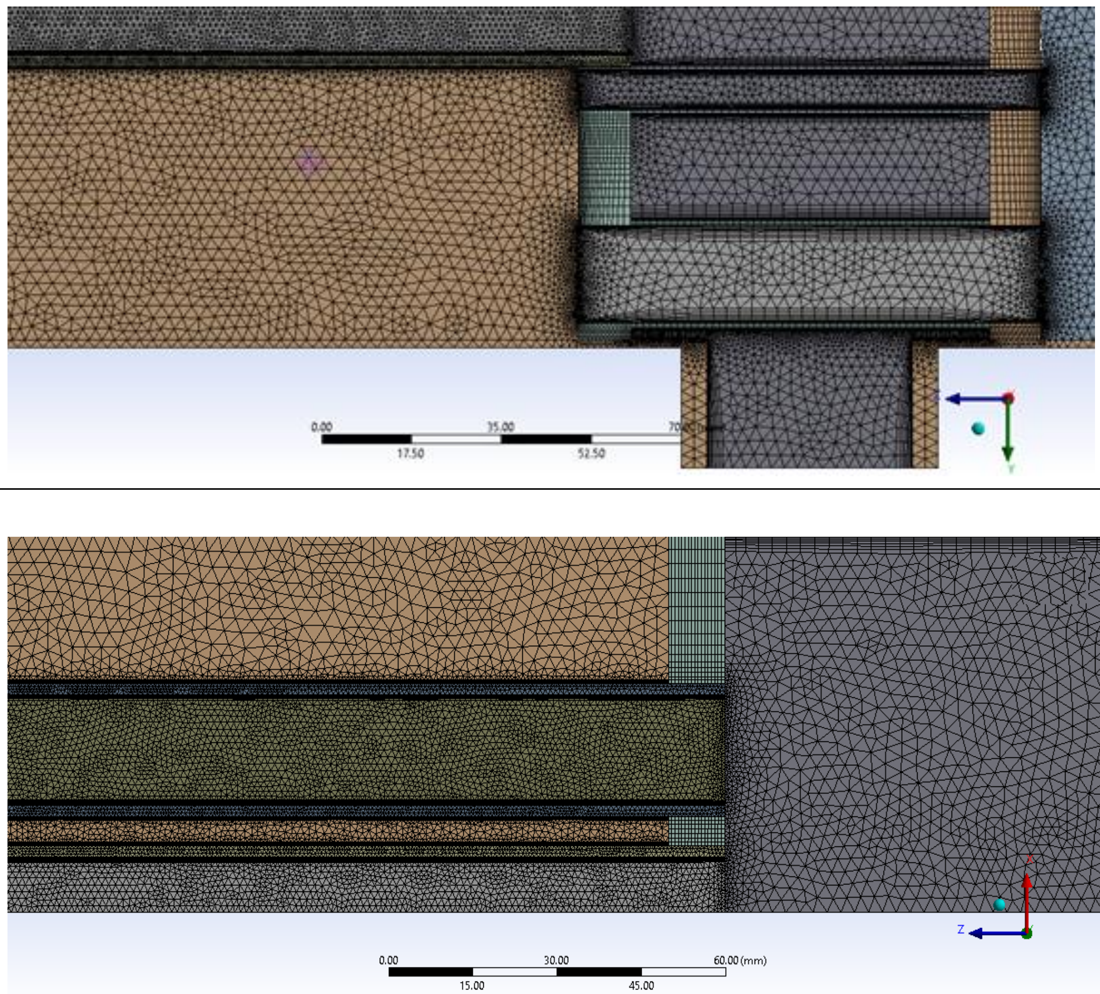

Figure 21: mesh in distribution/collection zones; YZ plane (top), XZ plane (bottom)

5.1.2 Solver and boundary conditions

Solver and tools

For the MD case studied in this thesis, the geometry was established using “Ansys Design Modeler”, for meshing “Ansys Mesher” was used to create the mesh, as a solver the adopted tool was “Ansys Fluent” version 2020 R1.

Boundary conditions

To match the DFR conditions, the boundary conditions (BC) for fuel was set to have a very low velocity 0.1 m/s. The coolant, however, has a larger velocity of 0.5 m/s. The DFR operates in atmospheric pressure, which was as well adopted in the case of the MD. Temperatures were assumed to be within the average operation temperature of fuel and coolant in the MD. A summary of the BC can be found in Table 4

Table 4 Mini Demonstrator boundary conditions.

Boundary conditions		
Fuel Boundary conditions	Velocity (m/s)	0.1
	Total pressure (atm)	1
	Total temp (K)	1473
Coolant Boundary conditions	Velocity (m/s)	0.5
	Total pressure (atm)	1
	Total temp (K)	873

Material properties

The core structure of the MD primarily comprises molten lead as the fluid medium, while the solid components of the MD, including the pipes, outside casing, and separation discs, are constructed using silicon carbide (SiC) material.

The preinstalled material properties in Ansys Fluent [50] encompass a wide range of materials; however, the properties specific to liquid lead and silicon carbide were not included in the default database. Therefore, it was necessary to manually incorporate the material properties of these substances into the Fluent software to facilitate accurate calculations.

This entailed adding piecewise linear values for each property, obtained through empirical correlations that accurately captured the behavior within the operational temperature range. The empirical correlations for liquid lead were sourced from a scientific report conducted by SCK•CEN [51]. As for silicon carbide, its material properties were obtained from the online database of the Ioffe Institute [52]. Silicon carbide specific heat was added to Ansys fluent as piece wise linear values corresponding to temperature.

The chosen correlations for each property of liquid lead can be found in Table 5

Table 5: Liquid lead material properties correlations[51]

Property	**Interpolation function**
Density *(kg/m3)*	$11463 - 1.32 \,.\, T$
Heat Capacity *(J/kg.K)*	$175.1 - (4.961 \,.\, 10^{-2} \,.\, T) + (1.985 \,.\, 10^{-5} \,.\, T^2) - (2.099 \,.\, 10^{-9} \,.\, T^3) - (1.524 \,.\, 10^6 \,.\, T^2)$
Viscosity *(Pa.s)*	$(1032.2/T) - 7.6354$

For silicon carbide the used material properties can found in Table 6 and Table 7

Table 6: Silicon carbide material properties correlation/values[52].

Property	**Interpolation/Value**
Thermal Conductivity *(W/cm/K)*	611/(T-115)
Density (kg/m^3)	3210

Table 7: Silicon carbide specific heat properties[52].

Temperature	**Specific heat C_p (J/g.K)**
880	500
1060	625
1100	750
1220	1000
1280	1250

5.2 Results Structuring

This section elucidates the structural organization of the results presented in this thesis, aiming to enhance comprehension of the sequential arrangement of information.

In the results, a detailed analysis was conducted for each zone of the MD individually. The examinations encompassed an assessment of heat transfer, wherein the description and evaluation of heat transfer were correlated with temperature fluctuations. Additionally, the influence of flow streamlines direction, geometric factors, and eddy viscosity on heat transfer were considered.

Furthermore, the description of mass flow rates and the velocity variation within each zone was provided through velocity profiles and streamlines.

The aforementioned methodology is implemented for the parallel flow configuration; however, a comparative analysis with counter flow is also undertaken to elucidate the significant distinctions between these two arrangements specifically in the context of the MD core.

Subsequently, an overview of measurement devices was conducted, encompassing a compilation of commonly utilized instruments, and suggestions were put forth regarding the installation locations. These recommendations were formulated based on the outcomes derived from the calculations conducted.

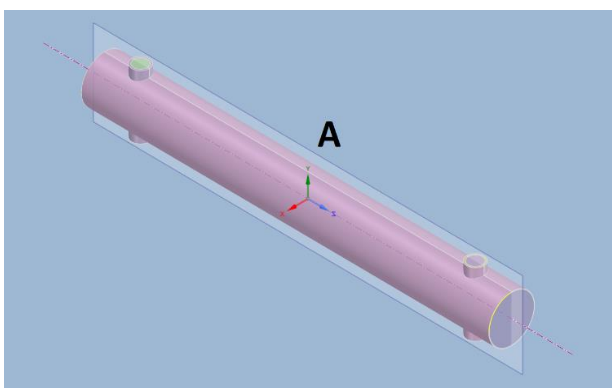

Figure 22: Longitudinal plane A

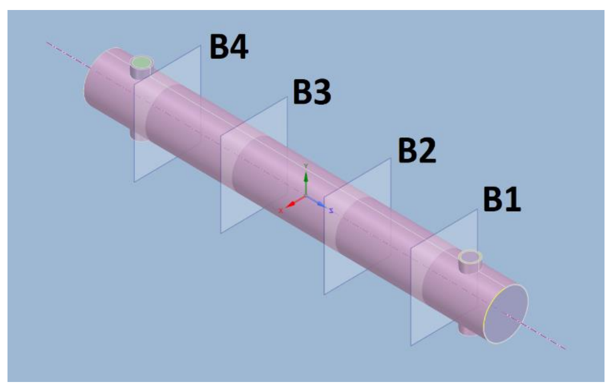

Figure 23: In core Transvers planes B1-B4

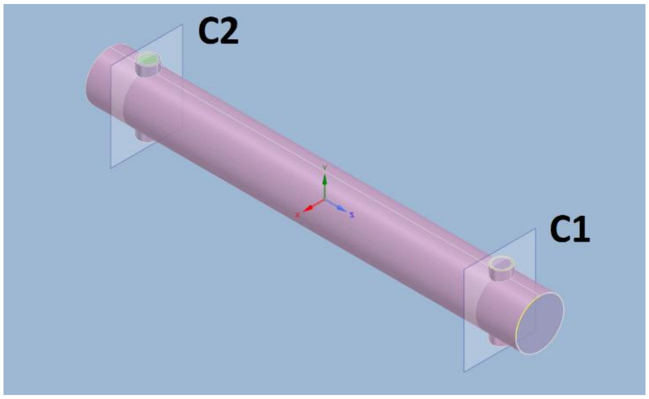

Figure 24: Transverse Inlet/Outlet plane C1, C2

In this thesis, the chosen planes (domain sections) for analysis are presented through the following figures (see Figure 22, Figure 23, Figure 24). These planes include the longitudinal plane labeled as A, the core transverse planes labeled as B1-B4, and the Inlet/Outlet transverse planes labeled as C1 and C2.

5.2.1 Heat transfer and temperature analysis

This subsection focuses on the comprehensive analysis and discussion of heat transfer outcomes within the MD core, specifically examining the temperature distribution and eddy viscosity distribution. To facilitate this analysis, streamlines and profile contours will be employed, with streamlines primarily used to illustrate the core flow and its associated flow velocity directions. These chosen parameters hold significant value in the analysis of heat transfer processes, as detailed justifications for their selection will be elucidated below:

Temperature in streamlines and contours: visualization is a crucial tool for gaining initial insights into the heat transfer processes occurring throughout the entire core. It serves as an effective means to comprehend the overall heat distribution and ascertain the range of the temperature, in terms of both the highest and lowest values attained.

Eddy viscosity in streamlines: on the other hand, represents the turbulent diffusion of momentum and accordingly, heat. A higher eddy viscosity implies stronger turbulence and increased mixing of the fluid, which can affect the heat transfer rates.

The colors of the streamlines in the figures coming in the next subsections are coded according to the previously mentioned key parameters. This color mapping provides a visual representation of the heat transfer phenomenon occurring within the MD core. Consequently, it enhances our comprehension of the heat exchange processes taking place in distinct zones within the MD. By considering these parameters collectively, we can gain valuable insights into the intricate heat interactions transpiring within the three zones of the MD.

Heat transfer in each zone has been calculated based on the parameters: temperature difference between inlet and outlet, heat capacity and mass flow rate.

5.2.2 Mass flow and velocity analysis

The mass flow rates, and velocity analysis were presented in this thesis basically by showing the velocity contours within each domain per zone. Additionally, the streamlines with the colors coded by velocity values. The choice of using velocity streamlines velocity profile contours is justified below:

Velocity Streamlines: provide a visual representation of the flow patterns within a fluid domain. They depict the direction and path that fluid particles follow within the flow field. This visualization aids in understanding the overall behavior of the fluid, identifying regions of interest, and revealing complex flow phenomena.

Furthermore, streamlines help identify areas where the fluid flow separates from surfaces or undergoes recirculation. By examining the streamlines, one can identify regions with vortices, eddies, or stagnation points. This information is crucial for assessing the aerodynamic performance of objects, analyzing fluid behavior around obstacles, and optimizing designs to reduce flow separation or recirculation.

Moreover, streamlines are used to validate CFD simulations by comparing them with experimental or analytical results. A close agreement between the simulated and observed streamlines confirms the accuracy and reliability of the numerical model. Deviations in streamlines may indicate errors or inconsistencies in the simulation setup or assumptions.

Velocity contour profiles: these contours offer a clear depiction of the spatial distribution of velocity within the flow field. This visualization aids in understanding the flow patterns, identifying regions of interest, and revealing areas of high or low velocity.

Also, they can be used to validate CFD simulations by comparing them with experimental or analytical data. A close agreement between the simulated and observed velocity contours confirms the accuracy and reliability of the numerical model. Discrepancies in the velocity profiles may indicate errors or inaccuracies in the simulation setup or assumptions.

5.3 Parallel Flow

Parallel flow in heat exchangers refers to a configuration where the hot fluid and cold fluid flow in the same direction, parallel to each other, within the heat exchanger. In this arrangement, the hot fluid (fuel) enters one end of the heat exchanger while the cold fluid (coolant) enters the same end and flows alongside the hot fluid in the same direction. As the fluids move through the heat exchanger, heat is transferred from the hot fluid to the cold fluid, resulting in a decrease in the temperature of the hot fluid and an increase in the temperature of the cold fluid. The fluids exit the heat exchanger at the opposite end, having undergone heat exchange in a parallel manner.

In this section, the results are divided into two main parts. The first part focuses on the analysis of heat transfer and temperature for both the fuel and coolant. The second part is dedicated to the analysis of mass flow rate and velocity for both fluids.

The analysis is structured based on the zones of the MD in the order of the flow direction. However, in the heat transfer and temperature analysis in the middle core zone the fuel and coolant fluids are discussed together due to the interconnected nature of the heat exchange phenomena between the two fluids in this particular zone. A summary of this structure can be found below in Table 8 and Table 9.

Table 8: Heat transfer and temperature results structure

	Fluid domain	Zone
Heat transfer and temperature	Fuel	Global overview
		Distribution zone
		Collection zone
	Coolant	Global overview
		Distribution zone
		Collection zone
	Fuel and coolant	Middle core zone

Table 9: Mass flow rate and velocity results structure

	Fluid domain	Zone
Mass flow rate and velocity	Fuel	Global overview
		Distribution zone
		Middle core zone
		Collection zone
	Coolant	Global overview
		Distribution zone
		Middle core zone
		Collection zone

5.3.1 Heat transfer and temperature analysis

In this subsection, a comprehensive analysis and discussion of the heat transfer and temperature phenomena will be conducted. The analysis will commence with a comprehensive overview of the fuel, encompassing an examination of the overall heat transfer characteristics. Subsequently, a detailed analysis of the fuel and coolant will be undertaken for each individual zone, including the distribution zone, middle core zone, and collection zone in regards of the heat transfer aspect.

5.3.1.1 Fuel Global Overview

The temperature of the fuel in the MD core varies from the highest temperature in the core 1473 K (fuel inlet temperature) to the lowest temperature in the core (coolant inlet temperature) Figure 25. This shows that the heat transfer between the fuel and the coolant is sufficient to decrease the fuel temperature to the most possible minimum based on the current flow conditions.

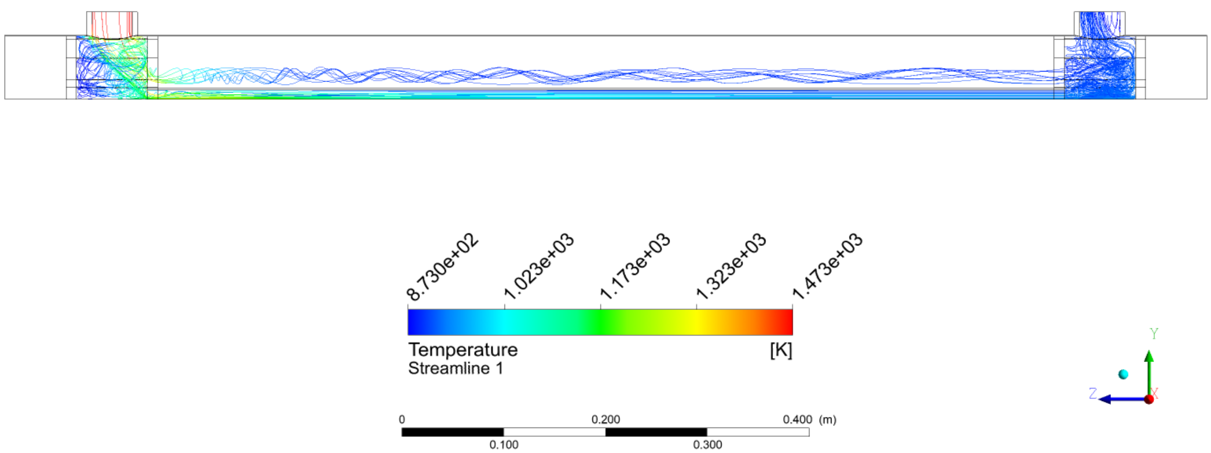

Figure 25: Fuel flow streamlines with temperature coded color.

The majority of the heat transfer seems to occur in the first third of the MD core, that includes the distribution zone and the first quarter of the fuel pipes in the middle core.

The highest turbulent diffusion can be observed in the eddy viscosity (Figure 26) within the distribution zone and the first quarter of the fuel pipes.

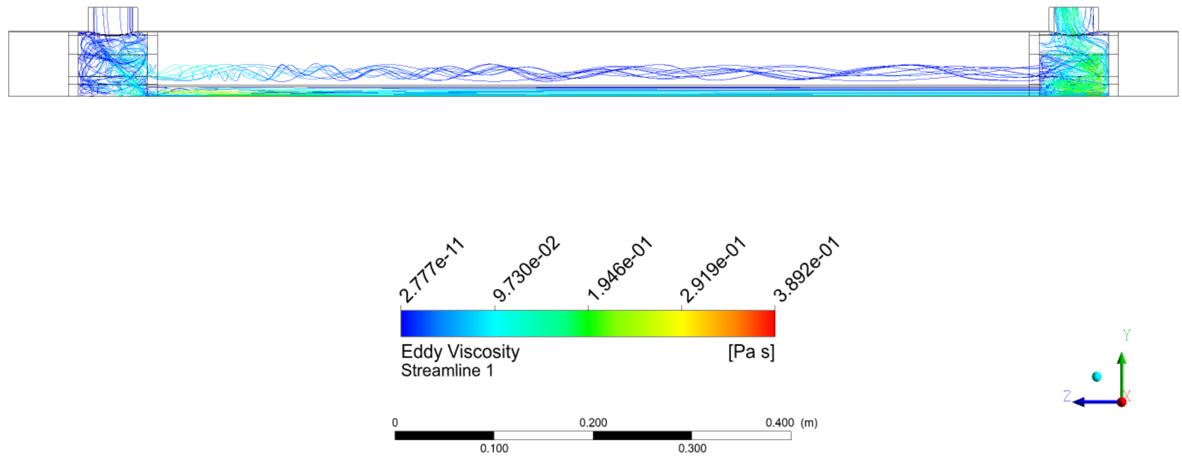

Figure 26: Fuel flow streamlines with eddy viscosity coded color.

5.3.1.2 Fuel Distribustion Zone

The fuel distribution zone is where the inlet fuel flow is distributed on the fuel pipe entering the MD middle core section. In the distribution zone, as the fuel has its highest temperature, surrounding the coolant pipes with the coolant in its lowest temperature. Consequently, a substantial amount of heat transfer takes place in this region.

It is clear from Figure 27 that the flow in the distribution zone has two volume sections with a large temperature difference. This is because the high temperature fuel enters from the MD inlet to deviate its direction upwards towards the fuel pipes due to its low density, leaving a lower temperature and velocity in the opposite section. This behavior will be discussed later in the mass distribution and velocity section, as well as in the counter flow section.

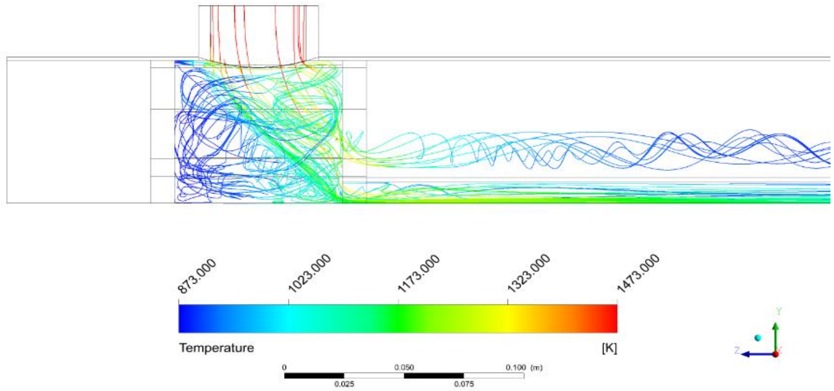

Figure 27: Fuel flow streamlines in the distribution zone with temperature coded color.

The eddy viscosity in the fuel distribution zone in Figure 28 indicates strong mixing in one section of the zone. The location of that section is as well on the same side as the high temperature fuel shown in Figure 27, this enhances the heat transfer in this area due to the high temperature difference, as well as the high mixing turbulence expressed in the high eddy viscosity values.

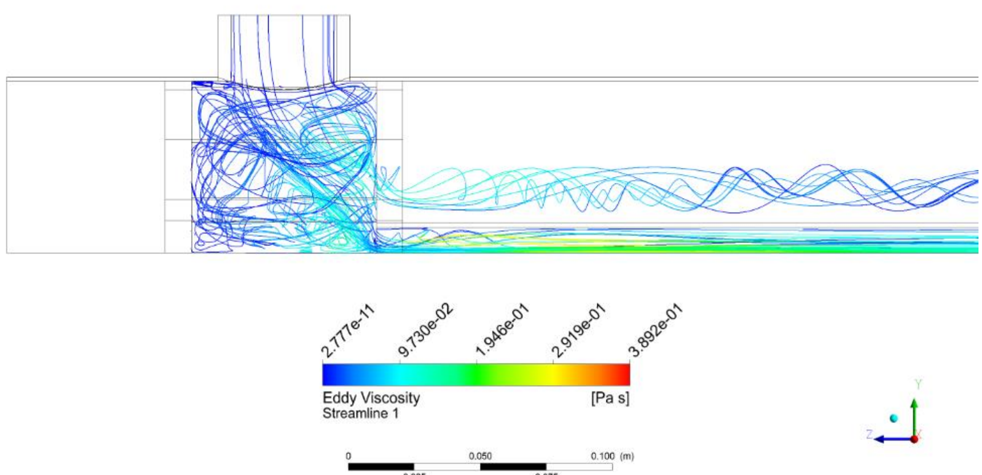

Figure 28: Fuel flow streamlines in the distribution zone with eddy viscosity coded color.

The heat transfer occurred in the distribution zone is 50.8 kW transferred from the hot fuel to the coolant including a minor heat transfer to the MD casing body.

5.3.1.3 Fuel Collection Zone

The fuel temperature in the collection zone is in the range of the coolant inlet temperature (873 K). It shows that most of the heat of the fuel has been transferred successfully to the coolant even before entering the collection zone Figure 29.

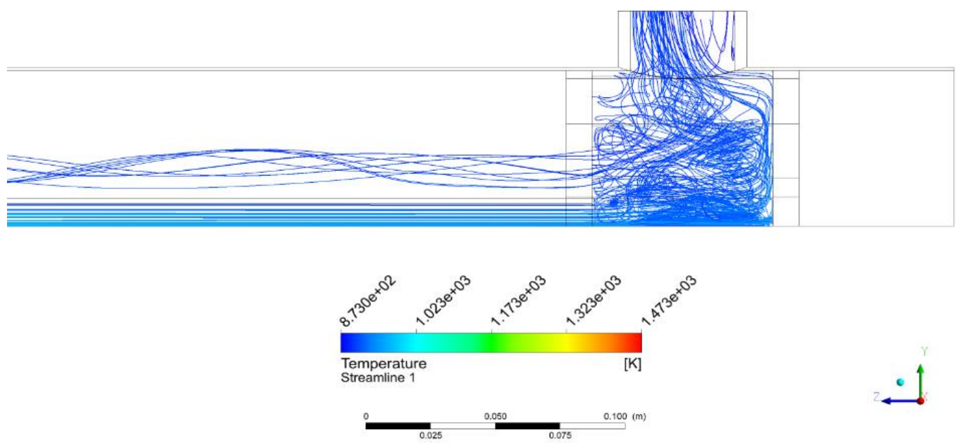

Figure 29: Fuel flow streamlines in the collection zone with temperature coded color.

The eddy viscosity diagram shows a high mixing in the collection zone, however, this significant mixing does not reflect in the heat transfer. This is due to the very small temperature difference - if any- between the two sides of the loops (coolant and fuel sides) Figure 30.

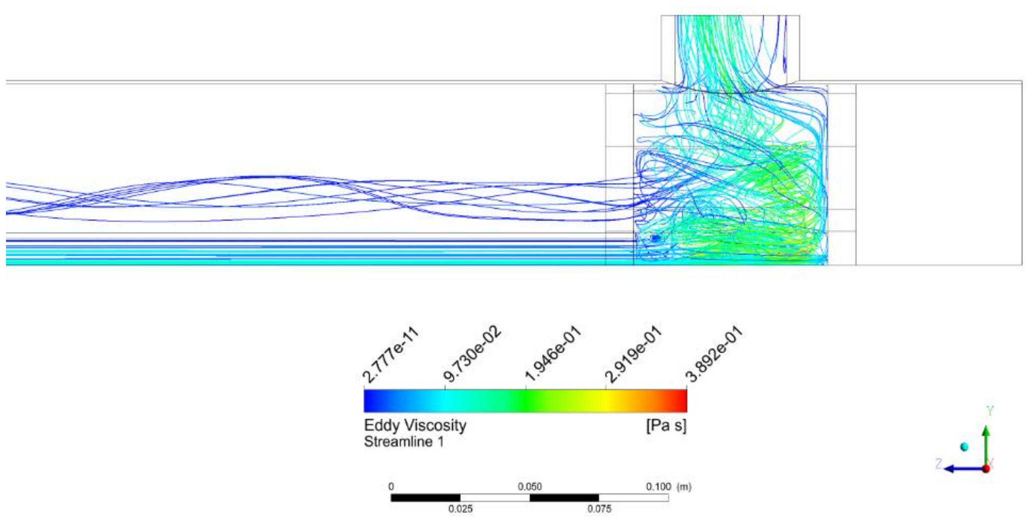

Figure 30: Fuel flow streamlines in the collection zone with eddy viscosity coded color.

5.3.1.4 Coolant Global Overview

The temperature of the coolant in the MD core varies between 873 k (inlet boundary condition) up to 1020 K in specific spots. The highest temperature of the bulk flow is by the outlet of the coolant in the collection zone. However, a hot spot was observed in the distribution zone and will be shown thoroughly in the discussion of the zone.

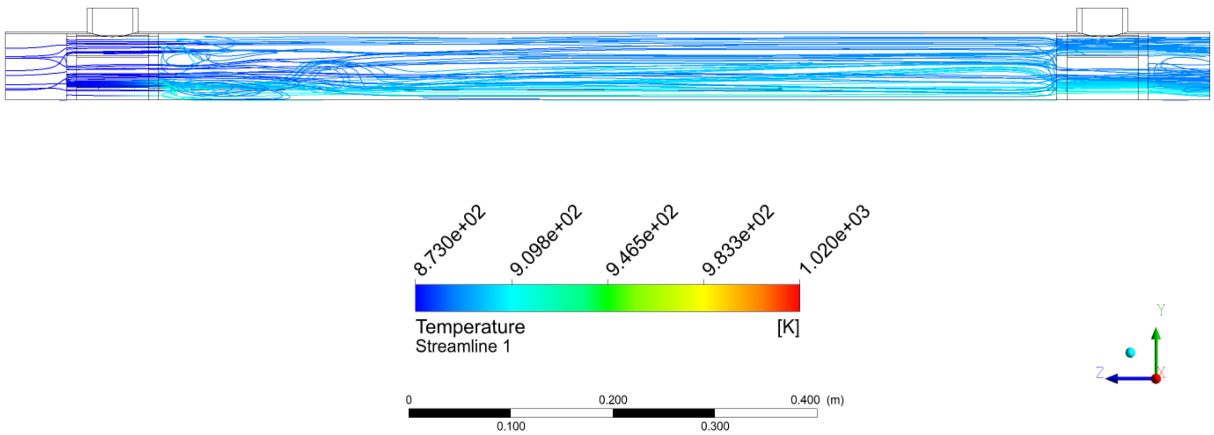

Figure 31: Coolant flow streamlines with temperature coded color.

By the first third of the middle core (left side), the highest eddy viscosity occurs. This is enhancing the heat transfer in this area, which to be added to the fact that in the same area a high temperature difference between fuel and coolant exists. The reason for the high eddy viscosity in the first third of the middle core is the sudden increase in the coolant flow cross sectional area, which led to a quick change in the velocities and random velocity profile. The eddy viscosity values increase again once more by the outlet. This will be explained later when discussing the collection zone Figure 32.

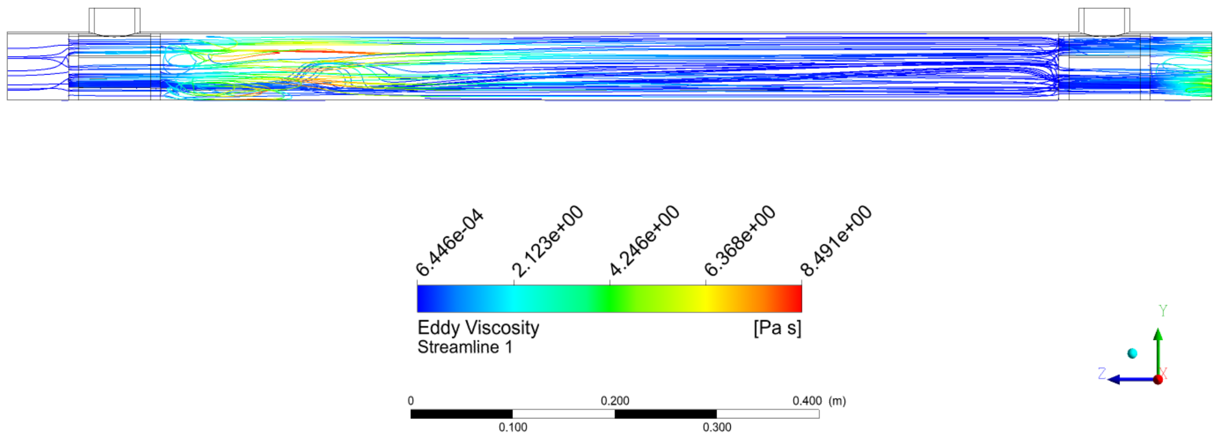

Figure 32: coolant flow streamlines with eddy viscosity coded color.

5.3.1.5 Coolant Distribution Zone

As the coolant enters from the bottom of the core (left) with its temperature 873 K, it gains a small amount of the heat before exiting the distribution zone due to the existence of the fuel in the zone with its highest temperature (1473 K). Figure 34 shows the fuel inlet temperature-colored streamlines as well as the coolant contours.

The figure clearly shows the interaction between the flow of the fuel and its temperature from one side, and the coolant temperature increase from other side. The coolant in the pipe located in front of the fuel inlet has the highest temperature of the coolant domain, however, this temperature is only on the surface close to the pipe wall facing the fuel inlet flow which might not have a large impact on the bulk coolant flow in the pipe Figure 33.

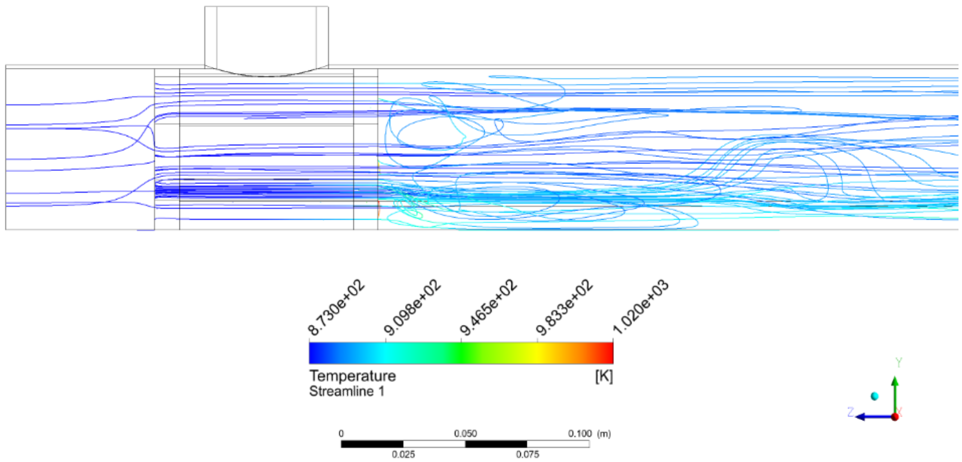

Figure 33: Coolant flow streamlines in the distribution zone with temperature coded color.

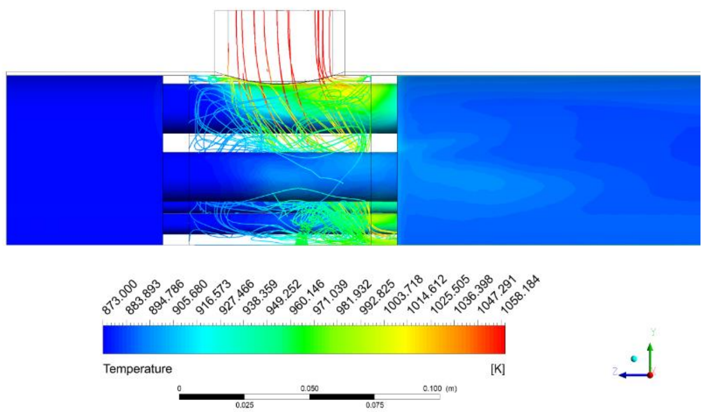

Figure 34: Coolant temperature contours in the distribution zone together with temperature-color coded fuel streamlines.

Due to the sudden increase in the coolant flow area (coolant pipes to the middle core zone), the diffusion caused by the high turbulence increases improving the heat transfer in this area of the middle core. This effect is visible in the increase of the eddy viscosity values as shown in Figure 35

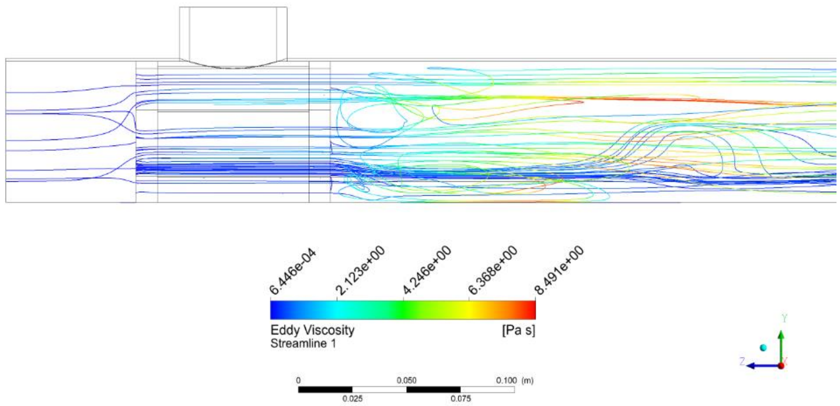

Figure 35: Coolant flow streamlines in the distribution zone with eddy viscosity- color coded.

5.3.1.6 Coolant Collection Zone

The coolant in this area has a temperature range that varies between 886 to 920 K. The increase of the coolant temperature is due to the heat gained in the first two zones (distribution and middle core zone). The heat gained in this zone is negligible Figure 36.

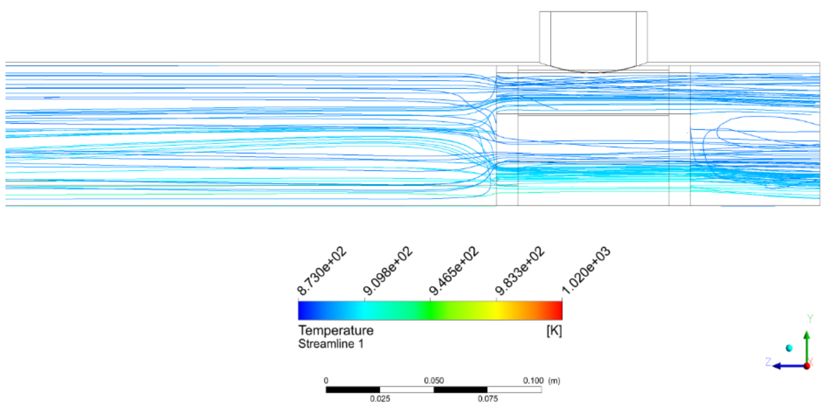

Figure 36: Coolant flow streamlines in the collection zone with temperature color coded.

Due to the high velocity of the coolant leaving the coolant pipes exiting the MD core, high turbulence was observed in this area concentrated in front of the coolant pipes flow direction Figure 37.

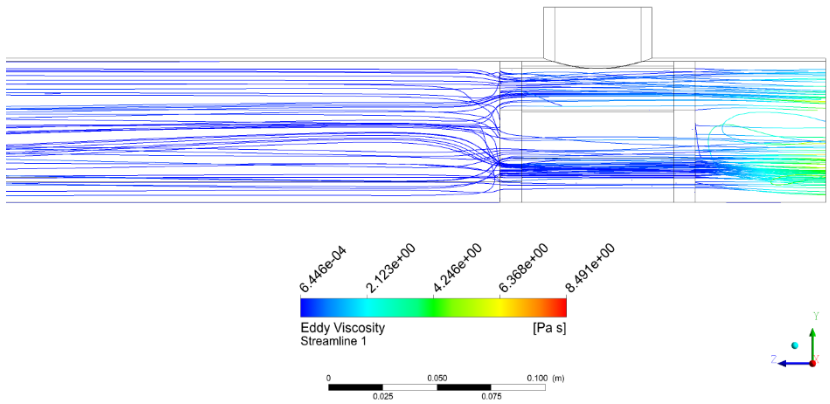

Figure 37: Coolant flow streamlines in the collection zone with eddy viscosity color coded.

5.3.1.7 Middle Core Zone

In the middle core, the fuel and coolant will be described together (not separately) for a better understanding of the heat transfer in the zone and its direct effect on both fuel and coolant sides.

Figure 39 shows the temperature profile of the fuel in the fuel pipes. As expected, the fuel temperatures in the beginning of the pipes are the highest in the middle core zone. Gradually the temperature decreases and becomes more uniform in all pipes.

The highest fuel temperature in fuel pipes is in pipes number 5 and 6 (Figure 38). This can be easily justified by looking at the previously showed Figure 27 which illustrates the fuel inlet to the "distribution zone" is driven forward by the inlet fuel momentum to directly reach the furthest pipe entrance with its highest temperature. The other pipes also have the same high temperature, however, due to the low mass flow rates in these pipes, the fuel loses its temperature quickly, thus this observation appears in the first plane in the middle core zone and continues in the other three planes as well.

Due to the temperature distribution of the fuel in the pipes, as well as the mass flow rates in each pipe, the heat transfer rates vary among the 7 pipes. The highest heat transfer rate is in pipes number 5 and 6, while the lowest is the middle pipe (pipe 7) Figure 38 and Table 10 : Heat transfer percentage per pipe out of the total heat transfer in the middle core zone. shows the heat transfer percentage per pipe out of the total heat transfer in the middle core zone. The figure and the table illustrate this result and summarize it respectively.

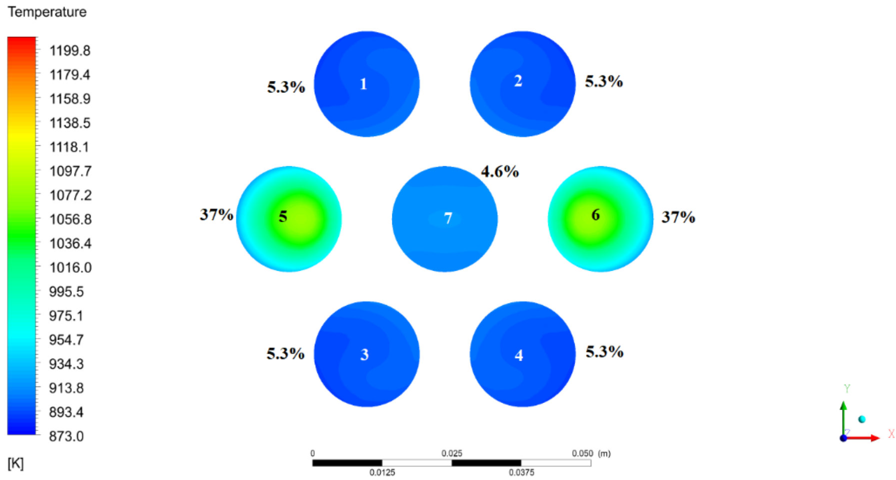

Figure 38: Fuel pipes (full domain) temperature contours in Plane B-1 with heat transfer percentage in each pipe along the middle core zone

Figure 39 shows the full domain of the fuel - fuel pipe – coolant domains in the four planes along the MD middle core zone, the diagram shows the gradual decrease in the fuel temperature, showing that the sharpest decrease in the fuel temperature occurred in the half of the zone (1200 K – 960 K). The figures come to confirm once more that most of the heat transfer takes place in the first quarter of the MD

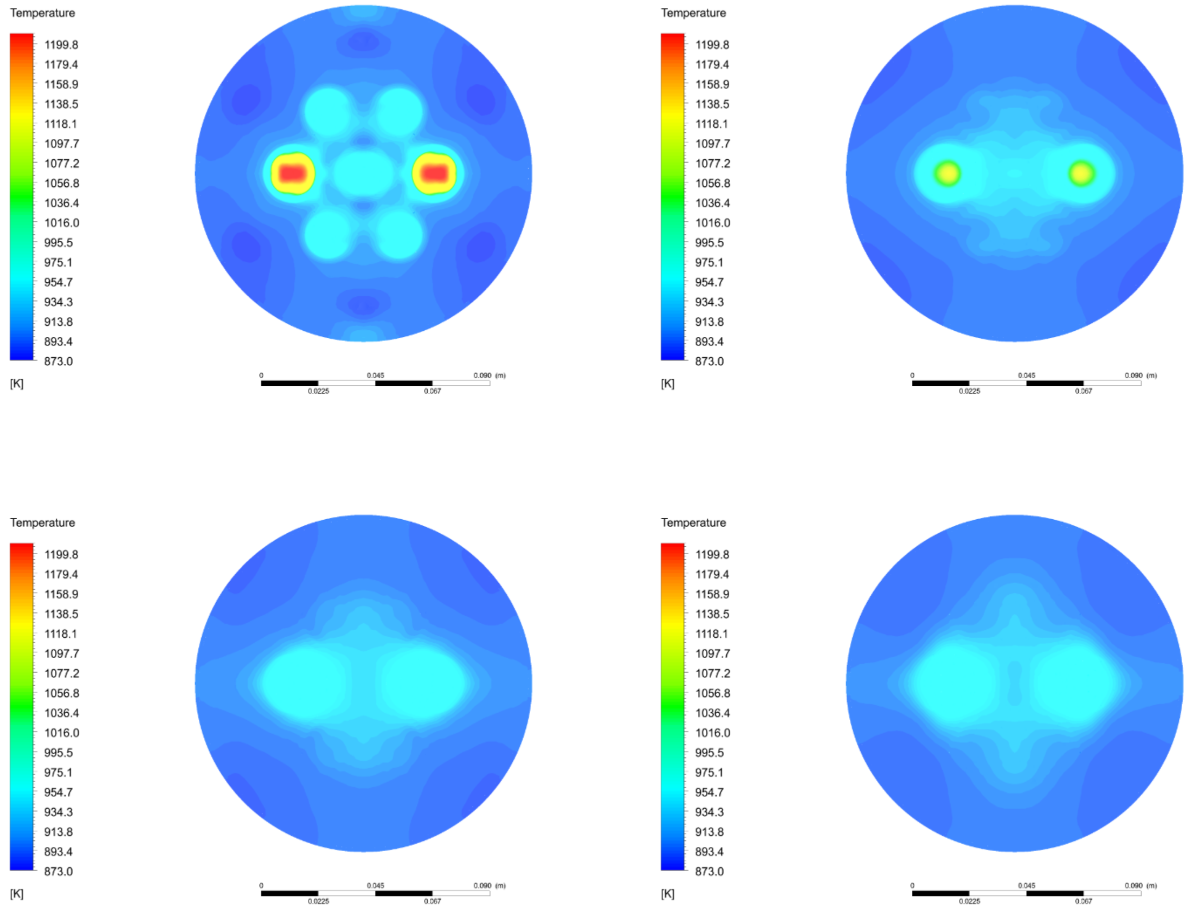

Figure 39: Fuel-pipe-coolant temperature contours in the middle core zone in planes B-1 to B-4

From the previous figures, the coolant temperature varies radially in the middle core section. This is due to the concentration of the hot fuel pipes in the middle of the core. To capture this temperature variations in the coolant domain within this zone, five lines has been added passing between the fuel pipes in the radial direction through the coolant domain only Figure 40.

Table 10 : Heat transfer percentage per pipe out of the total heat transfer in the middle core zone.

Pipe group	**Heat transfer rate per pipe [kW]**
Group A (pipes 1,2,3,4)	5.3%
Group B (pipes 5, 6)	37%
Group C (pipe 7)	4.6%

This line is then duplicated four times to have a total of five lines in five different sections along the middle core length as shown in Figure 41.

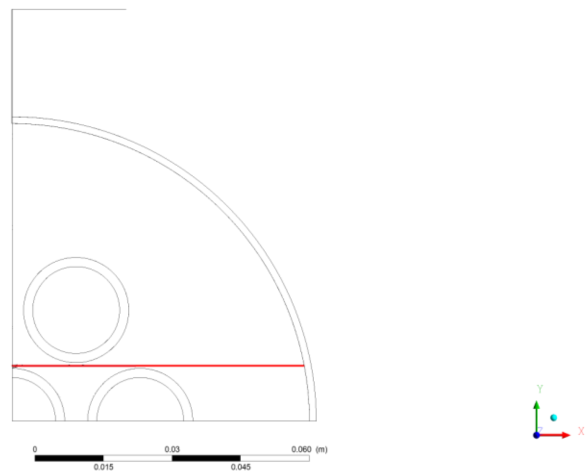

Figure 40: Lines positioning in the coolant domain.

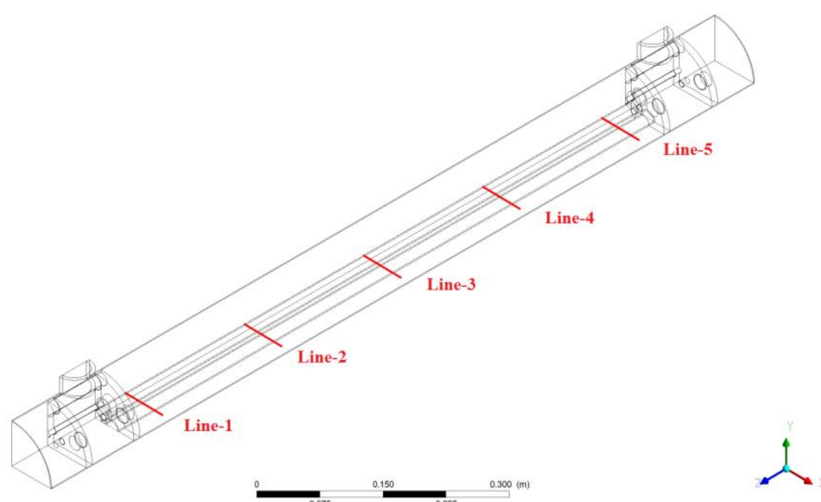

Figure 41: The positions of lines (1-5) along the coolant domain. (To be seen together with Figure 40)

Due to the small distance between the line and the higher temperature fuel pipes, the first line (line-1) has three temperature peaks in the first half of the line (middle core) coming from the effect of the three fuel pipes high temperature. Then on the other half (further from the core) the temperature tends to decrease to its lowest value by the MD casing Figure 42.

From line-2 to line-5 a similar pattern can be observed in the coolant temperature along the established lines. However, the temperatures are uniformly raised gradually while moving from line-1 to line-5 raising the curves upwards. The highest coolant temperature was expected to be in the middle of the core diameter; however, it was found to be in middle of the core radius, not diameter. This is due to two factors; the first factor is the low temperature of the fuel passing through the middle fuel pipe. The second factor is the low velocity of the same fuel pipe (velocity and mass flow will be explained in next section). These two factors affect the heat transfer in the middle core area and shift the highest temperature more towards the radial direction. In the context of the experimental facility under consideration, this characteristic could be perceived as advantageous with regard to safety considerations. In DFR with heat generation occurring in the fuel pipes, the case will have a different observation, and the highest temperature is then expected to be in the middle of the DFR core.

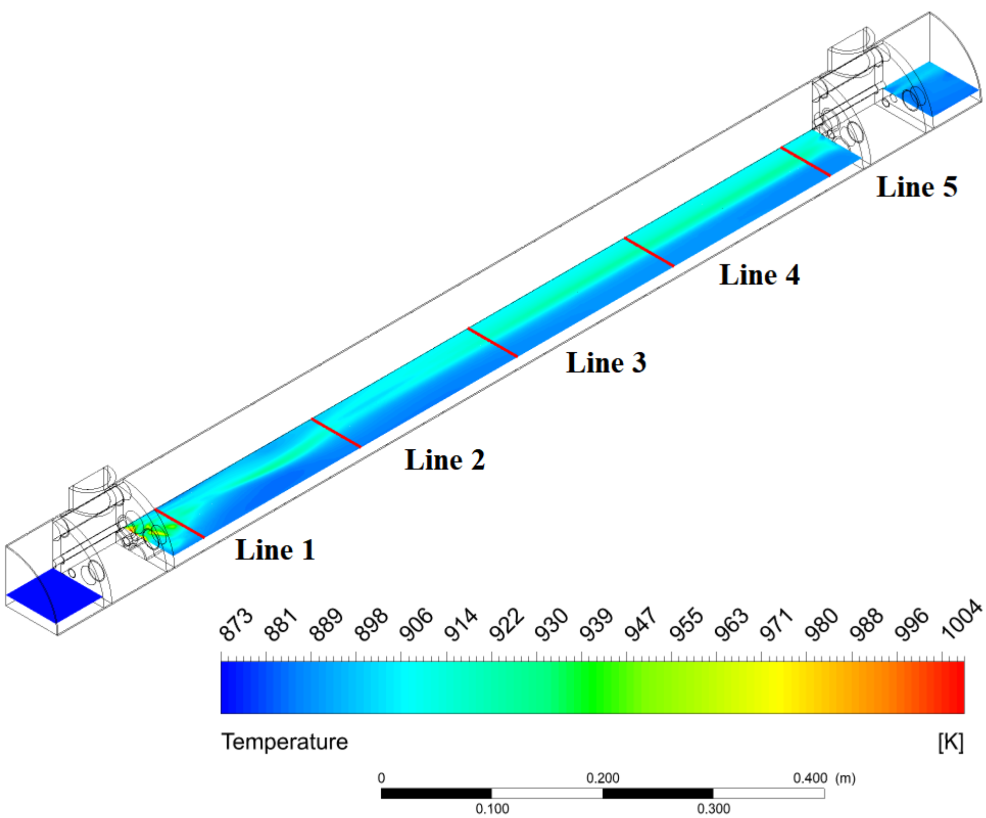

Figure 42: Temperature contours of the coolant domain in the plane passing through Lines 1-5

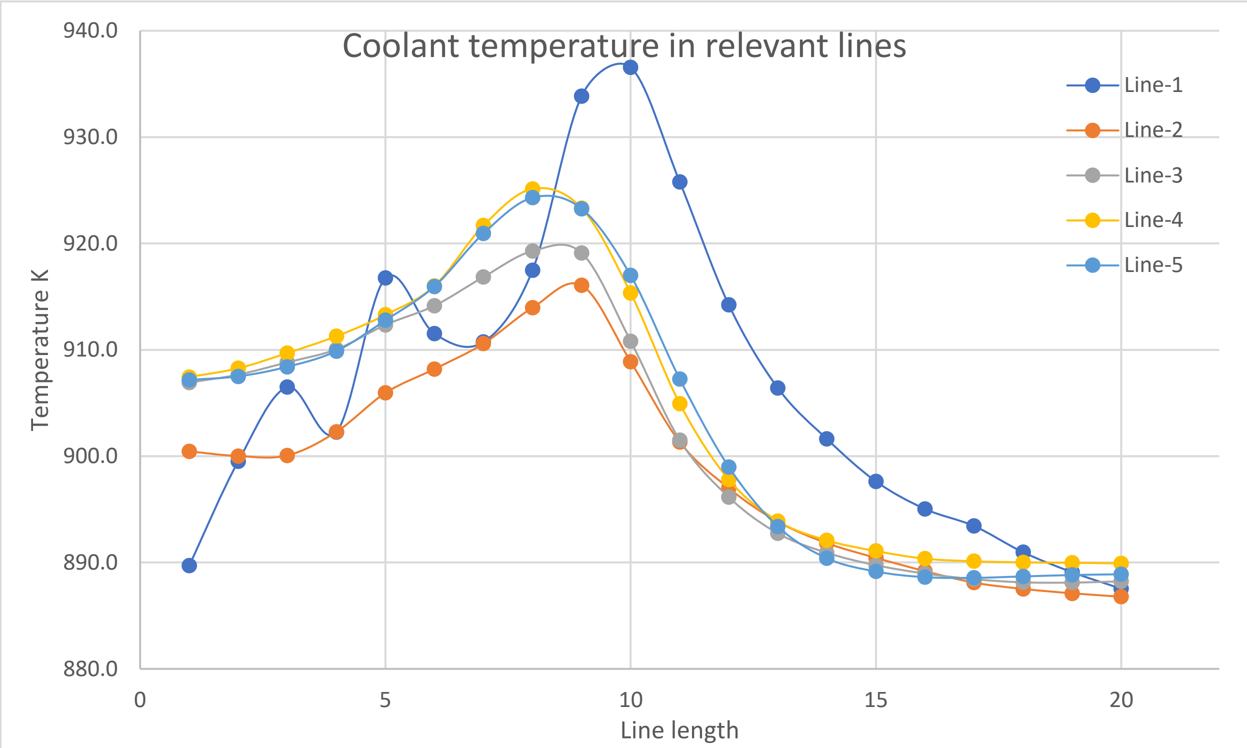

Figure 43: Coolant temperature distribution in the middle core zone in the relative lines (line 1-5)

The three peaks that appeared in line-1 have disappeared due to the stabilization of the heat transfer rate due to lower temperature differences occurred gradually Figure 43.

The highest temperature of the coolant in this zone is found to be in the second quarter of the MD radius (first quarter starts from the core exact middle, fourth quarter is the furthest from the core exact middle). In the opposite of the middle core conditions, this highest temperature of the coolant in the middle core zone corresponds to the highest temperature fuel pipe. This pipe not only has the highest temperature, but it also has the highest fuel mass flow rate. These factors exert a direct influence on heat transfer and the temperature of the coolant within this specific region. Despite that the peak temperature is not in the exact middle core, the temperature in the middle half diameter of the core is higher than the radial half due to the heat transfer from the fuel to the coolant that is concentrated in the middle half of the middle core zone diameter.

5.3.1.8 Zonal heat transfer in the MD

Based on the considered parameters and boundary conditions, the heat transfer in the MD predominantly takes place within the initial quarter of the middle core zone, followed by heat transfer in the distribution zone, whereas the collection zone exhibits minimal heat transfer.

Table 11 is summarizing the heat transfer in each zone in terms of kW and percentage of the total heat transfer.

Table 11: Heat transfer in each zone in case of parallel flow

Zone	Total Heat transfer rate per zone [kW]	Total Heat transfer percent per zone [%]
Distribution zone	19	41.6%
Middle Core zone	24.76	54.3%
Collection zone	1.84	4.0%
Total	45.6	100%

The change in the temperature of the fuel and coolant was captured in six different planes, namely, Inlet, B-1, B-2, B-3, B-4 and Outlet. In each plane the temperature was calculated based on the area average values of the temperature. Figure 44 shows the variation of the temperatures along the selected planes.

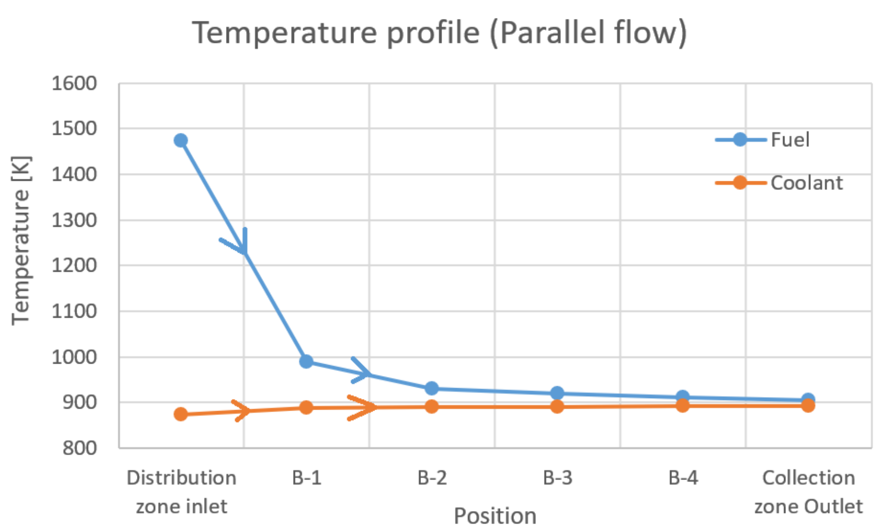

Figure 44: Area averaged temperature profile in case of parallel flow

Figure 44 confirms the heat transfer distribution findings as it shows that the fuel temperature decreases rapidly in the first fifth of the heat exchange process system within the MD core (from 1473 K to 990 K). This is followed by a considerable amount of heat transfer in the second fifth of the MD core shown in the fuel temperature declination (from 990 K to 920 K).

However, for the coolant side, considering its temperature and high mass flow rate (873 K and 68 kg/s) the increase in the temperature is much lower than the decrease of the fuel temperature (coolant increases from 873 K to 895 K when reached first fifth of the MD core (coolant inlet till plane B-1)). The coolant temperature didn't increase significantly from B-1 till the coolant outlet.

5.3.2 Mass flow and velocity analysis

Due to the DFR design which is based on a very low mass flow rate of fuel, the difference between the mass flow rates of fuel and coolant is large. The mass flow rate of fuel is 2.4 kg/s and while for the coolant it is 68 kg/s based on the current boundary conditions. In the next subsections the velocity and mass flow rates of fuel and coolant will be discussed.

5.3.2.1 Fuel Global Overview

The velocity variation within the distribution zone (bottom-right) in Figure 45 seems to have less variation the velocity values mostly lie in a range that is less than 0.1 m/s. However, the subsection number 5.3.2.2 will give a better insight to the zone and its effect on the mass flow rate in the fuel pipes.

The velocities in the fuel pipes (in my middle core zone) are higher especially at the pipe inlets. Then finally in the collection zone the velocities suffer a large amount of variation (0.4-0.05 m/s).

The variation in velocity ranges between the distribution and collection zones can be attributed to the distinct boundary conditions at the fuel inlets. In the distribution zone, the fuel is introduced through two inlets characterized by lower velocity boundary conditions (0.1 m/s - velocity inlet). In contrast, the collection zone comprises seven fuel pipes distributed at various locations with different velocities ranging from 0.05 to 0.4 m/s, resembling a jet flow effect. As a result, the high fuel velocities exiting the fuel pipes induce considerable turbulence within this region, leading to significant variations in velocities within the zone.

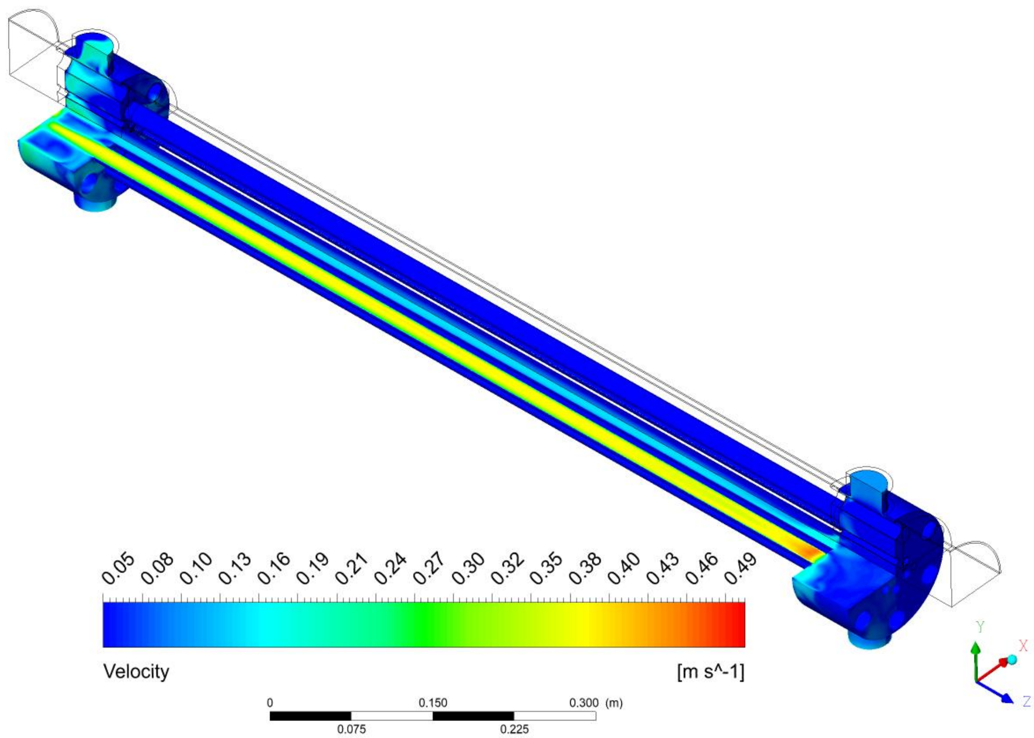

Figure 45: Velocity contour profile of fuel in the MD

5.3.2.2 Fuel distribution zone

With an inlet velocity of 0.1 m/s the fuel enters the distribution zone from two opposite inlets and from there enters the middle core zone. Right after the inlet the fuel flow faces 12 coolant pipes distributed as per the locations shown in Figure 46. The first coolant pipes in front of the fuel flow split the flow into two halves as shown in the same figure. This elevated the fuel velocity significantly compared to other areas in the same zone.

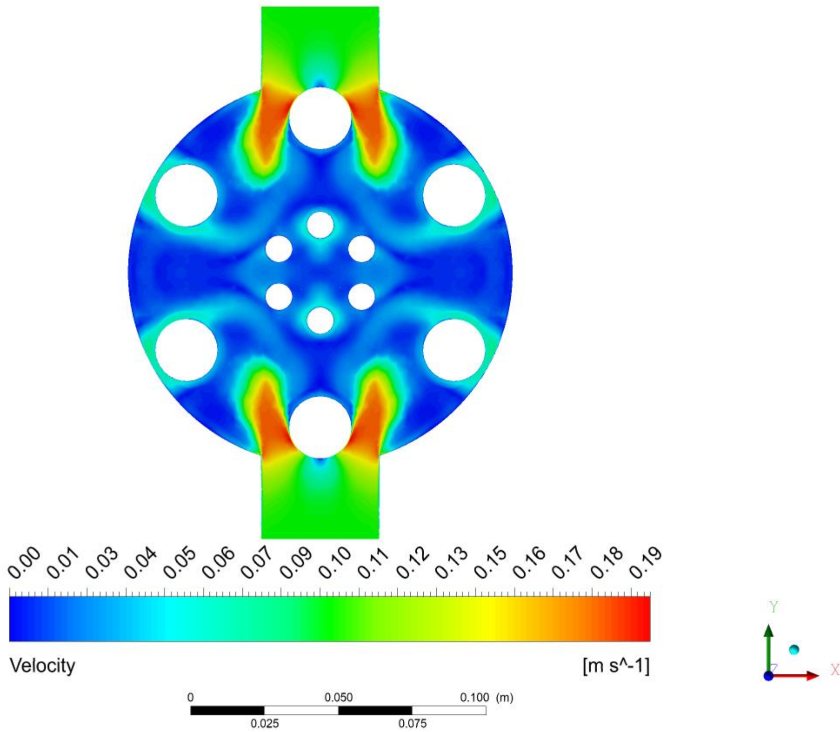

Figure 46: Fuel flow velocity in plane C-1 (distribution zone)

The fuel is now forced to pass through the fuel pipes in the core, which implies changing the direction of the flow by 90 degrees. Then due to the momentum of the flow, it tends to retain the direction and bend gradually to the direction of the fuel pipes. This creates a diagonal shape of the flow streamline (upper half of the zone) as shown in Figure 47. The reason of the diagonal shape with the fuel flow passing directly to the fuel pipes is because of the high temperature of the inlet fuel, which reflects on its density tending to direct the flow upward. The opposite of this behavior can be observed in the case of the counter flow that will be discussed in another section.

However, the flow below the diagonal (lower half of the zone) has a very low fuel velocities where in this area the flow separates from the flow heading to the fuel pipes and then circulates in the same area (lower half of the zone). This influences the heat transfer of this part of the flow, resulting in lower temperature of the fuel in this area due to the frequent circulation over the fresh cold coolant in the coolant pipes. For this reason, there is a noticeable velocity difference between the upper half of the diagonal with higher velocities and the lower half with low velocities.

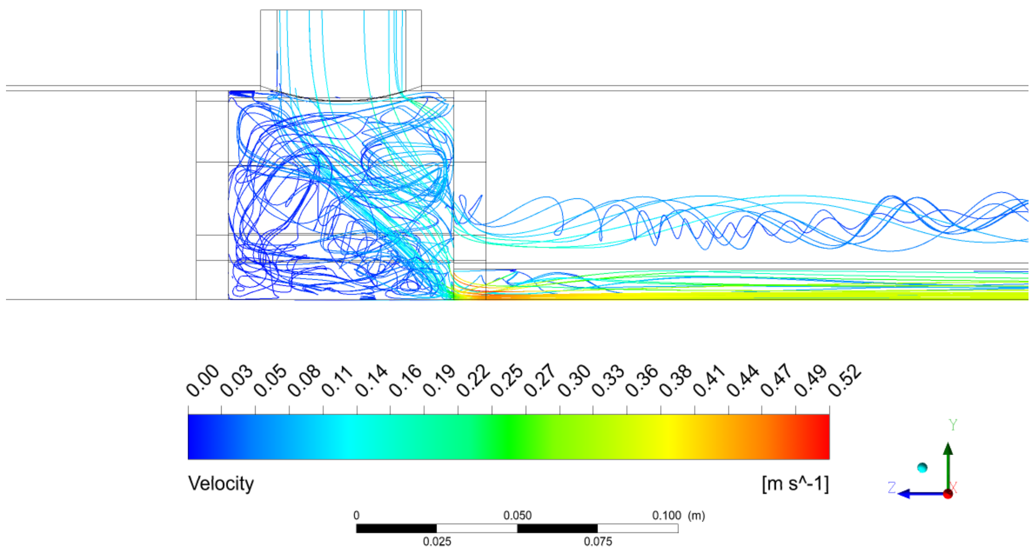

Figure 47: Fuel velocity streamlines in the distribution zone

5.3.2.3 Fuel middle core zone

Within the middle core zone, the fuel velocity in each pipe is different. Looking at the streamlines in the previously presented Figure 47 one can observe that a higher velocity is in pipes number 5 and number 6 which implies larger mass flow rate in these pipes.

Figure 48 illustrate the velocities *w* (the Z-direction with inverse rainbow color coding due to the negative Z direction of the flow) in plane B-1 with mass flow percentage in each pipe

As the mass enters the pipe in different velocities and different flow direction, as well as different mass flow rate, the flow behavior inside the pipes are as well different.

At the entrance of pipes 5 and 6, the flow has a higher momentum and higher velocity that causes a quick flow separation, decreasing the flow area and increasing the flow velocity even more. In the same area of the pipe, behind the separation area, back flow eddies were observed Figure 49.

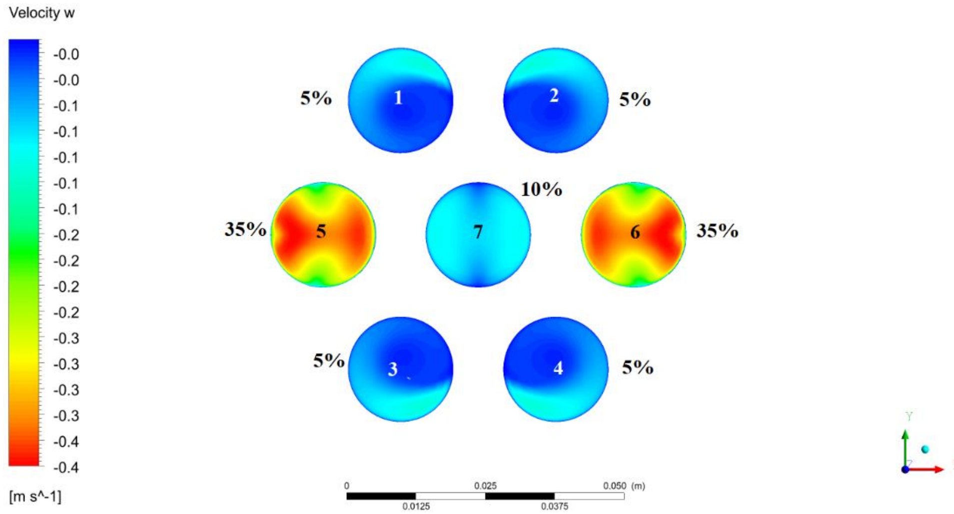

Figure 48: Fuel velocity *w* (in z-direction) profile in plane B-1 with the percentage of the coolant mass flow rate in each pipe – Inverse rainbow color code is used due to the negative z direction of the flow.

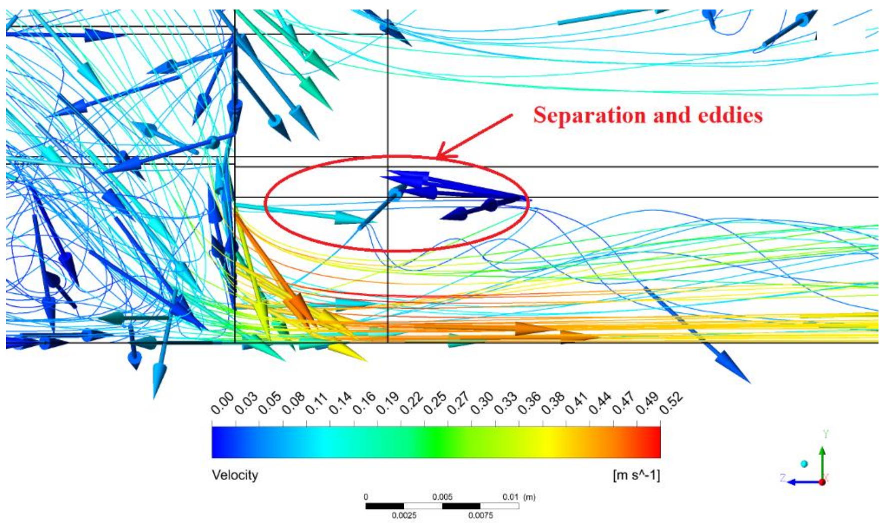

Figure 49: Fuel flow separation in pipe 5 and 6

In pipes 1, 2, 3 and 4, the modelling results showed a high swirling of the fuel flow in the first quarter of the pipes. This is due to the sharp change in the flow direction and short distance (the pipes are closer to the inlet than other pipes) which resulted in high turbulence and swirling as well as less mass flow rate entering these pipes.

Later along the pipe the swirling frequency decreases gradually. This is due to the further development of the flow based on the shear stress by the pipe inner wall, and it is expected that if the pipe was to be long enough, the swirling will tend to decline totally.

5.3.2.4 Fuel Collection zone

In this zone the flow enters from the middle core zone with a higher velocity in pipes 5 and 6 and lower velocities in the other pipes. The high velocity from pipes 5 and 6 continues carrying the flow momentum through the zone. This -jet like- flow effect makes the flow hit the separation disc with high velocity then change direction to the fuel exit with a relatively high speed in the range of 0.1 to 0.2 m/s. This velocity is larger than the inlet velocity of the fuel, this is due to the smaller flow outlet area caused by the flow separation. The rest of the outlet area in this case was left for backflows and circulation of some of the exiting flow.

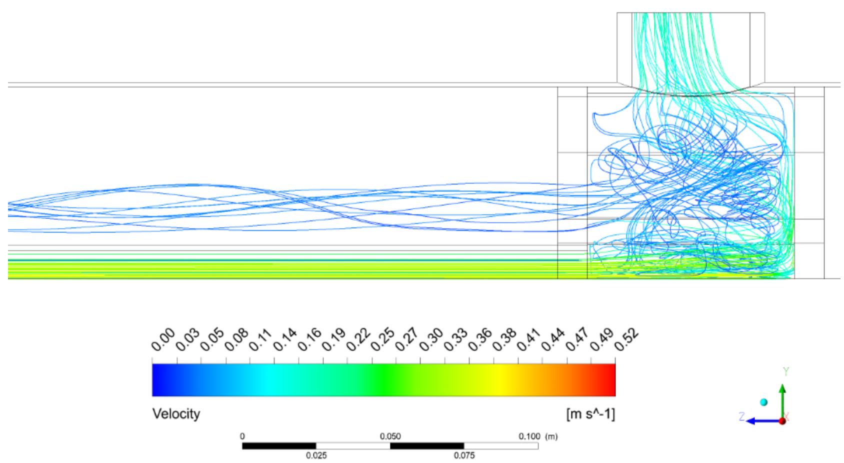

Figure 50: Coolant velocity streamlines in the collection zone.

5.3.2.5 Coolant Global Overview

The coolant in the MD core enters with 0.5 m/s as per the current design boundary conditions. The flow is then divided into 12 pipes, each six of the 12 pipes have a different diameter (six with larger diameter and the other six with smaller diameter located closer to the centerline of the MD and surrounded with the larger diameter pipes. Dimensions of the pipes can be found in Table 2 Dimensions of the DFR mini demonstrator core. The velocities and mass flow rates in the pipes are different as well in the case of the coolant. Figure 51 shows the coolant velocity profile contours in three quarters of the domain. The velocity varies from close to zero in some spots up to more than 5 m/s in some others (for example coolant pipes in both distribution and collection zones).

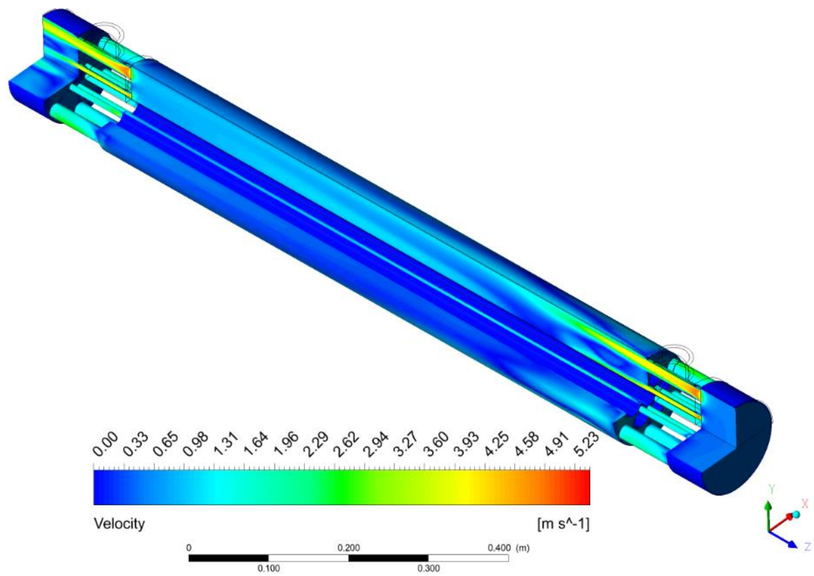

Figure 51: Coolant velocity profile contours

5.3.2.6 Coolant distribution zone

Although the coolant pipes in this zone have different diameters, a similar velocity profile pattern was found in all pipes Figure 53. This is expected as the coolant inlet direction is parallel to the coolant pipes, so no effect from direction changes or any other obstacles in the flow front Figure 52. This is unlike the fuel case where the coolant pipes in the distribution/collection zones exist as well as the sharp change in the direction.

Figure 53 shows the coolant velocities in the pipes in plane C-1. The figure also shows the percentage of the mass flow rate in each of the coolant pipes in this zone. The mass flow rate was found to be very similar per pipe size. The mass flow rate ratio between a large and small diameter pipe is equal to 5.6 while the diameter ratio between the large and small pipe is equal to 2.3.

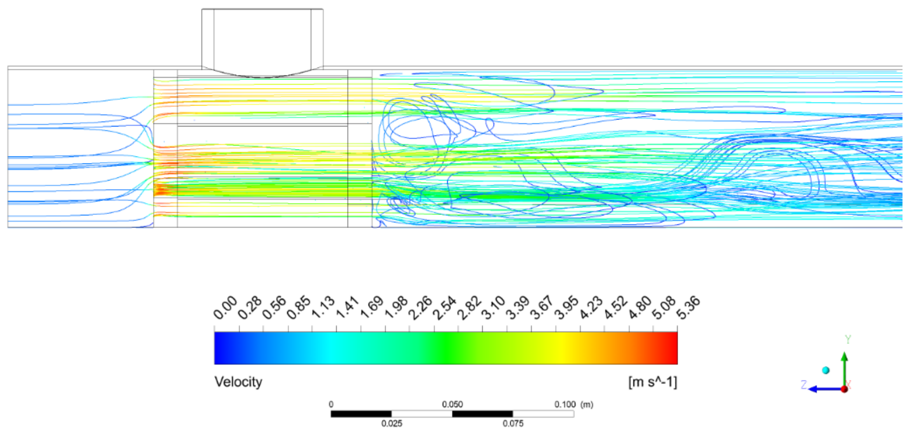

Figure 52: Velocity streamlines of coolant in the distribution zone.

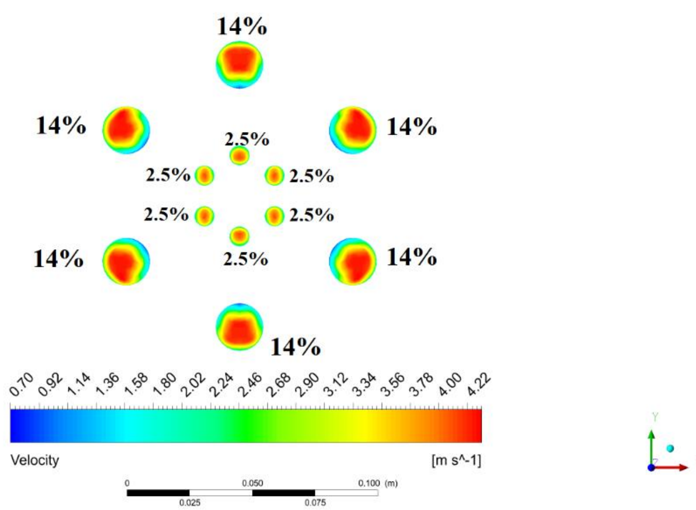

Figure 53: Coolant velocity contours in plane C-1 with mass flow percentage in each pipe.

5.3.2.7 Coolant middle core zone

The coolant in this zone suffers a lot of turbulence in the first quarter of the middle core. This is due to the sudden change in the flow cross sectional area, in addition to the fuel pipes located in-between the coolant flow. Also, the different velocities and mass flow rate in the two different diameter pipes causes anisotropic pressure in this area of the middle core which enhances the turbulence in the favor of heat transfer as discussed in the previous section. This turbulence can be captured through Figure 54 which shows that at the beginning (line-1) the flow velocity is high and random with backflow in different areas occur with negative velocity sign (Red color is backflow in the + direction of z-axis). This can also be noticed in Figure 55 which shows the velocity in the negative Z direction (*w*). From these figures one can observe that the velocities of the coolant along the middle core zone are in the same value range and have a similar profile with the first quarter as an exception.

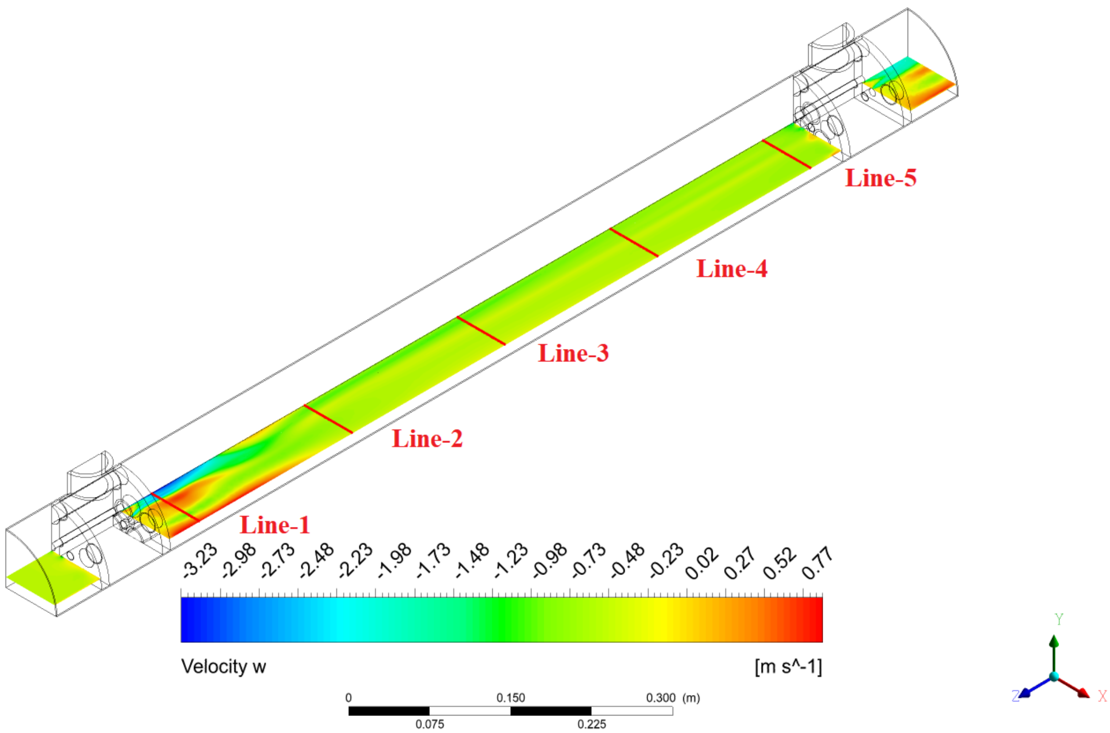

Figure 54: Velocity *w* (z- direction) contours of the coolant domain in the plane passing through Lines 1-5, – Inverse rainbow color code is used due to the negative z direction of the flow.

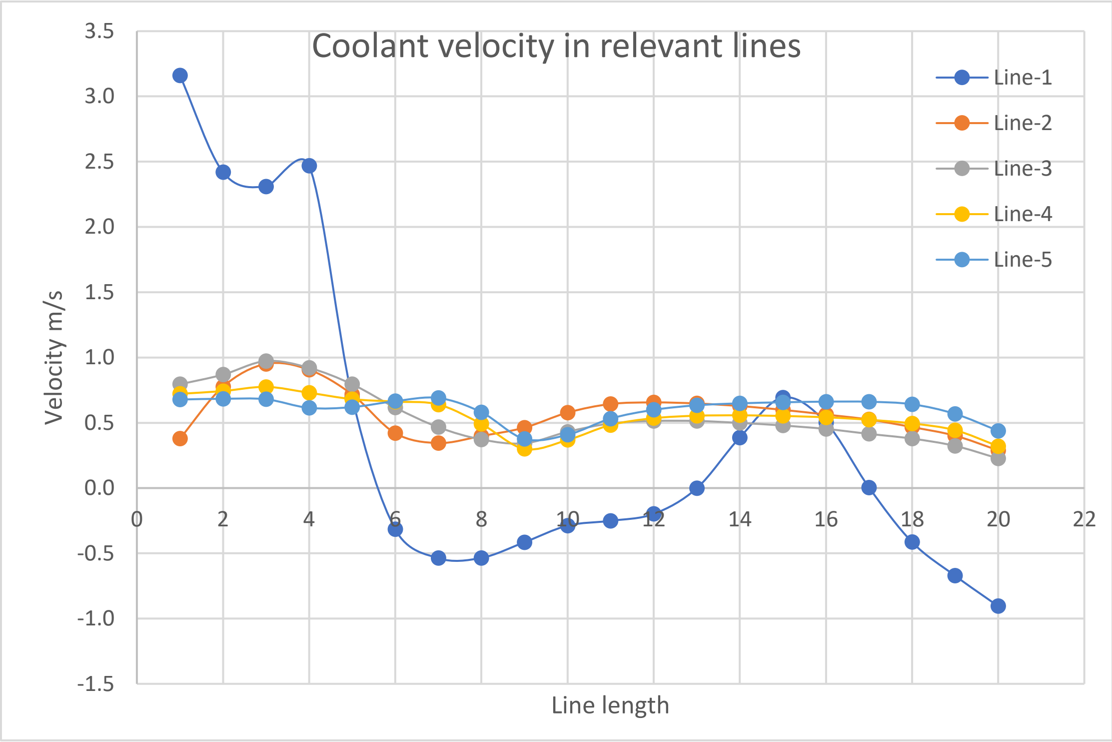

Figure 55: Coolant velocity variation in the middle core zone for the relative lines (1-5)

5.3.2.8 Coolant collection zone

In the collection zone the coolant has similar velocity values to that of the distribution zone, which means that the average mass flow rate percentage of each pipe is as well close to the ones in the distribution zone Figure 56. This is despite that fact, the velocity profile in the pipes has a crescent shape unlike the ones in the distribution zone where the higher velocities were in the middle of the pipe. Finally, the coolant exits the MD core again in a jet-like velocity profile with a highest velocity more than 0.7 m/s.

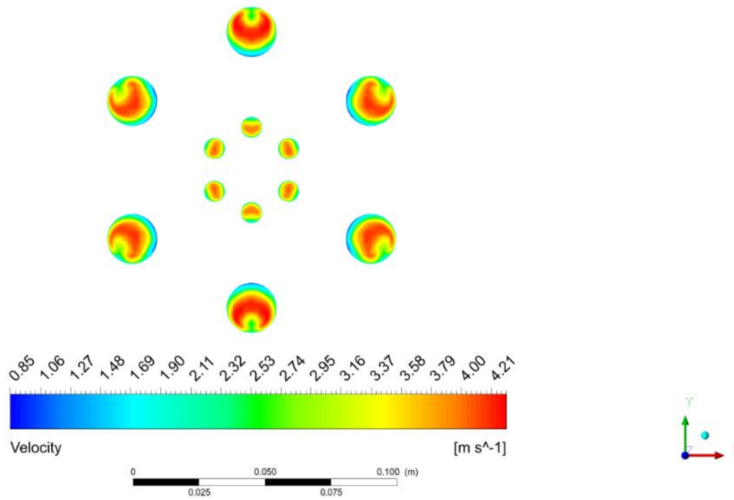

Figure 56: Coolant velocity contours in plane C-2 (collection zone)

5.3.3 Discussion

The heat transfer in the parallel flow case is highly affected by the direction of gravity which is in the opposite direction of both fuel and coolant flow directions.

The direction of the fuel in the distribution zone from the MD core inlet to the fuel pipes is the upwards direction. Two physical factors affected the direction of the fuel, the first is the position of the fuel pipes inlets (upper), the second is the buoyancy force of lower density fuel (due to high temperature). Both forces add up to direct the fuel to the fuel pipes inlet. Another geometrical factor had an important effect on the flow parameters. The existence of a coolant pipe in the exact front middle of the fuel direction caused the fuel flow to split into two halves. The combination of all these factors led the fuel flow to have a higher inlet velocity in some of the pipes, and lower velocity in other pipes. This has its effect on the mass flow rate in each pipe, and the heat transfer accordingly. It was observed that pipes number 5 and 6 together have 70% of the fuel mass flow, and a similar percentage of heat transfer within the middle core zone. Although in the DFR case, the heat generation occurs within the fuel pipes in the middle core zone, which will have a different effect on the flow and temperature distribution, still the same effect might be found as in the MD due to the expected higher temperature of the fuel compared to the coolant, in addition to the buoyancy forces of the heated fuel in the fuel pipes. The exact percentage is not expected to be found in the DFR, but it is expected to have ununiform mass flow rate distribution as well as heat transfer for similar reasons.

The incorporation of CFD analysis in a three-dimensional (3D) framework for the DFR is essential when coupled with a 3D neutronic analysis of the reactor. This coupling enables a bidirectional feedback loop, enhancing the comprehension of the reactor's behavior across diverse operational conditions. Although such investigations remain to be conducted in future endeavors, they hold promise in advancing our understanding of the DFR and its performance characteristics.

Due to the same mentioned observations, the fuel in the distribution zone was split into two volumes, one with the fuel passing from the inlet to the fuel pipes. This volume has a higher temperature and velocity. The other is the fuel circulating around the coolant pipes at a low velocity resulting in much lower temperature circulating flow. The heat transfer occurred in the middle core zone mostly existed in the first quarter, where the fuel was still retaining some of its high temperature. In the case of DFR, some of these conditions exist, which gives an idea about the expected flow and heat transfer within the reactor core.

A high swirling phenomenon is observed in certain fuel pipes, specifically pipes 1, 2, 3, and 4. This can be attributed to the variations in fuel entrance angles resulting from the different positions of the fuel pipe inlets in relation to the MD fuel inlet. This swirling pattern gradually lost some of its frequency along the fuel pipes. This behavior is highly affected by the type of the flow, the diameter of the pipe and inlet velocity magnitude and direction[53]. Although swirling has a positive impact on heat transfer enhancement, such swirling patterns might result in three main different types of problems. The first problem is mechanical vibrations, such vibrations could have a great impact on the pipe's mechanical stability in the long term especially if the swirling has a high swirl number[54][55]. This applies for circular and non-circular pipes[56]. A second drawback of the observed swirling is the higher corrosion rates. Where flow swirling occurs, a higher rate of shear stresses over the pipe wall is observed causing high rates of corrosion[57]. This effects the life of pipe material that tends more to failure, especially if this effect is to be added to the previous mechanical one[58]. Swirling has its impact on the pressure drop (increases) in pipes, which affects the mass flow rates in such pipes influencing the heat transfer and the temperature distributions[59]. This swirling phenomenon wouldn't be clearly observed if the modelled geometry was in 2-D. This fact raises the importance of the 3-D analysis in such complicated geometries.

The occurrence of swirling in the DFR core needs to be examined by considering the geometric and physical flow parameters specific to the DFR. Accurate analysis is required to determine if swirling in DFR will have a high impact on the reactor operation and safety. It is anticipated that certain pipes in the DFR may experience this phenomenon due to similar reasons observed in the MD case. Thus, the MD can be a good facility to examine such behavior, regardless of the size of the facility compared to the actual DFR. However, the use of flow straighteners discs in this zone, such as honeycombs, could potentially ensure a more uniform flow distribution at the inlets of the fuel pipes and can help reducing swirling[60].

In the same zone, coolant pipes in front of the fuel inlet resulted in a hot spot on one side of the coolant pipes. Such a setup is clearly not optimal due to several reasons. The first reason is mechanical reason; represented in high expansion of the pipe in a small area, this will cause high thermal stresses which will make the pipes tend to failure much faster than the expected life of other pipes. Another mechanical problem is due to the possible change in the fuel temperature, this will cause a direct expansion fluctuation especially on these specific pipes, causing fatigue stresses resulted from the continues change in the spot temperature[61][62]. Corrosion of these coolant pipes is another problem which is more likely to occur when compared to other coolant pipes in the same zone. This is because the coolant pipes are facing the momentum direction of the fuel flow right after entrance, increasing the shear stresses on the surface while fuel in this area has its highest temperature value[63]. These problems can be significantly reduced if the fuel inlet was to be shifted to a suitable distance so that the fuel flow will not be distracted by the coolant pipes by the entrance. The suggestion won't only help solve the mentioned problems, but it will also help in solving the swirling problem mentioned earlier. This is because the fuel flow will not suffer an early split right after the entrance, which was a reason of the high velocity and an angle that most likely helped in the swirling problem creation. More detailed studies can be useful in this point.

Once more the effect of the fuel flow inlet direction in the distribution zone reflects its impact on the coolant in the middle core zone. Due to the high temperature and high velocity of the fuel in specific pipes (not the central pipe), the highest coolant temperature isn't in the middle of the core. This is due to the relatively lower temperature of the fuel in the pipes within this area as mentioned earlier in the detailed description. Although such coolant temperature distribution is favorable when it comes to reactors safety, this effect might not exist in the case of DFR. Main reasons include the fact that the number of the fuel pipes in the DFR is much larger than in the MD (>1000 pipes), thus the high mass flow concentration observed in the MD might not be as significant in the case of the DFR. However, a detailed analysis of this should be explored.

5.4 Counter flow

In the context of heat exchangers, the term "counter flow" pertains to a particular flow configuration characterized by the direction of the hot and cold fluids within the exchanger. In this arrangement, the hot and cold fluids enter the heat exchanger at opposite ends and subsequently travel towards each other. This specific flow pattern enhances heat transfer between the two fluids as the temperature difference between them remains comparatively high along the entire length of the exchanger. Consequently, the counter flow arrangement facilitates a more efficient heat transfer process.

In the preceding subsection, a parallel flow configuration was employed. Nevertheless, the ensuing subsection will focus on a counter flow scenario and provide a comparative analysis against the parallel flow configuration. Given the minor distinctions in mass flow rates between parallel and counter flow heat exchangers due to the similar boundary conditions used by the inlet, this subsection will primarily concentrate on the discussion of heat transfer aspects.

The flow arrangement of the fuel and coolant, both in parallel and counter cases, is illustrated in Figure 57. To facilitate the observation of temperature changes along the MD core, the planes from B-1 to B-4 are utilized for comparisons of temperature contours. Furthermore, for the purpose of tracking heat transfer, the MD core is divided into five sections (Section 1 to Section 5) in addition to the previously defined three zones (distribution, middle core, and collection zones). The sections are arranged in opposite order to enable a valid comparison of heat transfer between the two cases, ensuring that the highest temperature difference is accounted for.

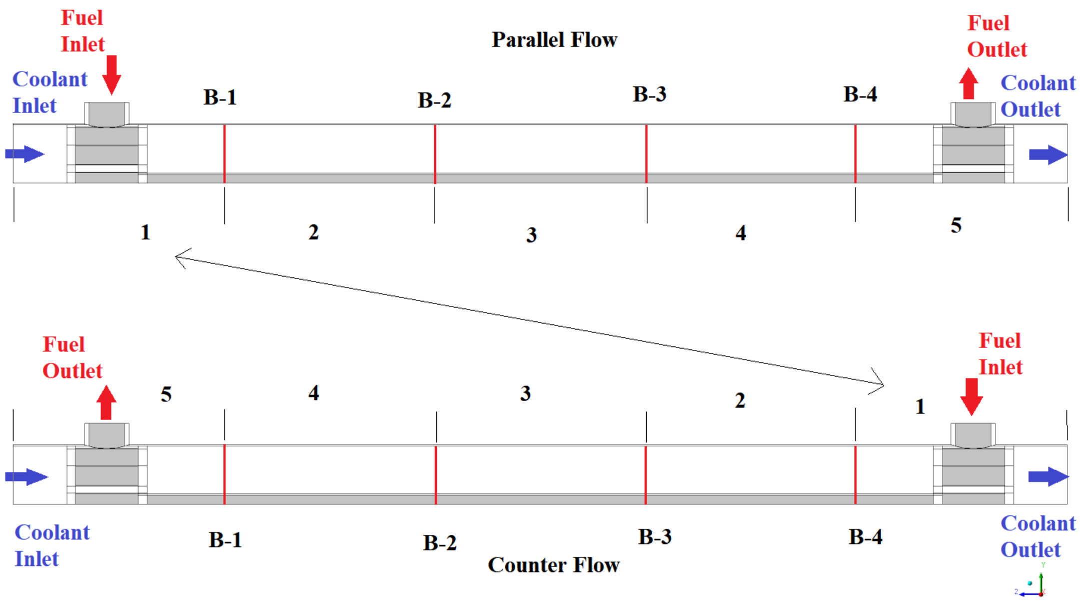

Figure 57: Parallel and counter flow (sections of comparison)

5.4.1 Fuel analysis

Although the same inlet fuel temperature in both parallel and counter flow cases is used (T_{in} = 1473 K), the flow enters the fuel pipes in different temperatures and conditions when comparing the two flow cases. The flow in the parallel flow case tends to move directly from the inlet to the fuel pipes (upwards) due to its high temperature and lower density (compared to fuel density after cooling). Oppositely, in case of the counter flow the fuel pipes inlets are in the bottom of the collection zone (fuel enters from the collection zone in case of the counter flow), however, the fuel flow is still directed upwards due to the same reason mentioned in the case of the parallel flow (lower density). Figure 58 shows this behavior.

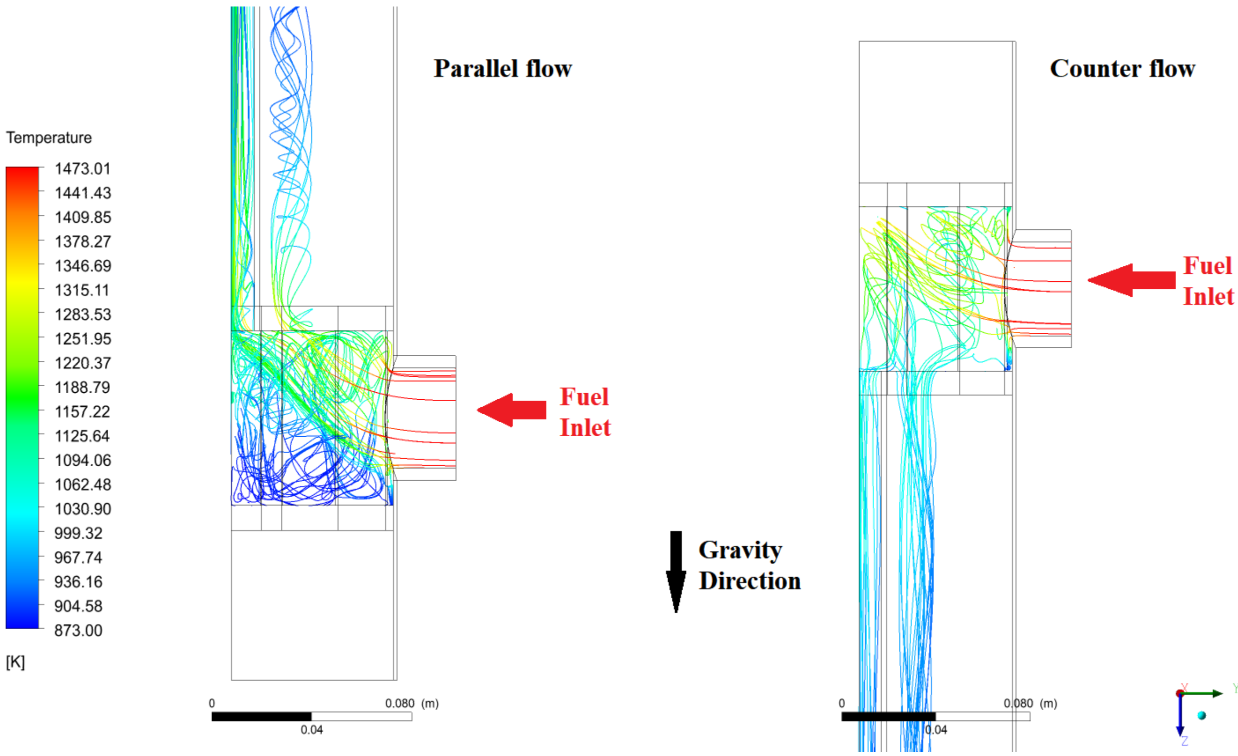

Figure 58: Fuel flow streamlines with temperature color coded by the fuel inlets in parallel and counter flows configurations.

Due to the mentioned behavior, in case of counter flow the fuel has to firstly move upwards then is forced to the bottom direction to enter the fuel pipes. This scenario made the fuel go through a longer pass in the collection zone which results in a better heat rejection in the fuel as well as a more uniform temperature distribution.

shows the differences in the fuel inlet conditions to the fuel pipes in the two cases (parallel and counter flows). It is observed that in the parallel flow the temperature is higher in some pipes, and lower in other pipes (nonuniform temperature distribution) compared to the counter flow case which has a uniform temperature distribution and profiles.

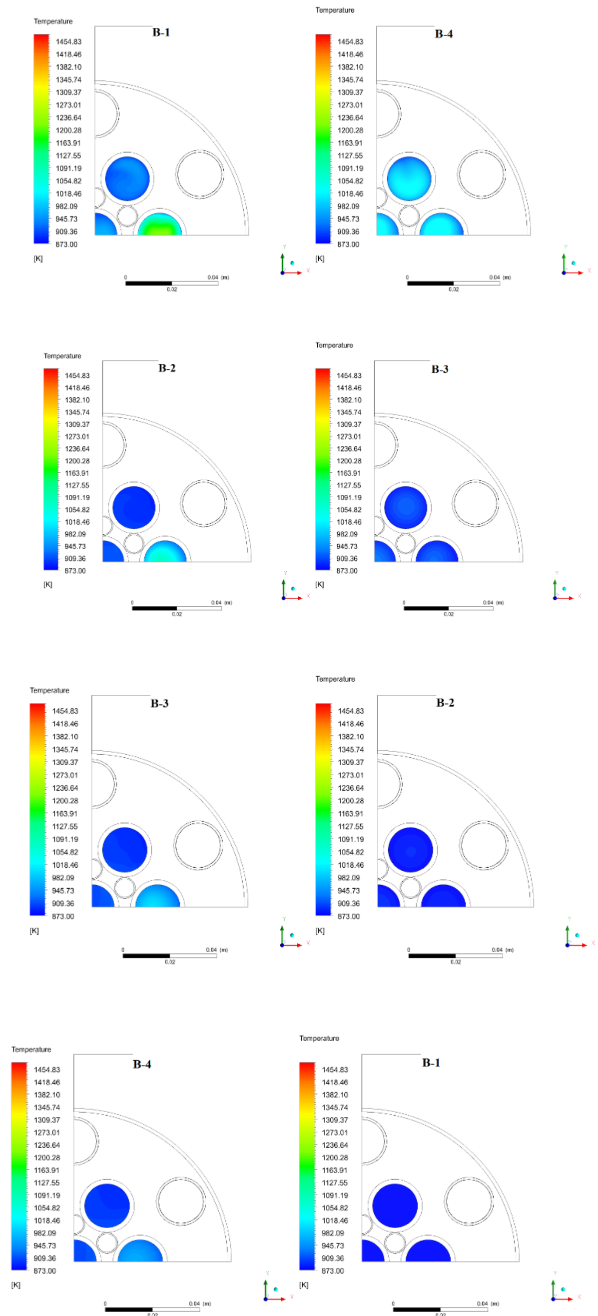

Figure 59: Fuel temperature contours; parallel flow B1 to B4 (left), Counter flow B4 to B1 (right)

Also in the fuel temperature stays relatively higher in some of the pipes in case of the parallel flow along the whole middle core zone. However, the temperature is quickly rejected in the case of the counter flow in early stages when compared to the parallel flow.

The Fuel velocity profile by the fuel pipes inlets in the counter flow case is much more uniform compared to the parallel flow. This is because what is mentioned before; that the flow isn't directly entering the fuel pipes with a high momentum in a sharp angle as in the case of the parallel flow, but rather going through a longer pass where the velocity has time to stabilize and become more uniform before entering the fuel pipes Figure 60.

The same reason significantly reduced the swirling occurred in the parallel flow Figure 61. With low swirling in pipes in addition to a uniform flow velocity, all result in a uniform mass flow rate in fuel pipes.

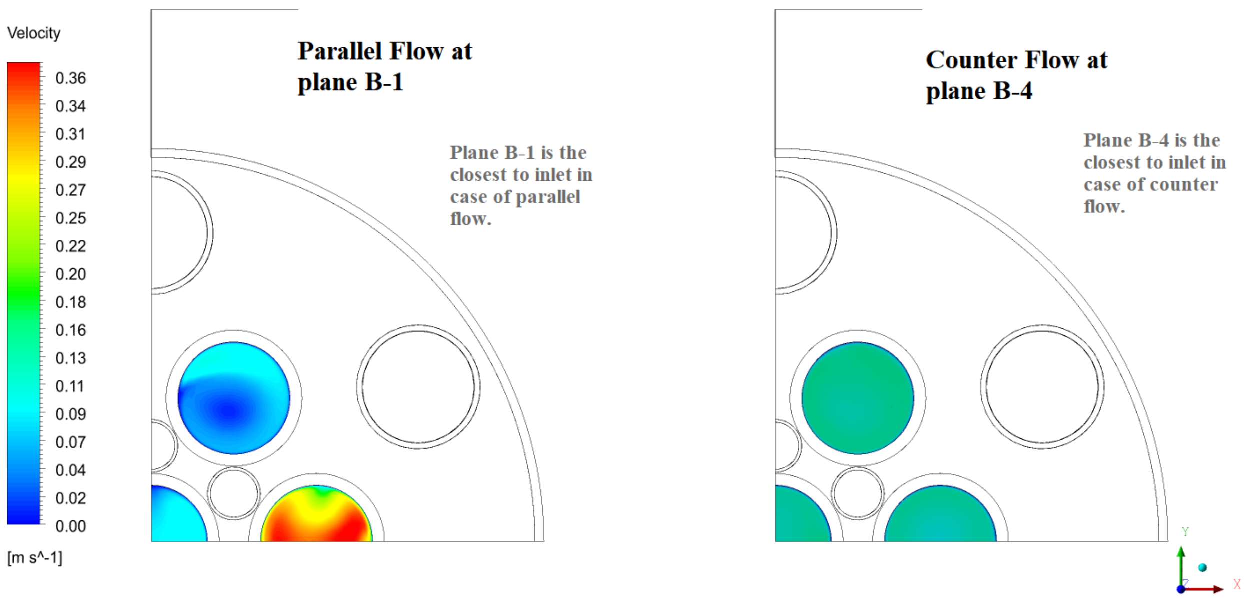

Figure 60: Velocity inlet to fuel pipes in plane B-1 (parallel flow-left), plane B-4 (counter flow-right)

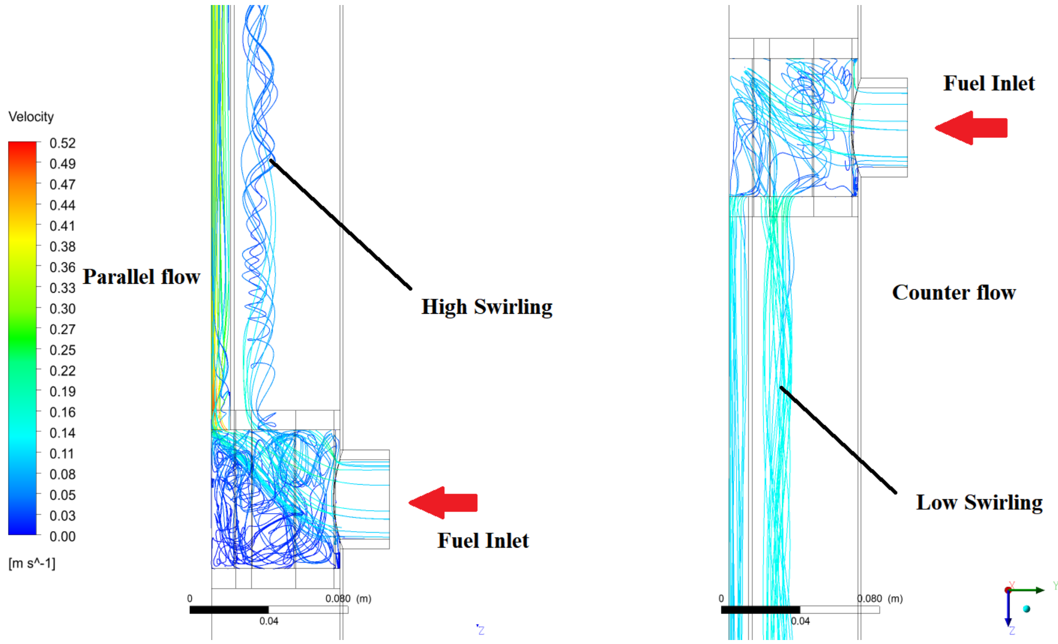

Figure 61: Fuel velocity streamline showing swirling in fuel pipe.

5.4.2 Coolant analysis

The disparity in temperature variation between the parallel and counter flows in the coolant side stems from the fact that, in the counter flow condition, the majority of the coolant temperature rise occurs primarily during the later stages (from B-4 to the coolant outlet). This stands in contrast to the parallel flow configuration where the coolant experiences a more gradual temperature increase Figure 62. However, it is crucial to note that even in the parallel flow case, substantial heat transfer takes place within the distribution zone and the initial quarter of the middle core zone (from the coolant inlet to B-1) as shown earlier in Table 11.

The observed behavior can have unfavorable implications from both material and mechanical perspectives. The presence of sharp temperature gradients within a confined area can potentially give rise to various drawbacks, particularly concerning the mechanical stability of the structure.

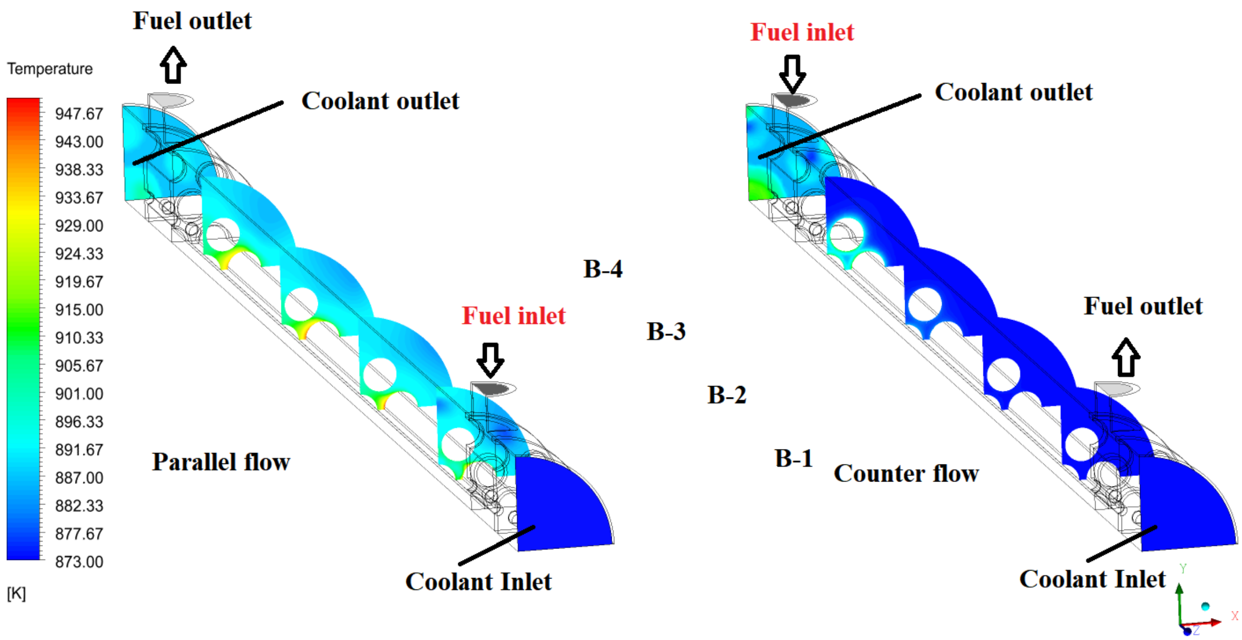

Figure 62: Coolant temperature contour profile in planes B-1 to B4; parallel flow (left), counter flow (right)

Given that the direction and velocity of the coolant in both parallel and counter flow cases remain constant, the dissimilar temperature gradients between the two configurations have minimal impact on the velocity and mass flow rate within various pipes. As a result, the discussion pertaining to the effects on velocity and mass flow rate will be omitted due to their negligible significance.

5.4.3 Global overview

In contrast to the parallel flow case, the counter flow configuration exhibited a significant amount of heat transfer primarily within the collection zone, specifically in close proximity to the fuel inlet. Comparatively, a lower amount of heat transfer took place within the middle core zone, while a negligible amount was observed in the distribution zone located just before the fuel outlet Table 12.

Table 12: Heat transfer per zone (counter flow case)

Zone	Heat transfer per zone [kW]	Heat transfer percent per zone
Collection zone	33.9	72.15%
Middle core zone	13.0	27.59%
Distribution zone	0.1	0.26%
Total	47.0	100%

In the case of the counter flow configuration in the MD core, the temperature variation exhibits an inverse pattern compared to that of the parallel flow, albeit with minor discrepancies in values Figure 63. By referring to the comparative sections depicted in Figure 57, it is evident that the rejection of fuel temperature as well as the temperature gain by the coolant predominantly occur during the initial contact of the two fluids. This can be attributed to the substantial temperature difference between the two fluids.

Notably, in the counter flow case, there is a slightly greater decrease in fuel temperature despite the coolant entering this section (section 1) at a higher temperature compared to the parallel flow case. This can be attributed to the effective mixing that takes place withite3n this section, facilitating enhanced heat transfer and resulting in the observed reduction in fuel temperature Figure 64.

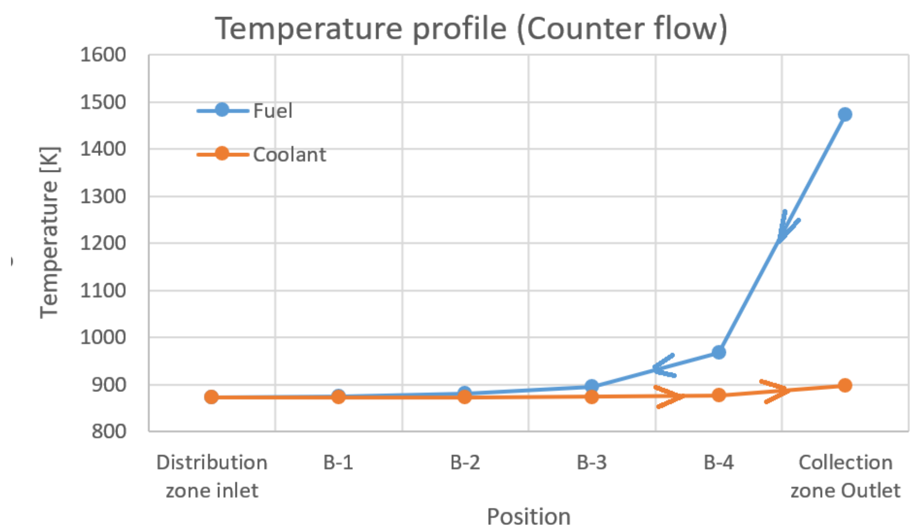

Figure 63: Area averaged temperature profile in case of counter flow

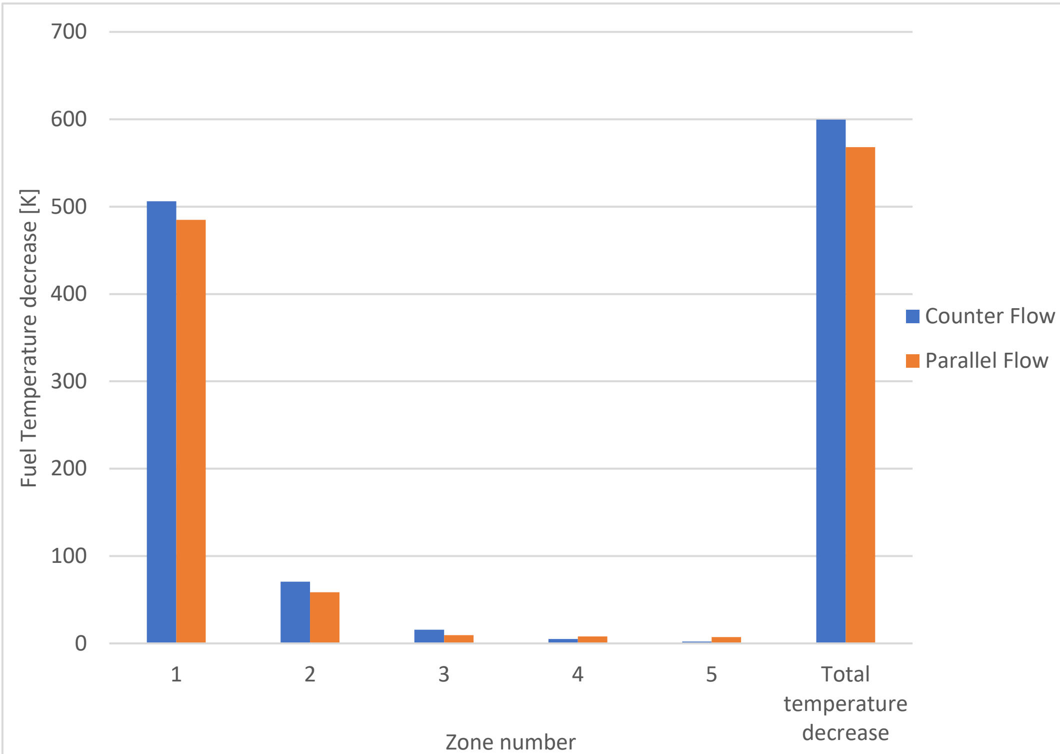

Figure 64: The decrease in fuel temperature in each section (1-5) in case of parallel and counter flows

The discrepancy in temperature rejection between the counter and parallel flow configurations across various zones/sections is directly attributed to the variation in heat transfer rates observed in each respective case and zone/section.

Figure 65 presents a comprehensive overview of the heat transfer rate distribution within the three zones of the MD core. Upon examination, it is evident that in the parallel flow case, over 90% of the total heat transfer transpires within the initial two sections, with the middle core zone accounting for the largest portion (55%), followed by the distribution zone (40%).

Nonetheless, in the counter flow scenario, the collection zone exhibits the greatest proportion of heat transfer, amounting to approximately 70%, while the middle core zone contributes around 27%. Overall, it can be concluded that the heat transfer performance in the counter flow case, under the specific parameters studied, is marginally superior to that of the parallel flow case.

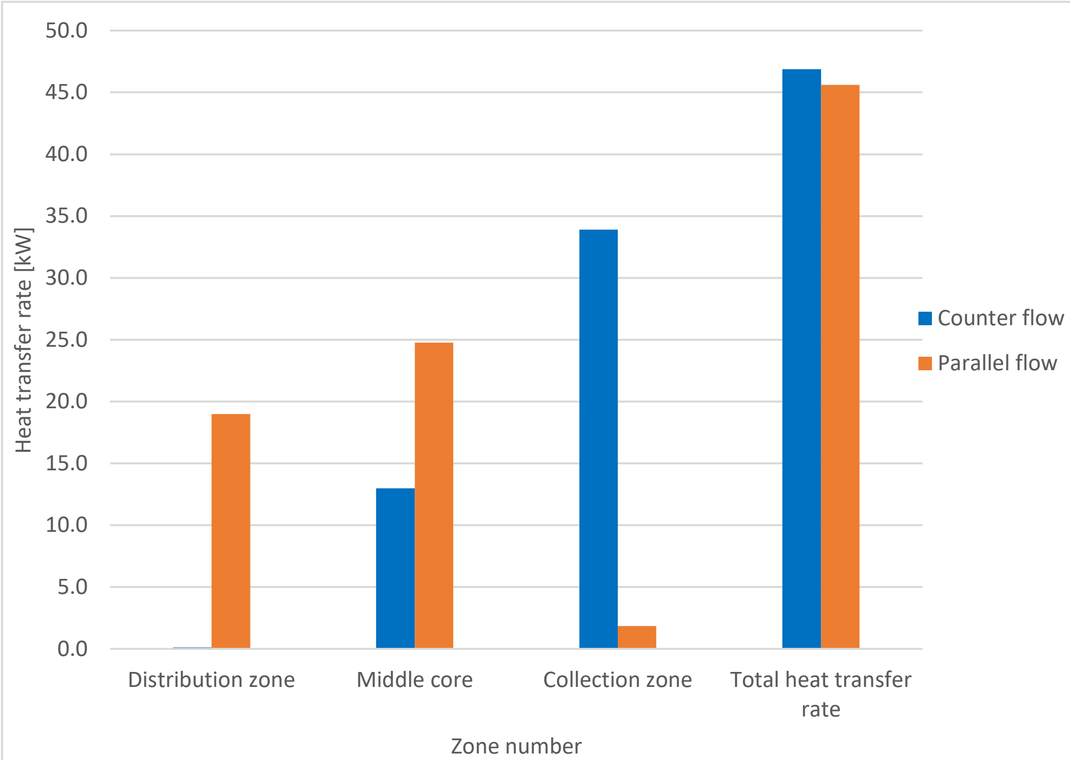

Figure 65: Comparison of heat transfer rate per zone in case of paralle and counter flows

5.4.4 Discussion

While the primary distinction between parallel and counter flows lies in the direction of the two fluids in the heat exchanger, the flow structure in the current case specifically reveals another notable difference. This difference is associated with the direction of the fuel flow after entering the MD core. In both cases, the hot fuel enters the core and tends to move in an upward direction due to its high temperature and resulting low density. In the parallel flow configuration, the fuel forms a diagonal barrier splitting the zone into high temperature volume (upper) and lower temperature volume (bottom). The high temperature volume extends from the inlet towards the upwardly positioned fuel pipes. Conversely, in the counter flow arrangement, the entrance to the fuel pipes is located at the bottom of the collection zone. This distinction has a significant impact on both the flow behavior and heat transfer characteristics.

From the perspective of heat transfer, it is observed that the fuel undergoes an extended journey, taking a longer path from the inlet, moving upwards, and then downwards before entering the fuel pipes. This prolonged path results in a significant loss of temperature and heat by the fuel, primarily occurring within the collection zone of the MD core. As a consequence of this fuel flow behavior, the coolant temperature experiences a sharp increase within the same zone.

From the flow perspective, the long path followed by the fuel from the MD core inlet to the pipe's inlets caused the flow to lose its straight direct high momentum vector that occurred in the parallel flow. Which reduced the high local momentum and velocity in the case of the counter flow, unlike the parallel flow where it caused a large difference in the velocities and mass flow rates in pipes letting the flow to enter the fuel pipes with uniform velocity and mass flow rate.

In the parallel flow a high swirling was observed in some of the pipes, in the counter flow case the swirling effect has been significantly reduced due to the more uniform inlet velocity magnitude and direction into the fuel pipes.

The counter flow case exhibits a slightly higher total heat transfer rate compared to the parallel flow case. Furthermore, upon examining the coolant temperature profile, which encompasses a larger domain characterized by relatively lower temperatures, one can anticipate an even more efficient heat transfer in the event of the case(s) of velocity or temperature variations in the fuel and/or coolant if these variations are to lead towards more heat transfer.

5.5 Measuring Instruments

In experimental flow analysis, the positioning of measuring instruments plays a crucial role in obtaining accurate and representative data. The selection of instrument locations depends on the specific objectives of the analysis and the flow characteristics being studied. Generally, measuring instruments should be strategically placed at locations that provide relevant information about the flow parameters of interest.

The main measuring instruments in the MD loops were highlighted in Figure 3. Considering more design details, more instruments shall be added, however this is not a part of this work due to the lack of the full detailed design of the MD loops. In this section, only for the MD core will be discussed in terms of the measuring instrument's locations based on the CFD analysis and observations.

To acquire significant data for conducting an extensive analysis of flow and heat transfer phenomena, as well as for the purpose of validating computational codes and models, this section will not only propose suitable positions for the installation of measurement instruments but will also provide recommendations on locations to be avoided. Furthermore, a list of commonly utilized devices will be mentioned, accompanied by a brief overview of their operational principles to aid in the device selection process. Additionally, challenges that should be considered when contemplating the implementation of these devices will be emphasized. In certain instances, attaining access to a particular location of interest may pose challenges, particularly in complex geometries such as MD. In such scenarios, it is necessary to reevaluate the situation and explore alternative approaches. This may involve selecting a different location for measurement, employing a different measuring device, or accepting a less precise methodology.

The ultimate selection of devices as well as the methodology for placing the device junctions/probes/sensors in specific locations will be deferred for subsequent investigations and is beyond the scope of this work.

5.5.1 Temperature Measuring Instruments

Several instruments can be used to measure temperature in high-temperature molten metals. Some commonly employed instruments include:

Thermocouples: Thermocouples are widely used for temperature measurements in high-temperature environments. They consist of two dissimilar metal wires joined together at one end. The temperature difference between the junction and the reference end generates a voltage, which can be correlated to the temperature.

Radiation pyrometers: Radiation pyrometers are non-contact temperature measurement devices that detect the thermal radiation emitted by the molten metal. They can be used to measure surface temperatures accurately without physically contacting the metal.

Optical pyrometers: Optical pyrometers also measure temperature based on the thermal radiation emitted by the metal. They utilize the principle of color temperature to determine the temperature by comparing the color of the emitted radiation to a calibrated scale.

Infrared thermometers: Infrared (IR) thermometers use infrared sensors to measure the temperature of molten metals without contact. They detect the thermal radiation emitted by the metal and convert it into a temperature reading.

Optical fiber thermometers: Optical fiber thermometers employ optical fibers to transmit temperature measurements from the high-temperature environment to a remote location. They can be used for real-time temperature monitoring in challenging environments.

It is important to select the appropriate instrument based on the specific requirements of the application, such as temperature range, accuracy, response time, and accessibility to the measurement location.

The above-mentioned instruments are able to measure the temperature with acceptable accuracy. These can be useful to measure the outside surface temperature of pipes and construction elements as they are classified as non-contact devices. However, measuring the temperature distribution inside the molten metal flow in the pipes is more challenging. This is because most of these devices depend on the reflected waves measurements, which in case of the molten metal reflects only the outer pipe/flow surface. More challenges and problems might be found when measuring the temperature of molten metals. Some common issues include:

Contact with the metal: Directly inserting a temperature sensor into the molten metal can cause the sensor to melt or corrode, leading to inaccurate temperature readings. The high temperature and corrosive nature of the molten metal can damage the sensor.

Heat transfer effects: The presence of the temperature sensor in the pipe can affect the heat transfer characteristics of the molten metal. It can alter the flow patterns, disturb the thermal equilibrium, and introduce measurement errors.

Inaccessible locations: In some cases, the location of the molten metal within the pipe might be challenging to access physically. This can make it difficult to install temperature sensors or retrieve accurate measurements. A good example is the fuel pipes in the MD middle core zone.

Radiation interference: Molten metals often emit thermal radiation, which can interfere with temperature measurements. This radiation can affect the accuracy and reliability of non-contact temperature measurement techniques such as infrared or optical pyrometers.

Rapid temperature changes: Molten metals can exhibit rapid temperature changes due to their high thermal conductivity. This can make it challenging to capture and measure the exact temperature at a specific point in the pipe.

To overcome these problems, specialized temperature measurement techniques and instruments designed for high-temperature environments may be required. These instruments should be able to withstand extreme conditions, provide accurate measurements, and minimize interference with the molten metal flow. Careful consideration and selection of the measurement method and sensor design are essential to ensure reliable and accurate temperature measurements in molten metal pipes.

Thermocouples emerge as a highly viable and practical solution for temperature measurement within the flowing molten metal, taking into account the aforementioned complexities. Overcoming these challenges, thermocouples can be seamlessly integrated into the MD core pipes by means of a capillary tube spanning the length of the pipe. This facilitates the strategic placement of multiple thermocouples, enabling the capture of temperature data across various points within the cross-section of the pipe.

Accurate calibrations are essential for assessing the potential errors arising from the presence of thermocouples within the flow, and their impact on velocity measurements and heat transfer.

5.5.1.1 Locations of Interest for Temperature Measurements

In order to ensure accurate temperature measurement, it is crucial to monitor the temperature at the inlet and outlet points of both the fuel and coolant. However, in scenarios characterized by significant turbulence or pronounced buoyancy effects, the outlets may experience backflows originating from the downstream flow. These backflows might be in a different temperature and can lead to variations in the measured temperature compared to the actual outlet temperature of interest, thereby impacting the precision of temperature measurements. Consequently, it is advisable to capture the outlet temperature immediately after it exits the final region where significant heat transfer is considered.

The number of junctions in each pipe may vary according to the possibility considering the small size of the pipes. However, to capture the temperature profile with minimum number of junctions it is recommended to have at least 3 junctions across each pipe diameter.

Note

1. The number of junctions depicted in the accompanying figures does not necessarily indicate the precise recommended count of junctions, but rather denotes the suggested positions for optimal placement.
2. It is essential to ensure that the junctions do not directly adhere to the inner wall of the pipes. This precaution is necessary to mitigate the influence of pipe temperature, which may differ from the temperature of the fluid being measured. For instance, in cases where fuel pipes come into contact with coolant, the pipe temperature could be higher than that of the fluid. Conversely, when fuel pipes interact with fuel, the pipe temperature could be lower. To address this issue, a small gap should be introduced between the junctions and the pipe wall, enabling temperature measurement within the boundary layers.

In Figure 66 the temperature measuring junction lines are located according to the previously mentioned considerations. Table 13 Summarizes the used abbreviations.

If counter flow case to be tested experimentally, then the backflow conditions shall be considered as well by locating additional junctions in the locations where backflows expected to have a significant effect on the temperature.

Table 13: Instruments location abbreviation (Inlets/Outlets)

Junction line/point	**Location**
F-1	Fuel inlet
F-2	Fuel outlet
CL-1	Coolant inlet
CL-2	Coolant outlet

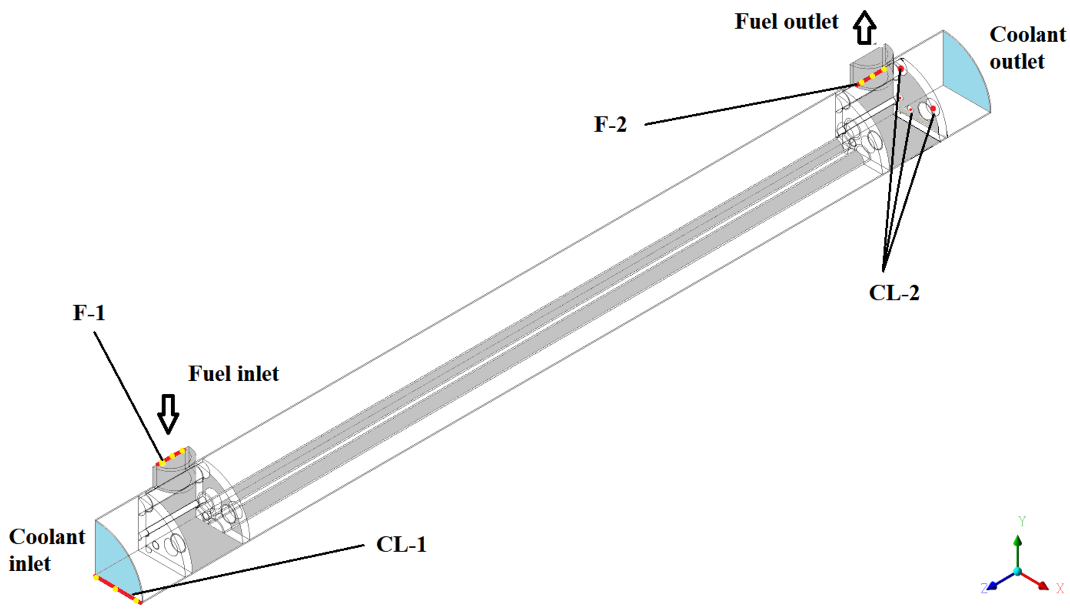

Figure 66: Inlets/outlets temperature measurment junctions locations.

The quantity of junctions in each pipe can vary due to constraints imposed by the small size of the pipes. Nonetheless, in order to capture the temperature distribution while minimizing the number of junctions, it is recommended to employ a minimum of three junctions across the diameter of each pipe.

In the case of the fuel system, the fuel inlet (F-1) and outlet (CL-1) are strategically positioned at the initial stages of the fuel/coolant flows respectively. This arrangement allows for the acquisition of temperature data pertaining to the incoming flows prior to any heat exchange interactions. This information holds significant importance for both heat transfer analysis and operational monitoring, as the fluids need to reach specific temperature thresholds before full operation can commence.

The selection of positions for F-2 and CL-2 was based on the aforementioned issue of backflow. Specifically, for CL-2, each outlet of the four coolant pipes is equipped with a minimum of one junction. This arrangement guarantees accurate measurement of the coolant outlet temperature, given that no further heat transfer occurs downstream (neglecting any heat transfer from the casing).

In earlier analysis, flow separation was observed in some of the pipes (Figure 49). The measurements in this area are affected by the high turbulence and mass flow concentration in a part of the pipe leaving other parts with much lower velocity and backflows in a different temperature. Such areas must be avoided when any measuring instrument is to be installed. This applies for temperature and velocity measurements (Figure 67). In these current flow conditions this area lies from the inlet of the fuel pipes and to 12 cm further measured in the flow direction.

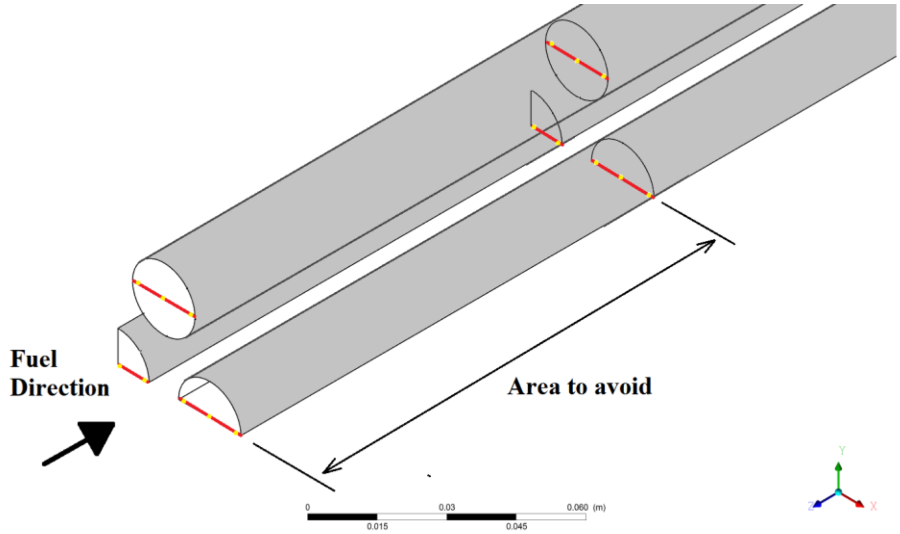

Figure 67: Fuel pipe temperature measuring junctions' locations.

Four to five levels along the fuel pipe length should have junctions for temperature measurements. It is also favorable to have the junctions in a different angle in each level (Figure 68). This is to capture the average temperature in each level regardless the flow profile pattern,

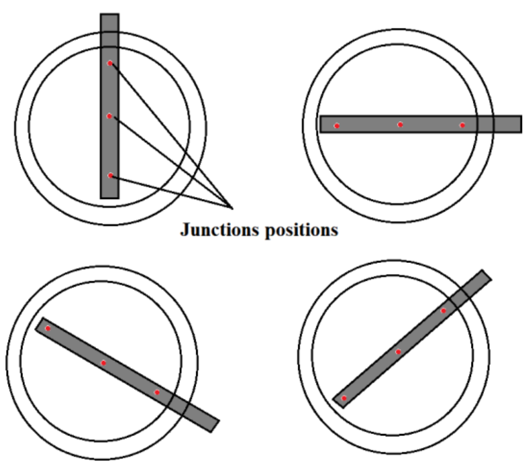

Figure 68: positioning of measuring devices junctions in different levels of a fuel pipe.

Considering the identical considerations as showed in Figure 67 along with the variations in positioning angles depicted in Figure 68 , a comparable technique can be employed when dealing with the coolant domain under consideration. However, in the case of measuring temperature in the coolant domain, it is a position of interest to capture the temperature profile variation along the core diameter. In this case more junctions shall be used to cover the relatively large MD diameter. The positions of the lines that shall include the measuring junctions can be seen in earlier figures: Figure 41.

5.5.2 Velocity Measuring Instruments

Several devices can be utilized to measure flow velocity and velocity profiles in molten metal. Given the extreme conditions and challenges associated with measuring molten metal flow, specialized instruments are typically employed. Some examples of devices commonly used for this purpose are as below:

1. **Electromagnetic Flowmeter:** An electromagnetic flowmeter can be utilized to measure the velocity of molten metal by utilizing Faraday's law of electromagnetic induction. It measures the induced voltage generated by the flow of conductive molten metal through a magnetic field.

2. **Laser Doppler Velocimetry (LDV):** LDV, an optical technique, can be adapted for measuring the velocity of molten metal. By analyzing the Doppler shift in laser light scattered off particles or bubbles within the molten metal, the flow velocity can be determined.

3. **Ultrasonic Doppler Velocimeter (UDV):** UDV can be applied to measure the flow velocity of molten metal. It uses ultrasound waves to analyze the Doppler shift in the reflected waves caused by the motion of particles or bubbles within the molten metal.

4. **X-ray Velocimetry (XRV):** XRV is a non-intrusive technique that employs X-ray imaging to measure the flow velocity of molten metal. By tracking the movement of tracers or solid particles suspended in the molten metal, the velocity profiles can be determined.

5. **Electrochemical Velocimetry:** This technique involves using an electrochemical probe to measure the flow velocity of molten metal. The probe detects changes in the electrical potential resulting from the fluid motion.

6. **Thermal Anemometry**: Thermal anemometry can be adapted to measure flow velocity in molten metal. By employing heated or cooled probes, it measures the velocity based on the heat transfer between the probe and the molten metal.

These devices are examples of commonly used instruments for measuring flow velocity and velocity profiles that can be employed in the MD core molten lead. However, it's important to note that the specific choice of instrument depends on factors such as the temperature and composition of the molten metal, the desired accuracy, and the accessibility of the measurement location.

These aforementioned devices, along with other suitable options, should be taken into consideration when making a selection. Multiple types of devices can be employed based on the desired accuracy and accessibility requirements of the specific location under consideration. When contemplating velocity measurement devices for a specific application involving molten metal, it is important to anticipate and address various challenges. Several examples of these challenges are provided below:

1. **High Temperature and Heat Transfer:** Molten lead (and molten metals in general) are typically at elevated temperatures, leading to significant heat transfer to the measurement equipment. This can cause thermal expansion, material degradation, or inaccurate readings if not properly accounted for.

2. **Corrosion and Erosion:** Molten metals can be highly corrosive and erosive, posing a risk to the measurement equipment and affecting its accuracy over time. The selection of materials that can withstand the corrosive properties of molten metal is crucial.

3. **Clogging and Blockages:** Molten metals may contain impurities or solid particles that can lead to clogging or blockages in the pipe or measurement devices. This can disrupt the flow and affect the accuracy of velocity measurements.

4. **Flow Turbulence:** Molten metal flow in pipes can exhibit turbulent behavior, resulting in fluctuations and irregular velocity profiles. Accurately capturing the velocity profiles in turbulent flow conditions can be challenging.

5. **Non-Newtonian Flow Behavior:** Some molten metals exhibit non-Newtonian flow behavior, where viscosity and flow characteristics change with shear rate or temperature. This can complicate the measurement of velocity profiles and require specialized techniques for analysis.

6. **Limited Access:** Accessing the measurement location within the pipe can be challenging due to the high temperatures, confined spaces, and safety considerations. Specialized probes or non-intrusive measurement techniques may be necessary to overcome these limitations.

7. **Interference from Magnetic Fields:** Some molten metals can generate strong magnetic fields due to their electrical conductivity. These fields can interfere with electromagnetic-based velocity measurement techniques or cause inaccuracies in the readings.

8. **Limited Measurement Points:** Obtaining velocity profiles across the entire cross-section of the pipe can be difficult due to limited access and the need for multiple measurement points. This can result in limited spatial resolution and less comprehensive velocity profile data.

Addressing these challenges requires careful selection of measurement techniques, proper sensor design, and consideration of the unique properties of molten metals. It is crucial to account for temperature effects, corrosion resistance, and potential blockages to ensure accurate and reliable velocity measurements in molten metal pipe flows.

5.5.2.1 Locations of Interest for Velocity Measurements

The suggested positions for velocity measurements in the MD coincide with the temperature measurement locations, primarily focusing on the inlets and outlets of the two fluids (both fuel and coolant) entering and exiting the MD core. It is important to note that special attention should be given to potential backflows induced by turbulence near the outlets, these should be avoided during measurements, as they can affect the accuracy of the data collected.

Despite the occurrence of high separation or swirling in certain pipes, it should be noted that these locations are not ideal for temperature measurements. However, from a flow perspective, these locations remain of interest Figure 69. It is imperative to investigate these phenomena by measuring velocities and mass flow rates. These measurements are crucial for assessing the impact on the DFR and validating the employed models. Specifically, the objective is to ascertain whether the models can accurately capture the pronounced variations occurring in localized regions. By doing so, it becomes possible to evaluate the accuracy and effectiveness of the models in representing such intricate flow dynamics.

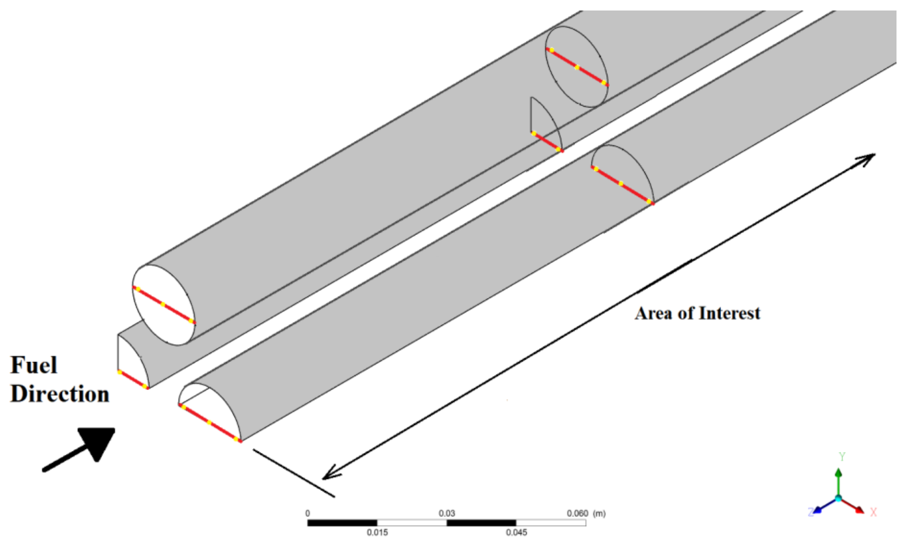

Figure 69: Fuel pipe area of interest (full pipe).

With respect to the velocity profile of the coolant within the middle core zone of the MD, it is crucial to emphasize the significance of capturing this profile. The variations in coolant velocities across the diameter of the MD significantly influence both the heat transfer rate and the temperature distribution within the MD. Figure 70 shows five locations where the velocity profile is important to measure. These locations are able to give a good understanding of the coolant flow, including the first quarter of the middle core zone where the coolant enters through the coolant pipes at a high velocity and different mass flow rates.

The velocities within the coolant pipes in the distribution and collection zones are also important, especially for the mass flow calculations. It would be very interesting to observe the mass flow distribution at different velocity inlets.

The availability of such data becomes particularly valuable if the testing procedure incorporates a wide range of parameter variations. In such cases, correlations can be established that hold importance for the safety and design aspects of the DFR. These correlations can provide valuable insights into the behavior of the coolant flow and aid in optimizing the performance and efficiency of the system.

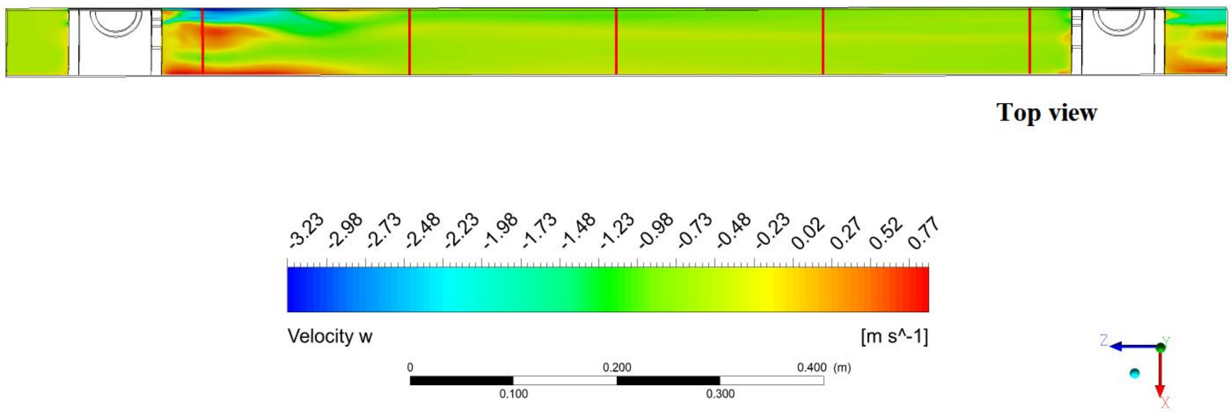

Figure 70; Top view of the MD core showing the variation of velocity (in z-direction) in a middle plane in the coolant domain with suggested testing Red-lines locations. (To be seen together with Figure 40)

5.5.3 Discussion

The quantity of data collected increases with an augmented number of measuring locations; however, in numerous instances, it is impractical to incorporate an extensive array of measuring devices. Several factors contribute to this limitation, including restricted accessibility resulting from spatial constraints or complex geometries. Additionally, cost considerations can pose challenges in deploying an abundance of measuring devices. Consequently, the selection of measuring instrument locations assumes paramount importance and necessitates careful and strategic deliberation.

Certain regions may necessitate the avoidance of temperature measurements due to the potential for misleading or inconclusive readings, often arising from factors such as high turbulence or mixing effects. Paradoxically, these very regions that render temperature measurements less useful can become areas of interest when considering velocity measurements. This is due to the same underlying reasons that initially made them unfavorable for temperature measurements. The turbulent or mixed flow characteristics present in these areas make them valuable for studying velocity patterns and understanding the fluid dynamics at play.

The suggested locations and available devices listed in this subsection only focus on the temperature and velocity measurements. More devices can be added, for example pressure gauges. However, only from the temperature and velocity measurements, one can collect a wide range of information. Some can be directly observed, and others can be calculated. below, some important parameters that can be collected/derived just from the temperature and velocity measurements:

1. **Flow Rate:** By integrating the velocity measurements across the cross-section of the flow, the volumetric or mass flow rate can be determined. This provides information on the amount of fluid passing through a given point per unit time.

2. **Reynolds Number:** The Reynolds number is a dimensionless quantity that characterizes the flow regime. It can be calculated using velocity, density, and viscosity data. The Reynolds number helps determine whether the flow is laminar or turbulent and is crucial in analyzing fluid behavior.

3. **Velocity Profiles:** The measured velocity data can be used to construct velocity profiles, which illustrate how the velocity varies across the flow cross-section. These profiles provide insights into flow patterns, boundary layer development, and the presence of turbulence.

4. **Temperature Profiles:** The acquired temperature data can be employed to construct temperature profiles, which depict the spatial variation of temperature across the flow cross-section. These profiles yield significant insights into the distribution of temperature, the evolution of the thermal boundary layer, and the existence of temperature gradients within the flow.

5. **Shear Stress:** Shear stress can be calculated using velocity gradient data. It represents the force per unit area acting parallel to a surface due to fluid viscosity. Shear stress is important for understanding fluid-solid interactions and assessing the potential for material erosion or wear.

6. **Heat Transfer Coefficients:** By combining velocity and temperature data, heat transfer coefficients can be determined. These coefficients quantify the rate at which heat is transferred between the fluid and its surroundings. Heat transfer coefficients are vital in designing heat exchangers and assessing overall system performance.

7. **Energy Balances:** The measured velocity and temperature data can be used to perform energy balances, allowing the calculation of parameters such as heat flux, thermal energy transfer, and convective heat transfer coefficients.

8. **Pressure Drop:** By analyzing the velocity data, pressure drop across a system or specific components can be calculated. This information is crucial for understanding the flow resistance and energy losses within the system.

9. **Turbulent Intensity:** Turbulent intensity can be derived from velocity fluctuations within the flow. It quantifies the level of turbulence present and is valuable for understanding flow stability, mixing, and heat transfer characteristics.

These are just a few examples of the calculations and derivations that can be performed using velocity and temperature data observed experimentally. The specific calculations depend on the nature of the required data and the phenomenon of interest.

6 Conclusions

The Dual Fluid Reactor (DFR) represents a promising reactor concept that offers numerous advantages compared to other Generation IV reactor types. The main advantages have been highlighted in section 1.4 of this study. However, the realization of such an innovative reactor design necessitates significant efforts to achieve an optimal design and to secure regulatory and public acceptance. While computer codes are commonly used for modeling, the credibility of actual experiments surpasses that of simulations. Therefore, the construction of a mini demonstrator (MD) is crucial. By comparing the experimental results obtained from the MD with the modeling outcomes, trust in the computer models dealing with these types of fluids (low Pr number fluids) can be enhanced. Consequently, once the model is validated under various operational conditions with different parameters, it can provide convincing evidence for regulatory bodies and the scientific community. This validation process enables reliable modeling of the DFR in a wide range of operational scenarios.

The turbulence modeling technique employed in this thesis demonstrated satisfactory agreement when compared to DNS/LES/Experimental data. Similar to other turbulence models, its performance can vary across different cases due to various factors, including geometric disparities and variations in boundary conditions. While the validation process utilized similar conditions and dimensionless numbers as those of the MD, it is important to acknowledge the potential deviations that may arise during the actual MD experiment. This highlights the significance of the MD in terms of validation, as utilizing experimental data to assess turbulence models and subject them to the necessary regulations plays a crucial role in the design, licensing, and operation of the DFR.

The computational results have yielded several noteworthy observations. It has been observed in the that the heat transfer and velocity of the fuel in the MD core are influenced by three primary factors. Among these factors, two are related to the geometry of the system. The first geometric factor pertains to the positioning of the fuel pipe inlets relative to the direction of the fuel inlet to the MD core.

The second geometric factor relates to the placement of the coolant pipes within the distribution zone facing the fuel flow inlet direction. The third factor is the buoyancy force exerted on the fuel, causing it to rise due to its elevated temperature. These three factors collectively determine the uniformity, magnitude, and direction of the inlet velocity into the fuel pipes. These last three parameters along with the path of the fuel in the distribution zone (or collection zone in the case of counter flow), significantly impact the heat exchange within this specific zone as well as the middle core zone. Furthermore, they have a substantial influence on the mass flow rates in each pipe, thereby affecting the heat transfer.

For the mentioned reasons, it was observed that the counter flow configuration, unlike the parallel flow, exhibited more uniform velocity inlets and higher heat exchange efficiency. Additionally, it displayed more uniform temperature gradients, at least for the fuel.

In the parallel flow configuration, noticeable swirling patterns were observed in certain pipes. While swirling can conceptually enhance heat transfer, its beneficial impact diminishes significantly as it results in higher pressure within the pipes, subsequently leading to reduced mass flow rates and diminished heat transfer. Furthermore, the presence of swirling poses the risk of vibration-induced pipe fractures, particularly under conditions of high velocity or long-term prolonged operation. Additionally, the intensified swirling contributes to increased corrosion of the internal pipe wall due to elevated shear stresses. Capturing this swirling behavior and the fuel flow splitting over the coolant pipes shows the significance of having 3D modelling instead of the 2D, as in 2D analysis such kind of observation would not be possible.

Heat transfer occurs in the initial zone of contact between the coolant and fuel in both parallel and counter flow cases. However, in the case of parallel flow, the heat exchange process extends over a broader region, encompassing a larger area of the middle core zone compared to the counter flow, which is advantageous in terms of achieving temperature uniformity. This behavior is considered beneficial as it promotes a more extensive heat exchange area and enhances temperature homogeneity. In contrast, in the counter flow configuration, the heat transfer in the initial zone of contact is exceptionally intense and substantial. However, this characteristic is not desirable from a safety perspective of a nuclear reactor control, also due to the heightened mechanical stresses it imposes.

A significant difference between parallel and counter flows is the mass flow rates in the fuel pipes. This is again due to the direction of the fuel flow right after entering the MD core. These mass flow differences have its effect on the heat exchange efficiency (positively for the counter flow configurations).

These discrepancies between the parallel and counter flows can be a point of interest to the DFR designers, to show the insights of different configurations.

Hot spots have been observed over the coolant pipes. Such pipes are located directly in front of the fuel inlets flow. These hot spots are highly undesired, as they result in high corrosion and mechanical stresses due to the high variation in the temperature within a small area in the pipes.

After the CFD analysis results are obtained, several locations of interest were specified for installing measuring instruments. The proposed locations were to give insights about the temperature and velocity profiles in several positions of the flows as well as to track the variations in the temperature and heat transfer parameters. For example, all inlets and a chosen outlet locations are indeed important to measure the temperature in several points to have an overview about the temperature profiles, velocity profiles can also be captured using suitable measuring instruments for these locations (for example Ultrasonic Doppler Velocimeter (UDV).

Capturing the temperature and velocity profiles within the middle core zone is crucial for both fuel and coolant to give a better understanding of the two flows and heat transfer. The exact measuring positions have been specified in section 5.5. Additionally, some locations were highlighted to be avoided and not to apply specific measuring devices, for example velocity and temperature measuring instruments in areas where backflows were observed, another example temperature measurements taken in flow separation areas will be misleading and should be avoided.

All in all, the mini demonstrator as an experimental facility is one of the most essential stages that needs to be made along with all the possible experiments and modelling validations if the construction of the DFR to be considered.

Bibliography

[1] Stephen Nalley, “INTERNATIONAL ENERGY OUTLOOK 2021,” *https://www.eia.gov/outlooks/ieo/pdf/IEO2021_ReleasePresentation.pdf*. EIA.

[2] UN, “https://www.un.org/en/climatechange/paris-agreement.”

[3] UNFCCC, “https://unfccc.int/process-and-meetings/the-paris-agreement.”

[4] N. Muellner, N. Arnold, K. Gufler, W. Kromp, W. Renneberg, and W. Liebert, “Nuclear energy - The solution to climate change?,” *Energy Policy*, vol. 155, p. 112363, Aug. 2021, doi: 10.1016/j.enpol.2021.112363.

[5] *Evaluation of High Temperature Gas Cooled Reactor Performance: Benchmark Analysis Related to the PBMR-400, PBMM, GT-MHR, HTR-10 and the ASTRA Critical Facility*.

[6] G. Locatelli, M. Mancini, and N. Todeschini, “Generation IV nuclear reactors: Current status and future prospects,” *Energy Policy*, vol. 61, pp. 1503–1520, Oct. 2013, doi: 10.1016/j.enpol.2013.06.101.

[7] T. Hanusek and R. Macian-Juan, “Analyses of the shutdown system and transients scenarios for the dual fluid reactor concept with metallic molten fuel,” *Int J Energy Res*, vol. 46, no. 12, pp. 17230–17246, Oct. 2022, doi: 10.1002/er.8387.

[8] A. Huke *et al.*, “Dual-fluid reactor,” in *Molten Salt Reactors and Thorium Energy*, Elsevier, 2017, pp. 619–633. doi: 10.1016/B978-0-08-101126-3.00025-7.

[9] “Dual Fluid Reactor-IFK,” 2013.

[10] A. Huke, G. Ruprecht, D. Weißbach, S. Gottlieb, A. Hussein, and K. Czerski, “The Dual Fluid Reactor – A novel concept for a fast nuclear reactor of high efficiency,” *Ann Nucl Energy*, vol. 80, pp. 225–235, Jun. 2015, doi: 10.1016/j.anucene.2015.02.016.

[11] IAEA,“https://www.iaea.org/resources/databases/power-reactor-information-system-pris.”

[12] “https://www.gen-4.org/.”

[13] U. DoE, “A technology roadmap for generation IV nuclear energy systems,” *Nuclear Energy Research Advisory Committee and the …*, 2002.

[14] Nuclear Energy Agency (NEA), “Technology Roadmap Update for Generation IV Nuclear Energy Systems. Technical report, U.S. DOE Nuclear Energy Research Advisory Committee and the Generation IV International Forum, 2014.”

[15] Paul R. Kasten, E. S. Bettis, and Roy C. Robertson, *Design studies of 1000-MW(e) molten-salt breeder reactors*.

[16] D. Weißbach, G. Ruprecht, A. Huke, K. Czerski, S. Gottlieb, and A. Hussein, “Energy intensities, EROIs, and energy payback times of electricity generating power plants.”

[17] C. BRAUN and R. FORREST, “CONSIDERATIONS REGARDING ROK SPENT NUCLEAR FUEL MANAGEMENT OPTIONS,” *Nuclear Engineering and Technology*, vol. 45, no. 4, pp. 427–438, Aug. 2013, doi: 10.5516/NET.06.2013.708.

[18] J. J. Laidler, J. E. Battles, W. E. Miller, J. P. Ackerman, and E. L. Carls, “Development of pyroprocessing technology,” *Progress in Nuclear Energy*, vol. 31, no. 1–2, pp. 131–140, Jan. 1997, doi: 10.1016/0149-1970(96)00007-8.

[19] D. A. C. H. G. M. J. T. R. L. G. Alexander, *Nuclear Characteristics of Spherical, Homogeneous, Two-region, Molten-fluoride-salt Reactors*. 1959.

[20] D. LeBlanc, “Molten salt reactors: A new beginning for an old idea,” *Nuclear Engineering and Design*, vol. 240, no. 6, pp. 1644–1656, Jun. 2010, doi: 10.1016/j.nucengdes.2009.12.033.

[21] James A. Lane, *Fluid Fuel Reactors*. Addison-Wesley Publishing Company, 2006.

[22] C. Smith, “Lead-Cooled Fast Reactor (LFR) Design: Safety, Neutronics, Thermal Hydraulics, Structural Mechanics, Fuel, Core, and Plant Design.” Feb. 22, 2010. Accessed: Jun. 12, 2023. [Online]. Available: https://inis.iaea.org/search/search.aspx?orig_q=RN:42093241

[23] X. Wang, C. Liu, R. Macian-Juan, X. Wang, C. Liu, and R. Macian-Juan, “Preliminary Hydraulic Analysis of the Distribution Zone in the Dual Fluid Reactor Concept,” 2017. [Online]. Available: https://www.researchgate.net/publication/317400436

[24] X. Wang, R. Macián-Juan, and M. Dabrowski, “Analysis and Evaluation of the Dual Fluid Reactor Concept.” Accessed: May 22, 2023. [Online]. Available: https://www.researchgate.net/publication/312534921_Analysis_and_Evaluation_of_the_Dual_Fluid_Reactor_Concept

[25] X. Wang and R. Macian-Juan, “Steady-state reactor physics of the dual fluid reactor concept,” *Int J Energy Res*, vol. 42, no. 14, pp. 4313–4334, Nov. 2018, doi: 10.1002/er.4171.

[26] J. Sierchuła, D. Weissbach, A. Huke, G. Ruprecht, K. Czerski, and M. P. Da¸browskida¸browski, “Determination of the liquid eutectic metal fuel Dual Fluid Reactor (DFRm) design-steady state calculations.” doi: 10.13140/RG.2.2.32706.91846.

[27] D. Weiβbach, J. Sierchuła, M. P. Dąbrowski, K. Czerski, and G. Ruprecht, “Dual Fluid Reactor as a long-term burner of actinides in spent nuclear fuel,” *Int J Energy Res*, vol. 45, no. 8, pp. 11589–11597, Jun. 2021, doi: 10.1002/er.5302.

[28] Thomas Dolan, *Molten Salt Reactors and Thorium Energy*. 2017.

[29] IAEA, “https://www.iaea.org/topics/construction-and-commissioning-of-nuclear-power-plants.”

[30] R.J. Lemire and L.W. Dickson, “Overview ofRelease Phenomenology in Phebus FP and Comparison with Out-of-Pile Experiments,” in *5th Phebus FP Seminar*, Aix-en-Provence, France, 2003.

[31] J. Sierchuła, M. P. Dąbrowski, and K. Czerski, “Negative temperature coefficients of reactivity for metallic fuel Dual Fluid Reactor,” *Progress in Nuclear Energy*, vol. 146, p. 104126, Apr. 2022, doi: 10.1016/j.pnucene.2022.104126.

[32] W. P. Jones and B. E. Launder, “The prediction of laminarization with a two-equation model of turbulence,” *Int J Heat Mass Transf*, vol. 15, no. 2, pp. 301–314, Feb. 1972, doi: 10.1016/0017-9310(72)90076-2.

[33] D. Wilcox, “Formulation of the k-omega Turbulence Model Revisited,” in *45th AIAA Aerospace Sciences Meeting and Exhibit*, Reston, Virigina: American Institute of Aeronautics and Astronautics, Jan. 2007. doi: 10.2514/6.2007-1408.

[34] F. Menter, “Zonal Two Equation k-w Turbulence Models For Aerodynamic Flows,” in *23rd Fluid Dynamics, Plasmadynamics, and Lasers Conference*, Reston, Virigina: American Institute of Aeronautics and Astronautics, Jul. 1993. doi: 10.2514/6.1993-2906.

[35] D. C. Wilcox, “Reassessment of the scale-determining equation for advanced turbulence models,” *AIAA Journal*, vol. 26, no. 11, pp. 1299–1310, Nov. 1988, doi: 10.2514/3.10041.

[36] B. E. Launder and B. I. Sharma, “Application of the energy-dissipation model of turbulence to the calculation of flow near a spinning disc,” *Letters in Heat and Mass Transfer*, vol. 1, no. 2, pp. 131–137, Nov. 1974, doi: 10.1016/0094-4548(74)90150-7.

[37] F. R. Menter, “Two-equation eddy-viscosity turbulence models for engineering applications,” *AIAA Journal*, vol. 32, no. 8, pp. 1598–1605, Aug. 1994, doi: 10.2514/3.12149.

[38] P.G. Saffman, “A Model for Inhomogeneous Turbulent Flow,” *Proc R Soc Lond A Math Phys Sci*, vol. Vol. 317, 1970.

[39] R. B. Langtry, F. R. Menter, S. R. Likki, Y. B. Suzen, P. G. Huang, and S. Völker, “A Correlation-Based Transition Model Using Local Variables—Part II: Test Cases and Industrial Applications,” *J Turbomach*, vol. 128, no. 3, pp. 423–434, Jul. 2006, doi: 10.1115/1.2184353.

[40] G. Grötzbach, “Challenges in low-Prandtl number heat transfer simulation and modelling,” *Nuclear Engineering and Design*, vol. 264, pp. 41–55, Nov. 2013, doi: 10.1016/j.nucengdes.2012.09.039.

[41] K. Mikityuk, “Heat transfer to liquid metal: Review of data and correlations for tube bundles,” *Nuclear Engineering and Design*, vol. 239, no. 4, pp. 680–687, Apr. 2009, doi: 10.1016/J.NUCENGDES.2008.12.014.

[42] K. Mikityuk, “Heat transfer to liquid metal: Review of data and correlations for tube bundles,” *Nuclear Engineering and Design*, vol. 239, no. 4, pp. 680–687, Apr. 2009, doi: 10.1016/j.nucengdes.2008.12.014.

[43] R. H. Notter, “Two problems in turbulence,” University of Washington, Seattle, 1969.

[44] R. ’Jenkins, “Variation of the eddy conductivity with Prandtl modulus and its use in prediction of turbulent heat transfer coefficients.,” *Proceedings of the Heat Transfer and Fluid Mechanics Institute*. Stanford University Press, Stanford, 1951.

[45] N. Z. Azer and B. T. Chao, “A mechanism of turbulent heat transfer in liquid metals,” *Int J Heat Mass Transf*, vol. 1, no. 2–3, pp. 121–138, Aug. 1960, doi: 10.1016/0017-9310(60)90016-8.

[46] W. M. ’, C. M. E. ’Kays, *Convective Heat and Mass Transfer*, 3rd edition. New York: McGraw-Hill, 1993.

[47] B. Weigand, J. R. Ferguson, and M. E. Crawford, “An extended Kays and Crawford turbulent Prandtl number model,” *Int J Heat Mass Transf*, vol. 40, no. 17, pp. 4191–4196, Oct. 1997, doi: 10.1016/S0017-9310(97)00084-7.

[48] M. Duponcheel, L. Bricteux, M. Manconi, G. Winckelmans, and Y. Bartosiewicz, “Assessment of RANS and improved near-wall modeling for forced convection at low Prandtl numbers based on LES up to Re_T =2000,” *Int J Heat Mass Transf*, vol. 75, pp. 470–482, Aug. 2014, doi: 10.1016/j.ijheatmasstransfer.2014.03.080.

[49] W. Ma, A. Karbojian, T. Hollands, and M. K. Koch, “Experimental and numerical study on lead–bismuth heat transfer in a fuel rod simulator,” *Journal of Nuclear Materials*, vol. 415, no. 3, pp. 415–424, Aug. 2011, doi: 10.1016/j.jnucmat.2011.04.044.

[50] *Ansys Fluent Theory Guide. ANSYS Inc.*

[51] “Database of thermophysical properties of liquid metal coolants for GEN-IV.” [Online]. Available: http://www.sckcen.be

[52] Ioffe Institute, “https://www.ioffe.ru/en/.”

[53] H. Li and Y. Tomita, “Characteristics of Swirling Flow in a Circular Pipe,” *J Fluids Eng*, vol. 116, no. 2, pp. 370–373, Jun. 1994, doi: 10.1115/1.2910283.

[54] G. Vignat, D. Durox, and S. Candel, “The suitability of different swirl number definitions for describing swirl flows: Accurate, common and (over-) simplified formulations,” *Prog Energy Combust Sci*, vol. 89, p. 100969, Mar. 2022, doi: 10.1016/j.pecs.2021.100969.

[55] H. A. Vaidya, Ö. Ertunç, B. Genç, F. Beyer, Ç. Köksoy, and A. Delgado, “Numerical simulations of swirling pipe flows- decay of swirl and occurrence of vortex structures,” *J Phys Conf Ser*, vol. 318, no. 6, p. 062022, Dec. 2011, doi: 10.1088/1742-6596/318/6/062022.

[56] H. HIBARA and K. SUDO, “Structure and Vibration Phenomenon of Swirling Flow through Conical Diffusers.,” *TRANSACTIONS OF THE JAPAN SOCIETY OF MECHANICAL ENGINEERS Series B*, vol. 68, no. 675, pp. 3049–3057, 2002, doi: 10.1299/kikaib.68.3049.

[57] D. E. Ramírez-Arreola, F. J. Aranda-García, C. Sedano-de la Rosa, M. Vite-Torres, E. A. Gallardo-Hernández, and J. G. Godínez-Salcedo, “Influence of swirl number and incidence angle on erosion-corrosion behavior of API 5L X-52 steel under swirling jets,” *Wear*, vol. 510–511, p. 204518, Dec. 2022, doi: 10.1016/J.WEAR.2022.204518.

[58] T. Sydberger and U. Lotz, “Relation Between Mass Transfer and Corrosion in a Turbulent Pipe Flow,” *J Electrochem Soc*, vol. 129, no. 2, pp. 276–283, Feb. 1982, doi: 10.1149/1.2123812.

[59] T. Takano, Y. Ikarashi, K. Uchiyama, T. Yamagata, and N. Fujisawa, “Influence of swirling flow on mass and momentum transfer downstream of a pipe with elbow and orifice,” *Int J Heat Mass Transf*, vol. 92, pp. 394–402, Jan. 2016, doi: 10.1016/j.ijheatmasstransfer.2015.08.087.

[60] Che Chung Fu, Q. Peng, Y. Li, D. Liao, J. Lyu, and B. Zhu, “Experimental study of flow straightening and turbulence reduction characteristics for porosity honeycomb,” Oct. 2016.

[61] X. Schuler and K.-H. Herter, “Thermal Fatigue due to Stratification and Thermal Shock Loading of Piping,” in *30th MPA-Seminar in conjunction with the 9th German-Japanese Seminar*, Stuttgart, Oct. 2004.

[62] R. Kumar, P. A. Jadhav, S. K. Gupta, and A. J. Gaikwad, “Evaluation of Thermal Stratification Induced Stress in Pipe and its Impact on Fatigue Design,” *Procedia Eng*, vol. 86, pp. 342–349, 2014, doi: 10.1016/j.proeng.2014.11.047.

[63] S.-T. Tu, H. Zhang, and W.-W. Zhou, “Corrosion failures of high temperature heat pipes,” *Eng Fail Anal*, vol. 6, no. 6, pp. 363–370, Dec. 1999, doi: 10.1016/S1350-6307(98)00057-0.